

INVESTIGATING THE PARAMETERS OF PRE-/POST-CONDITIONING ON HUMAN-DERIVED  
CANCER CELLS

INVESTIGATING THE PARAMETERS OF PRE-/POST-CONDITIONING ON HUMAN CANCER

CELLS

By

Jason Cohen, B.Sc.

A Thesis Submitted to the School of Graduate Studies

in Partial Fulfilment of the Requirements for the Degree of

Master of Science

McMaster University





## Abstract

There is a large amount of interest and research currently going into studying the effects of low dose radiation on humans, and bridging the gap with the data from the effects of high dose radiation. Much work is to be done to understand low dose exposures such as from medical treatments and those who work with or around radiation. Two popular and widely known examples of low-dose phenomena are the radiation induced bystander effects and the radioadaptive response (RAR). This research involves the study of the impact of a low dose of radiation that is administered several hours after a high – even fatal – dose is given, which contrasts the traditional RAR where a low priming dose is given before a high dose and can lead to increased cell survival. Many different parameters were checked to see if cell survival can be enhanced or diminished depending on the stage of the cell cycle, cell growth conditions, and cell profiling differences in protein function (namely the TP53 gene). Additionally, the post-conditioning response was contrasted to see if it was possible to see any effects from the newly emerging area of bystander signalling, UV BioPhotons, would be present in cell lines that either did or did not exhibit a post-conditioning effect. It was shown that post-conditioning has a protective effect on survival of the cells in certain dose ranges and certain cell lines. The post-conditioning effect also appears to be stronger in magnitude

than the classic RAR. No relationship between gamma-induced biophoton signalling and post-conditioning was observed, nor is it certain whether an acute gamma-field can induce significant UV biophoton damage. This thesis is aimed to explore the various parameters by which post-conditioning effects occur on various Human cancers.

## Acknowledgements

I would like to thank Drs. Carmel Mothersil and Colin Seymour, who have provided unending patience, support, and openness in their supervising during my thesis. They had allowed me the space, independence, and creativity for me to pursue this project that I had enjoyed to study and carry out. Their open-minded and curious attitudes are what propels science past its boundaries and into the unknown territory where true inventions and discoveries can take place.

I would also like to thank Drs. David Chettle and Fiona McNeill, who offered their time, support and knowledge during many meetings with them to help me with my project and ideas. They were always there for me despite their very hectic schedules and helped to be a foundation from which my research was able to build upon.

To the staff in Radiation Sciences and Health Physics: Fiona Ahlang, Terri Parker, all the members of the Health Physics Staff, thank you for providing your help and knowledge all the way. I would especially like to thank Scott McMaster for his guidance and help in many of my project ideas. He was always available and very kind and patient. He had given me ample knowledge and confidence when pursuing my ideas as well as the details for making the experiments carry out smoothly.

I would like to thank all the members of my lab: Dr. Michelle Le, Dr. Cristian Fernandez-Palomo, Dr. Christine Pinho, Dr. Xiaopei Shi, Dusan Vukmirovic, Gary Wong, and Chandula Fernando, as well as all of the co-ops who provided countless training, assistance, advice, and overall keeping me on the right track towards finishing my research. They were all amazing lab members and helped to keep the lab running smoothly and efficiently. I would especially like to thank Dr. Nathan TK Vo for his time, patience, support and knowledge in helping me with my experiments, especially his edits of our manuscript, and his time for teaching me the Western Blotting technique.

To our fellow Medical Physics Undergrad Class: Andre Laranjeiro, Marwan Shahid, Julianna Sebastianni Farazdak Ali and Suhier Seif, whom I wouldn't have even been at this point if it weren't for our solid group that worked together for the 4-years before this.

To my parents for their unimaginable patience, support, and love, without which I would not be even at this point today. They are both kind, honest, hardworking and great role-models who taught me many things, always encouraging me to pursue what made me happy. Thanks to our cat Jewel who also provided lot of unconditional love and furry companionship during this time.



## Table of Contents

<b>1</b>	<b>Introduction ..1</b>
<b>2</b>	<b>Background of Radiation Source ..7</b>
<b>3</b>	<b>Radiation Induced Pre-Conditioning &amp; Post-Conditioning Responses ..15</b>
3.1	Overview ..15
3.2	HT29 Materials and Methods ..16
3.3	Results ..19
3.4	Discussion ..22
<b>4</b>	<b>Parallel comparison of pre-conditioning and post-conditioning effects in human cancers and keratinocytes upon acute gamma irradiation ..26</b>
4.1	Supplemental Material ..56
<b>5</b>	<b>Protein Expression Resulting from Pre-/Post-Conditioning ..60</b>
5.1	Western Blotting Materials and Methods ..60
5.2	Results ..66
5.3	Discussion ..69

<b>6</b>	<b>Quantifying Cell Luminescence in a Gamma Field via Photon Detection ..70</b>
6.1	Photon Detection Overview ..70
6.2	Materials and Methods ..71
6.3	Results ..83
6.4	Discussion ..90
<b>7</b>	<b>Radiation Induced Bystander Effects and BioPhoton Cell-Cell Signalling ..94</b>
7.1	Radiation Induced Bystander Effects and BioPhoton Emission Quantification Materials and Methods ..94
7.2	Results ..101
7.3	Discussion ..104
<b>8</b>	<b>Future Directions ..106</b>
<b>9</b>	<b>References ..109</b>
<b>10</b>	<b>Appendix A: Raw Data ..126</b>

## List of Figures

Figure 1: Experimental outline of areas of interest	..6
Figure 2: Decay Scheme of Cesium-137 Gamma Radiation Source from the McMaster Taylor Source	..7
Figure 3: McMaster Taylor Source Cesium-137 Source Dose Rate as a Function of xyz position away from the centerline of the source origin	..9
Figure 4: Dosimeters and Dosimetric testing of McMaster Taylor Source dose uniformity	..11
Figure 5: Dosimeters and Dosimetric Testing results of McMaster Taylor Source. A shows the dosimeter placement and reading and B shows the evaluation copy	..12
Figure 6: HT29 Clonogenic Assay of Control Plating Efficiency after Staining	
3.2.1 Results from HT29 Cell Line Pre-/Post-Conditioning Trials	..20

Figure 7: Summary of experimental results for pre-/post-conditioning of HT29 cell line, n=9	..22
Figure 8: Cell concentrations check at 24h and 29h after seeding using an Automated Cell Counter	..58
Figure 9: Cell singlet and doublet percentage at 24h and 29h for n=3 triplicates. The method was done using 500 cells seeded and stained at the times given, then manually counted under the microscope.	..59
Figure 10: A: Microplate with working reagent and protein standards control (top three rows), and working reagent with unknown protein concentration samples. Note that the image was captured a couple of hours after creating the WR and protein samples, colors have faded in some areas. B: Absorbance versus Protein Standard Curve based on control known protein standards, from which a best fit equation was acquired and used to interpolate absorbance data from unknown protein samples to solve for the corresponding protein concentration.	..63
Figure 11: Actin control at 42 kDa in Wells 1, 3, 5, 6, 8-11 (from left-right).	..66
Figure 12: Original image of Western blot membrane investigating p53 status after pre-/post-conditioning treatments and controls, with visible protein standard ladder on the	

right side. ..67

Figure 13: Close-up and labelled p53 protein expression from each of the 8 treatment groups used in this experiment with the HCT116 p53+/+ cell line. ..67

Figure 14: p21 western blotting results. Image taken from BioRad ChemiDoc as an overlay of colorimetric and chemiluminescent image. ..68

Figure 15: A top-down view of the exact setup in how measurements took place. The flask is angled so that the wall containing the cells (or lack thereof) is parallel to the detector window, ~6 cm away. When the lid is on, this entire area is dark and free from stray light. ..74

Figure 16: A schematic of the photon detector in the gamma-irradiator ..75

Figure 17: Average Counts from 30s exposure to  $\gamma$ -Irradiation with a 610nm filter. The counts were subtracted from background (detection of stray gammas only) for each independent trial. ..84

Figure 18: Average Count rate from 30s exposure to  $\gamma$ -Irradiation with a 610nm filter. The counts were subtracted from background (detection of stray gammas only) for each independent trial, n=9. Different cell densities were used with Flask Only indicating no cells present during the measurements. ..85

Figure 19: Average Count rate from 30s exposure to  $\gamma$ -Irradiation with a 340nm filter. The counts were subtracted from background (detection of stray gammas only) for each independent trial. ..87

Figure 20: 4 million cells seeded, and no differences in observed count rate from changes in dose rate at highest dose rate ..88

Figure 21: 4 million cells seeded, and no differences in observed count rate from changes in dose rate at lowest possible dose rate. ..89

Figure 22: Photon emission detected immediately AFTER irradiation for 4 million cells, and compared to natural background or flask only. ..90

Figure 23: Schematic of flask arrangement to perform crude testing of cell-cell signalling through UV BioPhotons. Grey color here represents shielding, whereas black represents the enclosed case that was kept dark during measurements. The orange color represents gamma irradiation and the green represents potential BioPhoton signals.

..96

Figure 24: A layout of the flasks before the top cover was placed directly over the rest of the enclosure. ..97

Figure 25: A shows the direct setup of the experiment just before irradiation, including the shielding placement. B shows a rough schematic using stock images of how the flasks were placed relative to the Cesium 137 radiation source opening...98

Figure 26: HCT116 p53+/+ summary of experimental results, n=9, 3 independent trials. 0Gy control is completely unirradiated, control plating efficiency, BP Con is the BioPhoton control of flasks only signalling to 500 shielded reporter cells, 3Gy DIR BP is flasks containing 200,00 cells receiving ~3Gy Direct irradiation to signal towards 500 shielded

reporter cells, and CCCM and ICCM are the bystander medium transfer positive controls.

The graph is representing the survival fraction on according to various treatments.

..102

Figure 27: HCT116 p53-/- summary of experimental results, n=9, 3 independent trials.

0Gy control is completely unirradiated, control plating efficiency, BP Con is the BioPhoton

control of flasks only signalling to 500 shielded reporter cells, 3Gy DIR BP is flasks

containing 200,00 cells receiving ~3Gy Direct irradiation to signal towards 500 shielded

reporter cells, and CCCM and ICCM are the bystander medium transfer positive controls.

The graph is representing the survival fraction on according to various treatments.

..103

Figure 28: UV-NIR Spectrum and the most suitable reflecting materials as provided by the

Edmund Optics Company

..108





## 1 Introduction

There is a large amount of interest and research currently going into studying the effects of low dose radiation on humans, and bridging the gap with the data from the effects of high dose radiation. Outside of the studies from the Atomic Bombings of Hiroshima & Nagasaki in Japan, , which account for majority of the high dose data we currently base radiation safety and health physics protocols on, there is still much work to be done to understand low dose exposures such as from medical diagnostic treatments and those who work with or around radiation. This is needed now because the current LNT model cannot describe certain effects that occur on the very low dose range, which would either exacerbate or minimize the damage of targeted radiation effects. Two popular and widely known examples are the radiation induced bystander effects and the radioadaptive response (RAR). The goals of our group are to expand on the current knowledge of the traditional bystander and adaptive response modes, which have been suggested to be tied together by different key characteristics. This research involves the study of the impact of a low dose of radiation that is administered several hours after a high – even fatal – dose is given, which contrasts the traditional RAR where a low priming dose is given before a high dose and can lead to increased cell survival. Many different parameters were checked to

see if cell survival can be enhanced or diminished depending on the stage of the cell cycle, cell growth conditions, and cell profiling differences in protein function (namely the TP53 gene). The protein p53 expression was analyzed in further detail using Western Blot, along with p21 which may be involved as a mediator to p53 in the downstream cell cycle arrest. It was shown that p53 may be less expressive from pre-conditioning, with no change in p53 expression from post-conditioning. Additionally, this post-conditioning response was contrasted to see if it was possible to see any effects from the newly emerging area of bystander signalling, UV BioPhotons, would be present in cell lines that either did or did not exhibit a post-conditioning effect. It was shown that post-conditioning has a protective effect on survival of the cells in certain dose ranges and certain cell lines. The post-conditioning effect also appears to be stronger in magnitude than the classic RAR. No relationship between gamma-induced biophoton signalling and post-conditioning was observed, nor is it certain whether an acute gamma-field can induce significant UV biophoton damage. There are, however, large implications for post-conditioning effects on cell survival within the field of radiation therapy, such as if a patient had been imaged with CT scans after receiving radiation therapy treatment. This thesis is aimed to explore the various parameters by which post-conditioning effects occur on various Human cancers.

The radioadaptive theory or adaptive response phenomenon has been well documented since it was first coined in 1984 (*Wolff et. al. 1984*). Their research suggested that a low dose of radiation given at various times before a larger dose resulted in a lower yield of

chromatid aberrations for the damaged human lymphocytes than when the same human lymphocytes were only subjected to the large dose of radiation. This study was followed up with using other cell lines shortly after (Sanderson & Morley (1986); Ikushima, 1987)). The mechanisms behind this adaptation have been largely unclear (Matsumoto et al., 2004; Stecca & Gerber, 1998; Szumiel, 2005; Tapio & Jacob, 2007; Wodarz et al., 2014).

There are many workable hypotheses of basic mechanisms behind the response, such as induction and suppression of genes during a period of time (Tapio & Jacob, 2007; Wodarz et al., 2014). Additionally, the molecular pathways may be related to ATM signal cascading leading to cell cycle arrest, phosphorylated ATM at ser1981, or DNA-dependent protein kinase activation (Marples, Wouters, Collis, Chalmers, & Joiner, 2004; Marples, Wouters, & Joiner, 2003; Short, Bourne, Martindale, Woodcock, & Jackson, 2005). Reactive oxygen species (ROS) and nitric oxide may also play a role in these cellular changes (Hamada, Matsumoto, Hara, & Kobayashi, 2007; Matsumoto et al., 2001; Matsumoto, Takahashi, & Ohnishi, 2007; MIURA, 2004). Authors today have gone even further to suggest the role of p53 with ROS and surviving-associated adaptive responses (Murley, Miller, Weichselbaum, & Grdina, 2017). Another model suggests cells may emit signals to nearby cells via gap junctions or other ways and cause a type of warning to prepare those not-yet damaged cells (Hamada et al., 2007; Ojima, Eto, Ban, & Kai, 2011; Snyder, 2004; Wodarz et al., 2014).

The question has also been raised if non-targeted effects such as the bystander effect, in which cellular damage is seen in cells that were not directly exposed to radiation due to signalling from damaged cells (Liu et al., 2006; Maguire, Mothersill, Seymour, & Lyng, 2005; C Mothersill, 1997; Carmel Mothersill & Seymour, 1997, 2002) are related to the radiation-induced adaptive response (Ryan, Seymour, Joiner, & Mothersill, 2009).

The relationship may be linked to a phenomenon called hyperradiosensitivity and increased radioresistance, or HRS/IRS, in which cells are much more sensitivity to acute doses of ionizing radiation, and yet highly radioresistant, both past a certain threshold of around 0.2Gy (M. C. Joiner & Johns, 1988; M. C. Joiner, Denekamp, & Maughan, 1986; Marples & Joiner, 1993; Carmel Mothersill, Seymour, & Joiner, 2002; Parkins & Fowler, 1986). These effects are again related to p53 because of its role as a target down the latter of ATM. P53 or tumor protein TP53 codes for cell cycle regulation and tumor suppression. To this day, it can be found that researchers are connecting the and plausible molecular pathways in order to get a fuller view of the interconnectedness of such mechanisms (Guéguen, Bontemps, & Ebrahimian, 2019).

The nature of low-dose phenomena seems to be linked in ways that are still being mapped out, the newest of which is the more recent area of BioPhoton research, in which damaged cells may emit signals in the form of cellular luminescence, or photons.

Of specific interest to this area of cellular luminescence is when damaged cells emit UV photons that can damage nearby unirradiated and healthy cells after a prolonged period of time. The work in this thesis (schematic pictured in Figure 1) presents a building block of seeing whether there is any vague link between cells that have shown classic bystander effect and strong biophoton signalling will also reveal any patterns of adaptive responses. More specifically, if there are any patterns between the status of the protein p53, which was described as seen playing a role as a potential molecular pathway for the adaptive response, and these phenomena.

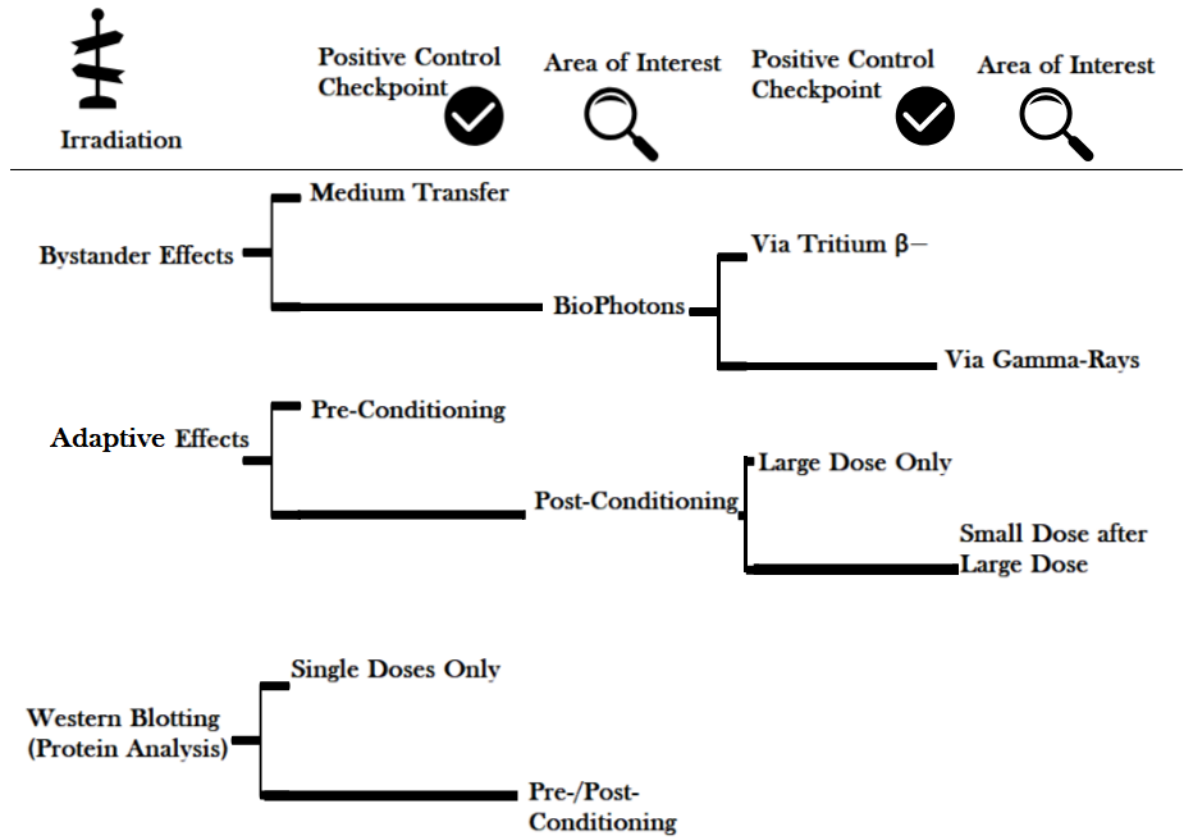


Figure 1: Experimental outline of areas of interest

## 2 Background of Radiation Source

On the main campus of McMaster University is the Taylor Radiobiology Source, which is a room with a contained radiation source: 1 kCi Cesium-137. Cesium-137 is primarily a gamma-emitter with a half-life of about 30.2 years, and its activity of 1 kCi was the original activity upon installation (the current activity is estimated to be approximately 500 Ci). The decay scheme is shown below in **Figure 2**

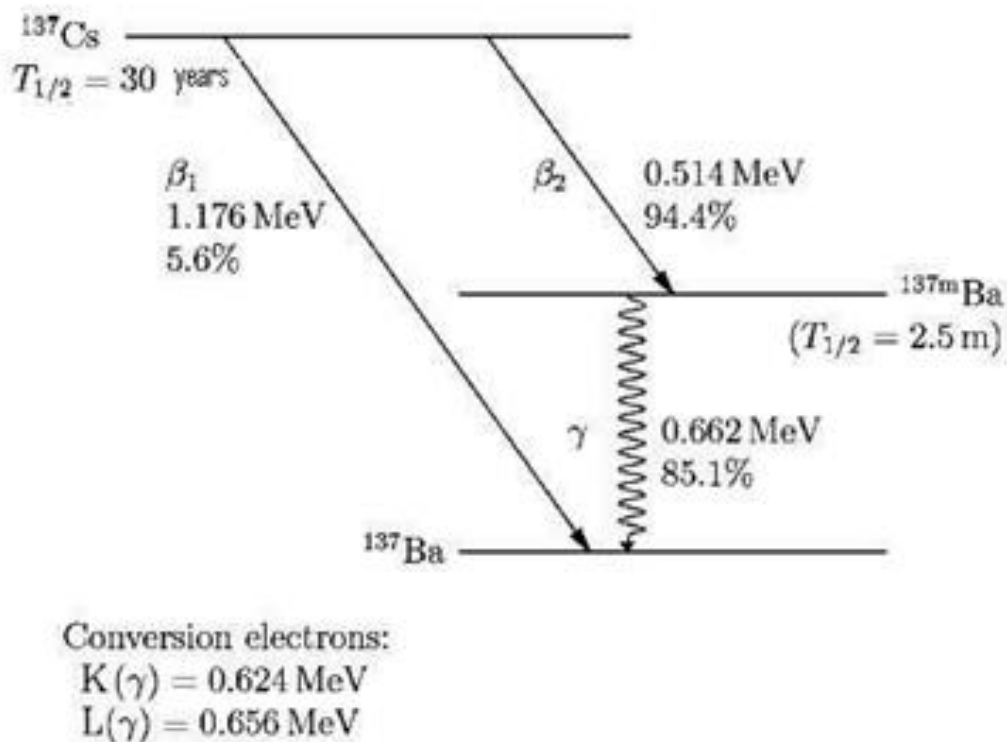


Figure 2: Decay Scheme of Cesium-137 Gamma Radiation Source from the McMaster Taylor Source



At the time of irradiations, the Cs137 source had an activity of approximately:

$$A = A_0 e^{-\lambda t} = 500 \text{ Ci}$$

Where the initial activity,  $A_0$ , was 1 kCi, the time  $t$  was 11,000 days since the initial calibration (source retrieval date), and the  $\lambda$  decay constant is 0.0000629 per day.

The radiation source is located inside of a heavily shielded cubic container with a circular shutter of ~6cm in diameter on the bottom face of the cube. It is assumed that the Cs137 source has a roughly even particle distribution inside of its containment, which eliminates major beam inequalities that would otherwise affect measurements at larger distances ( $Z > 27$  cm) from the source, and allows the approximation of the Cs137 source as a crude point source. Beam inequality, or dose uniformity, was examined in detail, as shown in **Figure 3**

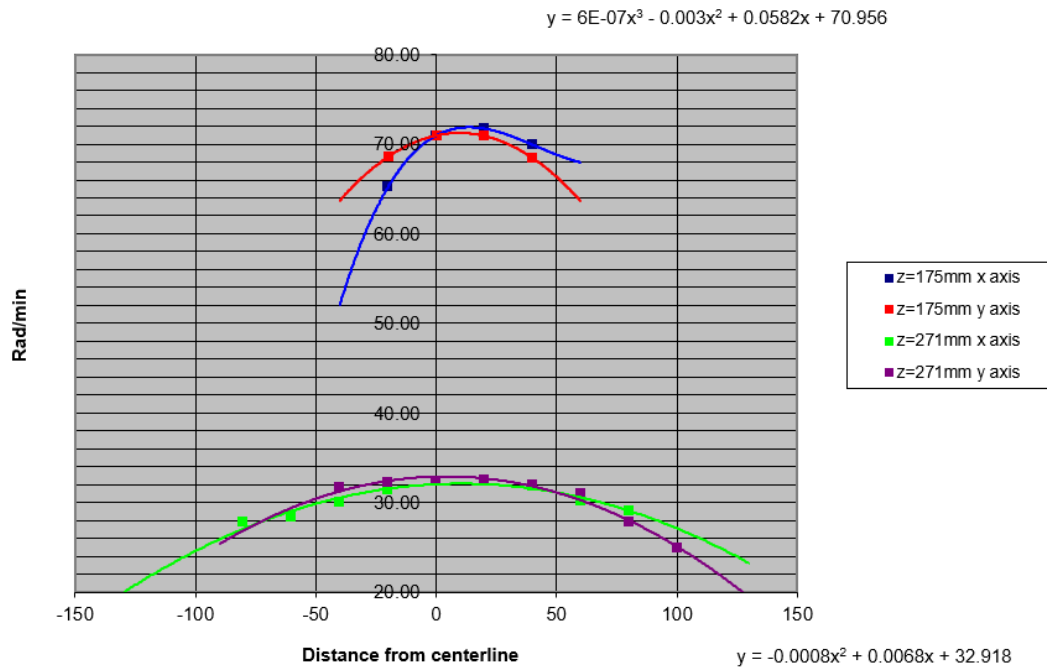


Figure 3: McMaster Taylor Source Cesium-137 Source Dose Rate as a Function of xyz position away from the centerline of the source origin

In **Figure 3**, the data shown as a dose mapping graph which graphs the dose distribution across an x-distance and y-distance (xy plane that flasks containing cells are placed on) for a given z-distance, which is the distance from the Cs137 radiation source to the cells. The z-distances shown are for either 17.5 cm or 27.1 cm, which are within the range of distances used for the majority of irradiations in this thesis. For the majority of experiments in this thesis, including all experiments presented in the manuscript, a z-distance of 27.1 cm was chosen. Since

experiments are designed in treatment groups contained 3 replicate flasks (triplicate flasks) per treatment group, the experimental design typically involved 6 flasks being irradiated at a time, with one treatment group aligned symmetrical to the centerline with the other treatment group. This setup was primarily for the administration of challenge doses, thereby setting up 3 control-treatment flasks facing back-to-back with the other 3 conditioned-treatment flasks, all destined to receive the same radiation dose. Flasks were aligned so that there would be as small deviation as possible (within roughly 1.5 cm x or y alignment error) from the centerline, in order for the 3 flasks on the right of the centerline to receive the same overall average dose as the 3 flasks on the left of the centerline. It is important to note that centerline in this case refers to either the  $x = 0$  or  $y = 0$  axis, where the triplicate flasks of one treatment are in contact with the other.

For some experiments utilizing the HT29 cell line at 2Gy analysis, a distance of  $Z = 20.3$  cm was used. In order to analyze the dose-distribution, it should be first noted that due to  $1/r^2$  fall off of dose-rate, that at  $Z = 17.5$ cm (ie. **Figure 3**) a very large deviation in dose-distribution along concentric circular distances in the xy-plane away from the source will be present, compared to the actual source-flask distance used which was 20.3cm. Therefore Thermoluminescent

Dosimeters (TLDs) were obtained and used in a separate experiment to determine the absorbed dose along different x-y coordinates at  $Z = 20.3\text{cm}$ , as shown in **Figure 4** and **Figure 5** below.

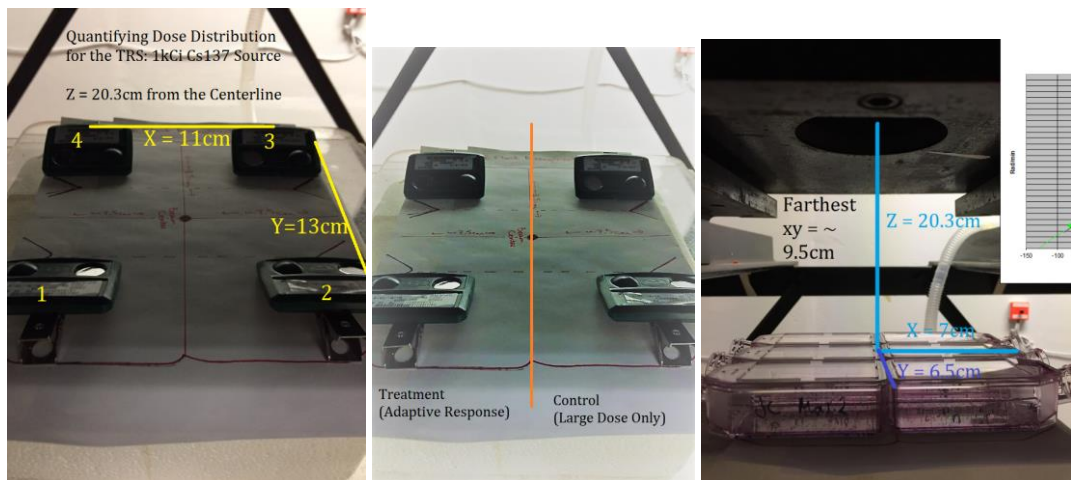


**Figure 4:** Dosimeters and Dosimetric testing of McMaster Taylor Source dose uniformity

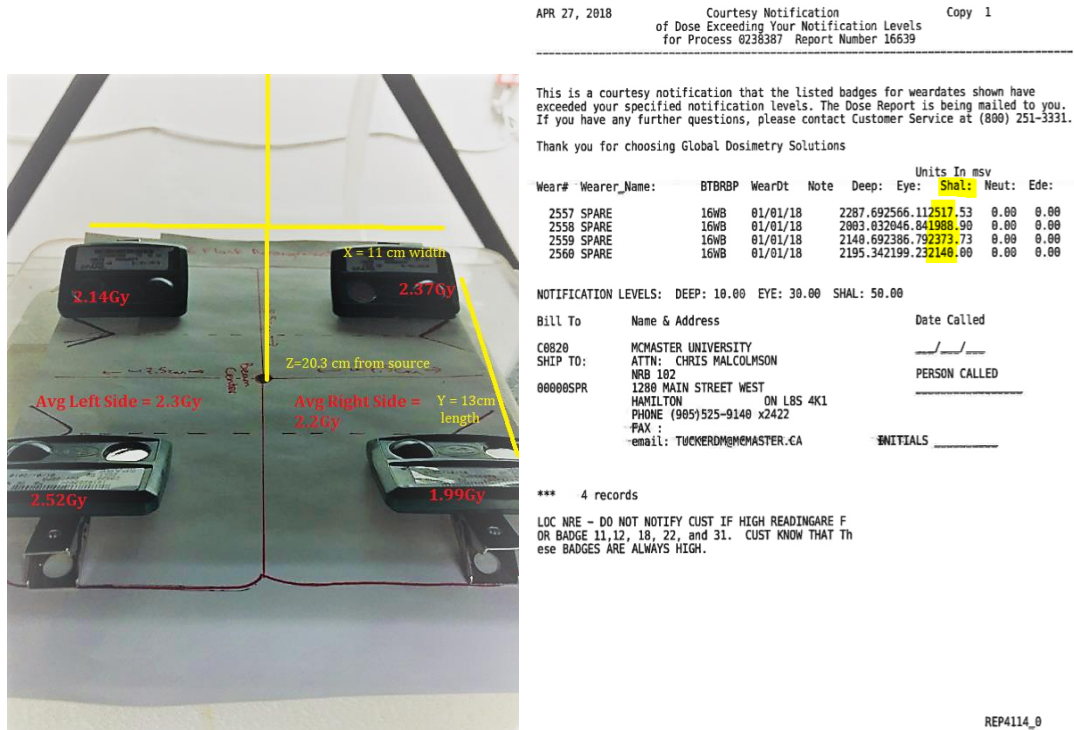


Figure 5: Dosimeters and Dosimetric Testing results of McMaster Taylor Source. A shows the dosimeter placement and reading and B shows the evaluation copy

The results from the TLDs placed at approximately the same xy distances away from the centerline of the source are shown in Figure 5 A B. In Figure 5 A the TLD arrangement is shown with the corresponding shallow doses written on them. All TLDs were destined to receive a theoretical 2Gy after 4 min. 40s of exposure at a distance of Z = 20.3cm from the Cs137 source. It should be noted that the shallow

dose is calculated based on radiation track penetrating the corner windows of the TLD, and that these were symmetrical along the diagonal, but not along the centerline plane. The shallow dose recording was taken as the more conservative recording because the dose-variation between left side and right side was larger than for the deep dose. Additionally, cells expose to gamma rays, separated only by liquid non-viscous medium and a thin plastic containment flask, will be more appropriately represented by shallow dose. The overall shallow difference between TLDs across the diagonal was 0.15 Gy and 0.15 Gy for the left side versus the right side. The overall shallow dose difference on average between the left side versus right side was 0.1 Gy. These results are within the error of the destined dose of  $2 \pm 0.23$  Gy. This error can be considered for both the error of the TLD reading as well as the error of the theoretical radiation dose calculations, or dose mapping for all four TLDs which is represented in the standard deviation equation below:

$$S.D. = \sqrt{\frac{\sum(x - \bar{x})^2}{N - 2}}$$

The equation gives an error of 10% or and so the previous expression of simply square root of the dose is used as a more conservative error for the beam inequality at the close source-flask distance of  $Z = 20.3$ cm.

However, these results at  $Z = 20.3$  cm from the source still suggest that either the TLDs were slightly misaligned within error or that at  $Z = 20.3$  cm, the beam

inequality is such that a difference of 0.15 Gy more on average is received between the left side of the centerline and the right side of the centerline. This is in agreement with the dose mapping from **Figure 3**, which shows that at 17.5cm, there may be a slight dose variation due to spatial distribution, particularly along the x-axis. It is again important to state that based on the dose mapping and TLD measurements that at  $Z = 27.1$  cm away from the source, a much more uniform beam should be observed.

All experiments were set up at a source – flask distance of  $Z = 27.1$  cm away from the Cs137 gamma source, giving an approximate dose rate of 0.26 Gy/min or 260 mGy/min. The only exception a few experiments mentioned with the HT29 cell line at 2Gy challenge dose testing versus pre-/post-conditioning which were set up at  $Z = 20.3$  cm away from the source, with a corresponding dose rate of 0.42 Gy/min or 420 mGy/min.

### 3 Radiation Induced Pre-Conditioning & Post-Conditioning Responses

#### 3.1 Overview

Low dose effects have been categorized by a number of different studies and backgrounds, one being an area of hormesis or adaptation work. The radiation induced pre-conditioning, or classical adaptive, response is one that involves a small (low, single acute radiation) dose that is administered to prime an enhanced survival or protective effect towards a larger radiation dose, which is given afterwards. The classical adaptive response has been of large interest and many studies have been published in the years on this low dose research. However, administering the large dose before the smaller dose, which for the duration of this thesis will be termed post-conditioning, has not been widely looked at. While the mechanisms remain unclear, this area of research has been predominantly showcased in physiology research, namely cardiac reperfusion for myocardial infarctions. Myocardial infarction, or heart-attack, has been shown to have lesser severity (such as infarct size) after subjects were treated with brief post-conditioning coronary occlusions (oxygen restriction) upon reperfusion (Paglia & Penna, 2011).



This thesis outlines several cell lines of interest: HT29 human colon colorectal adenocarcinoma, HCT116 p53+/+ and HCT116 p53-/- human colon colorectal carcinoma, T98G human glioblastoma, and HaCaT human keratinocytes. A direct comparison between pre-conditioning and post-conditioning effects was performed to elucidate further understanding of cellular responses to high damage mitigated by low dose intervention.

### 3.2 HT29 Materials and Methods

#### **Cell Culture**

HT29 Cell line is an in-vitro human colon adenocarcinoma with a wild type expressive p53 status. HT29 were bathed in RPMI 1640 cell culture medium that was supplemented with 10% Fetal Bovine Serum (Invitrogen, Burlington, ON, Canada), and 5 mL of 10,000 units of penicillin (Gibco, Burlington, ON), and 5mL of L-Glutamine, and kept in incubation at 37°C in an incubator with 5% CO<sub>2</sub> and 95% relative humidity.

All cell culturing and experiments were performed in BioSafety Level 2 laminar flow cabinets. Cell stocks were maintained in T75 flasks (Falcon) with 20 mL of medium and cell passaging was performed at approximately 60-80% confluency. Subculturing

routines were performed using a 0.25% dilution of 1:1 trypsin buffer and DPBS and 1 mM EDTA in order to create single cell suspensions for cell passaging.

### **Challenge irradiation and Clonogenic Assay Technique**

The cell survival of the control and the irradiated cells were assessed using the clonogenic assay technique developed by Puck and Marcus (1956) after the irradiations were completed. All experimental flasks were T25, including the irradiated cells, and were incubated at 37°C for 24 h after being seeded from the stock T75 flask. After trypsinization, cells were neutralized with equal volume of medium and depressed out of a serological pipette against the flask wall 3 times to break apart clusters. Afterwards, the cell stock was centrifuged at 1000rpm for 5 min. The cell pellet was resuspended in 10mL of fresh medium, and cell concentration was counted using a BioRad Automated Cell Counter.

While the 0 Gy control set remained in the incubator, another control set labelled “Sham” was taken to the irradiation facility along with the other cells to be irradiated, except the “Sham” set was not subjected to any dose. This was to mimic the conditions of the irradiated flasks during the time they were out of the incubator for the experiment. In total there were three flasks per set, resulting in n=12 or n=9 flasks per set in total, as the experiment was independently repeated 3 times. Adaptive Response and 2Gy irradiated

controls were repeated 4 times resulting in n=12 flasks per set in total.

The flasks that were irradiated were each were labelled corresponding to their subjected radiation: 2Gy for a single 2Gy dose, AR for an adaptive response test (0.1Gy priming dose – 5 hour incubation wait – 2Gy challenging dose), and PC for a post-conditioning test (2Gy – 5 hour incubation wait – 0.1 Gy dose). It should be noted that the adaptive response set of flasks were also acting as a positive control because these human colon adenocarcinoma cells have been shown before to exhibit an adaptive response at the challenge dose range (Ryan *et al.* 2009). Additionally, it was shown from the previous published work that the microcolonies were scored during the 5 hours of wait period between dose administrations to make sure that cells did not divide during this period. The 2Gy control was irradiated after the 5 hour wait period together with the adaptive response positive control. After radiation treatment, flasks were placed in an incubator in the next room to the irradiation unit, to limit temperature fluctuation. During this 5 hour wait time the cells were kept in 37°C without CO<sub>2</sub>. Once the second radiation treatment was complete all flasks were carried back to the main incubator at 37°C in with 5% CO<sub>2</sub> and 95% relative humidity.

All colonies were stained with CarbolFuschin (Ricca Chemical Company, Alington,

TX) and scored after cell cultures were incubated for 9 days for the HCT line and 10 days for the HT29 cell line in conditions previously described. Cell colonies were inspected under the microscope and a few were marked on the flask as a reference to determine whether a colony on the flask exceeded 50 cells. The marked colonies were used as a reference and all colonies exceeding 50 cells were scored as representing surviving cells.

### **Statistical Analysis**

Data are presented for three independent experiments containing triplicate flasks per group, and either three or four trials (n=12 & n=9 for post-conditioning treatments). The data are characterized as the mean of the 12 or 9 flasks normalized to a mean plating efficiency, which was calculated by using the plating efficiencies of the 0 Gy controls of the experiments and averaged. The errors for these data are standard error of the mean for each individual result. An unpaired t-test using GraphPad Software was used to measure significance of the experiments. A confidence interval of 95% and  $p < 0.05$  were selected to be statistically conclusive of a difference between the treatment groups studied.

### **3.3 Results**

The HT29 Human Colon Colorectal Adenocarcinoma cells were one of the cell lines used to test the effects of pre-/post-conditioning by using Cesium 137 irradiation at a dose rate of  $\sim 0.23$  Gy/min. The first radiation dose was administered

~24 hours after seeding the cells in experimental flasks. The doses were given as 0.1Gy for the priming dose and 2Gy or 5Gy for the challenge dose. After the first dose of radiation was administered, the flasks were immediately placed in the incubator for 5 hours before the second dose. The control flasks, stand-alone 2Gy or 5Gy treatments, had doses administered at the time when all first doses were administered after 24 hours. This is in the form: 2Gy-5h-0Gy, or 5Gy-5h-0Gy, for explicit notation. Results were scored as n=9, three replicates per experiment as three independent experimental trials, and revealed in **Figure 7**.

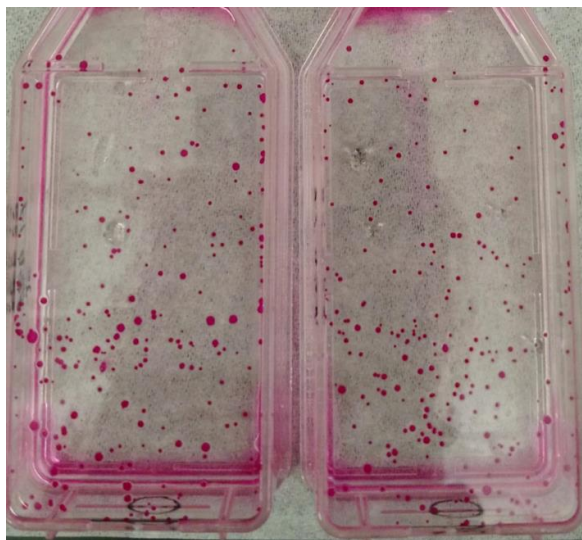


**Figure 6: HT29 Clonogenic Assay of Control Plating Efficiency after Staining**

### **3.3 Results from HT29 Cell Line Pre-/Post-Conditioning Trials**

The results suggest that there was non-significant pre- and post-conditioning adaptation leading to enhanced cell survival upon 2 Gy challenge doses. The higher

clonogenic survival was independent of whether the 2Gy challenge dose was given (preceding or following the 0.1Gy priming dose). The results show that similar non-significant enhanced survival is observed for both pre- and post-conditioning treatments compared to the control.

For the 5Gy treatments, pre-conditioning led to a significant ( $p < 0.05$ ) enhanced survival of cells, compared to the 5Gy control alone (5Gy-5hr-0Gy). The post-conditioning treatment led to a non-significant small enhancement of survival, compared to the stand-alone 5Gy treatment alone (5Gy-5h-0Gy). When comparing pre-conditioning to post-conditioning, the pre-conditioning treatment had a larger significant effect compared to the post-conditioning treatment.

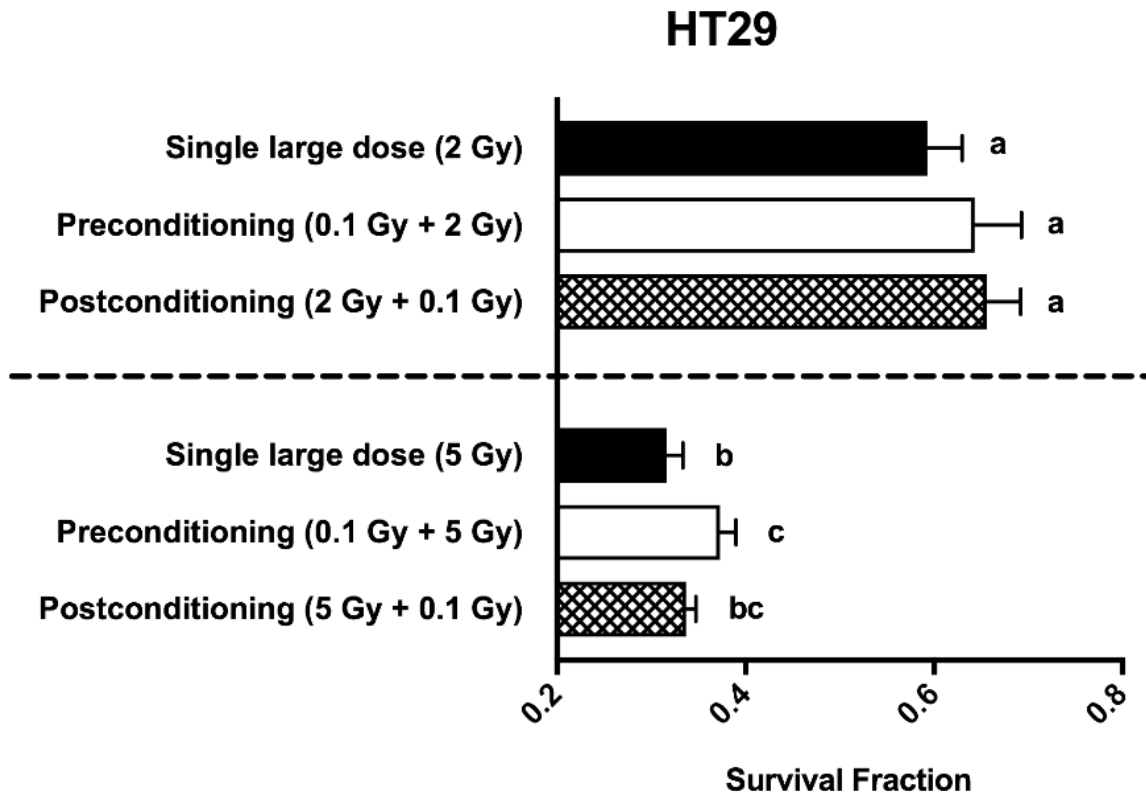


Figure 7: Summary of experimental results for pre-/post-conditioning of HT29 cell line, n=9.

Letters a, b, and c indicate statistical significance; a significant difference between any group within the given 2Gy or 5Gy experiment will be indicated by separate letters.

### 3.4 Discussion

There has been extensive research looking at the effects of low doses of radiation on mammalian specimens. Much of the research in this field has been to show of the varying degrees that low doses can impact the survival of living systems (Wolff et al 1988, Mothersill et al 2002, Mothersill et al 2016). There is an abundance of data showing that

that low doses of radiation can stimulate protective effects in vivo and in vitro (Boreham et al 2015, Ryan et al 2007, Mothersill et al 2018, Wolff et al 1988). There has also recently been research uncovering the mechanisms of the adaptive response in cancerous versus normal cells (Cai et al. 2016). Their research shows that the ataxia telangiectasia mutated (ATM) pathway increased CDK4/CDK6/cyclin D1 expression through AKT/ GSK-3 $\beta$ , as well as the nuclear accumulation of Nrf2 which ultimately led to an increase in antioxidant levels and subsequent damage reduction. This is because of the well-known connection that radiation produces reactive oxygen species (ROS) (Mothersill et al. 2004). However, those effects from the pathways described were absent in the carcinoma line used in the study (Cai et al. 2016). Recently, some researchers have suggested that the gamma radiation induced adaptive response is due to concerted activation of transcription factors NF- $\kappa$ B and Nrf2 (Paraswani et al. 2018). The group similarly proposes that the function of ATM is involved, along with extracellular signal-regulated kinase (ERK) and NF- $\kappa$ B.

Previously, it was thought that hyper-radiosensitivity/increased-radioresistance (HRS/IRR) and the adaptive response result from the same underlying mechanism (Marples and Joiner 1995), and the earlier work done by our group showed a significant positive correlation between the adaptive response and the HRS/IRR (Ryan et al. 2007, Mothersill et al. 2002). Another group that had also used a glioblastoma cell line suggested the involvement of nitric oxide (NO) radicals which lead to the accumulation of NO synthase may be responsible for radioresistance (Matsumoto et al 2007). Interestingly, their model




suggested that the induced iNOS through the activation of Hdm2 suppressed the accumulation and activation of p53, and that based on the observations seen from their work, wild-type p53 response may be dampened by chronic irradiation followed by an acute radiation. Additionally, it was reported that NO radicals released from irradiated mutant p53 cells caused radioresistance in wild-type p53 (Matsumoto et al. 2000, Mastumoto et al. 2001). Even recently the role of p53 is being researched as a mechanism of mediating the radio-adaptive response in human tumors (Murley et. Al 2017).

For the post-conditioning response, it is possible that the effect shares repair mechanisms as that of the adaptive response. To our knowledge it is the first instance for these cell lines to exhibit a post-conditioning effect leading to increased survival. Though post-conditioning has been shown in other specimens, such as improving cancer morbidity in mice (Boreham et al. 2017). Again p53 status seems to be an important indicator of radio-adaptivity, and the phosphorylation of H2AX histones around DNA double-stranded breaks, forming  $\gamma$ -H2AX, during DNA repair may serve as a scaffold for more repair complexes (Boreham et al. 2017).

In these experiments, an evaluation of the cell survival for the human colon cancer (HT29) is shown after cells were treated with challenge doses ranging from 2Gy or 5Gy, preceded

or followed by either 0.1Gy priming doses from  $^{137}\text{Cs}$  gamma radiation. Adaptive and post-conditioning effects were observed in all cell lines used, with the strongest pre-conditioning effect for a treatment of 0.1Gy five hours before a 5Gy dose ( $p < 0.05$ ). Even though the HT29 cell line had demonstrated a post-conditioning effect at 2Gy, it did not reach a significant response in this study. However, it was observed that giving a small priming dose before or after a large dose generally had a beneficial effect for these cancer cell lines. The prominence of each effect could have implications when determining at which dose the cell line has significant adaptive effects and whether the mechanisms involving cellular adaptation are more similar than previously thought. Further studies looking at p53 status in more detail during post-conditioning treatments would prove to be a useful comparison to these data.

4 Parallel comparison of pre-conditioning and post-conditioning effects in human cancers and keratinocytes upon acute gamma irradiation



International Journal of Radiation Biology

Taylor & Francis  
Taylor & Francis Group

ISSN: 0955-3002 (Print) 1362-3095 (Online) Journal homepage: <https://www.tandfonline.com/loi/irab20>

---

**Parallel comparison of pre-conditioning and post-conditioning effects in human cancers and keratinocytes upon acute gamma irradiation**

Jason Cohen, Nguyen T. K. Vo, Colin B. Seymour & Carmel E. Mothersill

To cite this article: Jason Cohen, Nguyen T. K. Vo, Colin B. Seymour & Carmel E. Mothersill (2019) Parallel comparison of pre-conditioning and post-conditioning effects in human cancers and keratinocytes upon acute gamma irradiation, *International Journal of Radiation Biology*, 95:2, 170-178, DOI: [10.1080/09553002.2019.1547850](https://doi.org/10.1080/09553002.2019.1547850)

To link to this article: <https://doi.org/10.1080/09553002.2019.1547850>



Accepted author version posted online: 29 Nov 2018.  
Published online: 04 Jan 2019.

**Purpose:** To determine and compare the effects of pre-conditioning and post-conditioning towards gamma radiation responses in human cancer cells and keratinocytes.

**Material and methods:** The clonogenic survival of glioblastoma cells (T98G), keratinocytes (HaCaT), and colorectal carcinoma cells (HCT116 p53<sup>+/+</sup> and p53<sup>-/-</sup>) was assessed following gamma ray exposure from a Cs-137 source. The priming dose preceded the challenge dose in pre-conditioning whereas the priming dose followed the challenge dose in post-conditioning. The priming dose was either 5 mGy or 0.1Gy. The challenge dose was 0.5–5Gy.

**Results:** In both pre- and post-conditioning where the priming dose was 0.1Gy and the challenge dose was 4Gy, RAR developed in T98G but not in HaCaT cells. In HCT116 p53<sup>+/+</sup>, pre-conditioning had either no effect or a radiosensitizing effect and whereas post-conditioning induced either radiosensitizing or radioadaptive effect. The different observed outcomes were dependent on dose, the time interval between the priming and challenge dose, and the time before the first irradiation. Post-conditioning effects could occur with a priming dose as low as 5 mGy in HCT116 p53<sup>+/+</sup> cells. When HCT116 cells had no p53 protein expression, the radiosensitizing or radioadaptive response by the conditioning effect was abolished.

**Conclusions:** The results suggest that radiation conditioning responses are complex and depend on at least the following factors: the magnitude of priming/challenge dose, the time interval between priming and challenge dose, p53 status, cell seeding time prior to the first radiation treatment. This work is the first parallel comparison demonstrating the

potential outcomes of pre- and post-conditioning in different human cell types using environmentally and medically relevant radiation doses.

Keywords: Cancer, p53, pre-conditioning, post-conditioning, gamma radiation

PURPOSE: To determine and compare the effects of pre-conditioning and post-conditioning towards gamma radiation responses in human cancer cells and keratinocytes

MATERIALS AND METHODS: The clonogenic survival of glioblastoma cells (T98G), keratinocytes (HaCaT),

and colorectal carcinoma cells (HCT116 p53<sup>+/+</sup> and p53<sup>-/-</sup>) was assessed following gamma ray exposure from a Cs-137 source. The priming dose preceded the challenge dose in pre-conditioning whereas the priming dose followed the challenge dose in post-conditioning. The priming dose was either 5 mGy or 0.1 Gy. The challenge dose was 0.5 – 5 Gy.

RESULTS: In both pre- and post-conditioning where the priming dose was 0.1 Gy and the challenge dose

was 4 Gy, RAR developed in T98G but not in HaCaT cells. In HCT116 p53<sup>+/+</sup>, pre-conditioning had either no effect or a radiosensitizing effect and whereas post-conditioning induced either radiosensitizing or radioadaptive effect. The different

observed outcomes were dependent on dose, the time interval between the priming and challenge dose, and the time before the first irradiation. Post-conditioning effects could occur with a priming dose as low as 5 mGy in HCT116 p53<sup>+/+</sup> cells. When HCT116 cells had no p53 protein expression, the radiosensitizing or radioadaptive response by the conditioning effect was abolished.

CONCLUSIONS: The results suggest that radiation conditioning responses are complex and depend on at least the following factors: the magnitude of priming/challenge dose, the time interval between priming and challenge dose, p53 status, cell seeding time prior to the first radiation treatment. This work is the first parallel comparison demonstrating the potential outcomes of pre- and post-conditioning in different human cell types using environmentally and medically relevant radiation doses.

## INTRODUCTION

In biology and medicine, pre-conditioning refers to exposing organisms or cells to a large damage inducing dose of a stressor preceded by a smaller non-toxic dose of the same stressor whereas in postconditioning a large dose of the stressor is followed by a smaller dose (Calabrese et al., 2007). The conditioning effect is generally built upon the hormesis concept (Calabrese and Mattson, 2017). In principle, conditioning enables the activation or enhancement of protective programs and therefore helps reduce the

damaging effect caused by the stressor (Calabrese et al., 2007; Calabrese and Mattson, 2017). The conditioning effect is perhaps best studied in vascular biology. Ischemic conditioning contributes to cardioprotection by reducing oxidative stress and thus minimizing or preventing myocardial infarction (Aimo et al., 2015).

The concept of pre-conditioning also applies to radiation biology where radiation is the stressor. Radiation pre-conditioning describes the irradiation of subjects to a large damage-causing dose after a smaller dose (known as priming dose), subsequently leading to a more radio-resistant phenotype (Wolff 1998). Olivieri et al. (1984) were the first group to report the protective effect of radiation preconditioning in human lymphocytes exposed to low-dose radioactive thymidine. Radiation preconditioning, now widely known as “radioadaptive response” (RAR), is observed with different types of radiation and in many biological systems (Azzam et al., 1994; de Toledo et al., 2006; Maguire et al., 2007; Ryan et al., 2008; 2009; Day et al., 2006; Smith and Raaphorst, 2003; Audette-Stuart and Yankovich, 2011; Tang et al., 2016; Vo et al., 2017a; Smith et al., 2011). In cancer onset, radiation preconditioning can extend the latent period (Lemon et al., 2017b). The protective effect can occur with the priming dose of as low as 0.001 mGy (Day et al., 2006). The mechanism governing radiation pre-conditioning or RAR appears to be evolutionarily conserved (Calabrese and Mattson, 2017). As life evolved with radiation for millions of years, this concept largely contributes to the big picture of adaptation, longevity, and evolution of biological entities living in environments with low radioactivity as well as their interactions with other bystander participants within the ecosystem. In

medicine, cancer patients are subjected to diagnostic imaging procedures (low dose exposure) prior to an actual therapeutic radiation regimen (high dose exposure). Thus the pre-conditioning-induced radio-resistance may reduce the effectiveness of the intended radiation therapy program.

Radiation post-conditioning, on the contrary, is the procedure of irradiating subjects with a large dose before a very small priming dose. To date, the literature on radiation post-conditioning is relatively small with significantly fewer studies (Day et al., 2007; Lemon et al., 2017a; Lin and Wu, 2015). In general, radiation post-conditioning exerts a similar RAR-like effect as seen in pre-conditioning (Day et al. 2007; Lemon et al., 2017a). The protective effects of radiation post-conditioning include enhanced protection against chromosomal damage (Day et al., 2007) and increased lifespan (Lemon et al., 2017a). The lowest priming dose inducing a RAR in radiation post-conditioning recorded to date was 0.01 mGy (Day et al., 2007). Currently, how comparable the extent of radioprotection is between preconditioning and post-conditioning is not well understood. We previously observed that a smaller dose preceding a large dose had a less damaging effect than the reverse order (Mothersill and Seymour, 1993), suggesting that different mechanisms might underlie low and high dose response and that irrespective of the order of delivery both mechanisms were activated by experience of different doses. The data also suggested immediate and delayed death levels involved different mechanisms. Lin and Wu (2015) later showed that differences in effects were cell type- and species-dependent in a complex multi-dose fractionated radiation setup.



Interestingly, in one of their two-dose experiments with a human colon cancer cell line HT-29, post-conditioning had a more protective effect than preconditioning.

Increasing evidence has suggested that there are a number of factors that are associated with or directly involved in RAR, especially in the context of low-dose radiobiology. Nitric oxide radicals and other reactive oxygen species are key players mediating the RAR (Matsumoto et al. 2007; Miller et al., 2016; Murley et al., 2017; 2018). More interestingly, factors in the irradiated cell conditioned medium can alleviate some of the damages caused by high dose in bystander cells (Maguire et al., 2007; Matsumoto et al., 2000; 2001). Cells that can develop RAR also have traits of hyper-radiosensitivity/increased radioresistance (HRS/IRS) (Ryan et al. 2009). Additionally, the tumour suppressor p53 protein is important in regulating RAR. While p53 regulates apoptosis in low-dose radiation hypersensitivity (Enns et al., 2004), its expression is suppressed during RAR (Takahashi, 2001), which would be consistent with the protective survival mechanism although sparing potentially damaged cells may have a role in postradiotherapy tumour recurrence. However, in p53-null or -mutant cells, priming cells with a lower dose before a larger challenge dose makes cells more radiosensitive (the complete opposite to the traditional RAR) (Miller et al., 2016; Murley et al., 2017; 2018). A lot of this knowledge has been gained from the radiation pre-conditioning perspective. Yet nothing is known regarding the other conditioning view, i.e. radiation post-conditioning. Most recent research by our group has evidence suggesting that

postconditioning effects can occur on a quantum biological level (Mothersill et al., 2018), possibly via UV biophoton-mediated mechanisms (Le et al., 2017a).

This current paper shows possible outcomes associated with radiation pre-conditioning and postconditioning effects in different human cell types.

## MATERIALS AND METHODS

### Cell Cultures

Four human cell lines were used in this study. They were two colorectal cancer lines HCT116 p53<sup>+/+</sup> and HCT116 p53<sup>-/-</sup>, one brain glioblastoma multiforme cell line T98G, and one spontaneously immortalized untransformed keratinocyte cell line HaCaT.

HCT116 p53<sup>+/+</sup> had wild-type TP53 gene and (Brattain et al., 1981; Popanda et al., 2000).

HCT116 p53<sup>-/-</sup> had both TP53 alleles inactivated via the homologous recombination technology (Bunz et al., 1998) and therefore expressed no p53 protein as confirmed by our group (Mothersill et al., 2011; Le et al., 2017b). HCT116 p53<sup>+/+</sup> was HRS-positive and HCT116 p53<sup>-/-</sup> was HRS-negative (Enns et al., 2004). The cell lines were cultured in the Roswell Park Memorial Institute (RPMI)-1640 medium supplemented with 10% fetal bovine serum (FBS), 2 mM L-glutamine, 25 mM HEPES, 100 U/ml penicillin, and 100 µg/ml streptomycin. All tissue culture reagents were obtained from Gibco/Life Technologies (Grand Island, NY), unless otherwise specified. Both cell lines were provided by Dr. Robert Bristow (University Health Network, University of Toronto, Toronto, ON).

T98G had a p53 mutant with a single-nucleotide variant leading to an amino acid switch from Met to Ile at codon 237 (Van Meir et al., 1994). T98G displayed HRS (Short et al 1999). T98G was routinely maintained in the Dulbecco's modified Eagle medium F12 (DMEM/F12), 10% FBS, 2 mM L-glutamine, 25 mM HEPES, 100 U/ml penicillin, and 100 µg/ml streptomycin. The cell line was provided by Dr. Brian Marples (Department of Radiation Oncology, William Beaumont Hospital, Royal Oak, MI).

HaCaT had a mutated p53 gene with two heterozygous mutations: one with a single-nucleotide variant leading to an amino acid switch from His to Tyr at codon 179 and the second with a double-nucleotide variant leading to an amino acid switch at codon 282 (Lehman et al., 1993). HaCaT displayed no HRS (Ryan et al., 2009). The growth medium for HaCaT was the same growth medium used for HCT116 cells with the addition of 1000 ng/mL cortisol. The HaCaT cell line was kindly provided by Dr. Petro Boukamp (German Cancer Research Center, Heidelberg, Germany).

All cell lines were grown at 37°C in an atmospheric environment equilibrated at 5% CO<sub>2</sub> and 95% air. Subculturing was performed with trypsin/EDTA as previously described by our group (Vo et al. (2017b) for HCT116 p53<sup>+/+</sup> and Fernandez-Palomo et al. (2016) for T98G and HaCaT).

Challenge Irradiation and Clonogenic Assay Technique

The cell survival of the control and the irradiated groups was assessed using the clonogenic assay technique developed by Puck and Marcus (1956). Briefly, adherent cells were detached from the tissue culture surface and dissociated into single cells by trypsin/EDTA along with excessive pipetting. Cell concentrations were determined using a BioRad T20 Automated Cell Counter. In T25 tissue culture flasks (BD Falcon), depending on the plating efficiency of the cell lines and the magnitude of the lethal dose, cultured cells were seeded at densities of 20-60 cells/cm<sup>2</sup>.

Depending on the cell lines, cells were seeded in triplicate flasks for 6h or 24h prior to irradiation challenge. Two non-irradiated controls were used. The first control group, regarded as “0 Gy control” was kept at all times in the incubator. The second control group, regarded as “sham-control” (to control for unknown variations imposed by temperature, transport, and background radiation), was brought to the irradiation facility and was subjected to zero radiation dose. Irradiated flasks were subjected to a first radiation dose, incubated at 37 for 3-5h, challenged again for a second dose, and finally returned to the 37 incubator (as illustrated in Figure 1). All flasks were left undisturbed for 9 or 10 days and cell colony survivors (having at least 50 cells) were stained with Carbol Fuschin (Ricca Chemical Company, Alington, TX) and scored. The gamma radiation source was 1 kCi <sup>137</sup>Cs housed in the Taylor Radiation Source (TRS) suite at McMaster University (Hamilton, ON). Irradiated flasks were 27.1 cm away from the radiation source for the dose rate of 260 mGy/min. Thermoluminescent dosimeters were

used to measure radiation doses and to ensure the uniformity of the radiation dose delivery. Three independent experiments were performed.

The schemes for the pre-conditioning and post-conditioning response experiments are shown in Figure 1. For the pre-conditioning experiments, the first dose was a small dose (5 mGy or 0.1 Gy) and the second dose was a large dose (0.5-5 Gy). For the postconditioning response experiments, the first dose was a large dose (0.5-5 Gy) and the second dose was a small dose (5 mGy or 0.1 Gy). The small dose of 0.1 Gy was used for all four cell lines while the small dose of 5 mGy was used only for HCT116 p53<sup>+/+</sup> because (1) the wild-type p53, but not mutant p53, can facilitate RAR (Miller et al., 2016; Murley et al., 2018) and (2) 5 mGy was previously shown to be effective to induce RAR in the HCT116 p53<sup>+/+</sup> cells (Murley et al., 2017).

#### Statistical Analysis

Data are presented mean of clonogenic survival fraction  $\pm$  SEM (n=9 or n=12). A one-way ANOVA with Tukey's post test and a confidence interval of 95% or a student's t-test was used to determine statistical significance via the GraphPad Prism software.  $p < 0.05$  were deemed statistically significant.

## RESULTS

### Effects of radiation pre- and post-conditioning in the human glioblastoma cell line T98G

The clonogenic survival was statistically significantly higher in both pre- and post-conditioning than in the no priming dose control (Figure 2). Pre-conditioning and post-conditioning resulted in 7.3 % and 5.3 % increases in clonogenic survival. Therefore, both pre- and post-conditioning induced the RAR in T98G. There was, however, no significant difference in clonogenic survival between pre- and postconditioning was observed (Figure 2).

### Effects of radiation pre- and post-conditioning in the human normal keratinocyte cell line

#### HaCaT

The clonogenic survival in pre-conditioning was slightly higher than that of the no priming dose control (Figure 3). In contrast, the clonogenic survival in post-conditioning was slightly lower than that of the no priming dose control (Figure 3). But both cases had no statistical significance. Therefore, no RAR was observed in both pre- and post-conditioning in the HaCaT cells. However, the pre-conditioning clonogenic survival was significantly higher than the post-conditioning clonogenic survival (Figure 3).

Effects of radiation pre- and post-conditioning in the human colon cancer cell line HCT116 p53<sup>+/+</sup>

When the priming dose was 0.1 Gy, the pre-conditioning clonogenic survival was similar to that of the no priming dose control at all three challenge doses (2, 3, and 4) (Figure 4). On the other hand, the post-conditioning clonogenic survival was significantly lower than those in the control and preconditioning at the 2 and 3 Gy challenge doses but not at the 4 Gy challenge dose (Figure 4). Therefore, pre-conditioning did not induce RAR while post-conditioning induced radiosensitization effects in HCT116 p53<sup>+/+</sup>.

To further see if RAR could be achieved in the HCT116 p53<sup>+/+</sup> cells at more environmentally relevant doses, the priming dose was chosen to be 5 mGy while the larger challenge dose was 0.5 Gy. In the pre-conditioning, the clonogenic survival was higher (an 5.2 % increase) but not statistically significant than that of the no priming dose control (Figure 5). In the post-conditioning, the clonogenic survival was significantly higher (an 8.4 % increase) than the no priming dose control (Figure 5). However, there was no difference in the clonogenic survival between the pre- and post-conditioning (Figure 5).

When HCT116 p53<sup>+/+</sup> cells were seeded for 24 h and then followed the radiation conditioning and exposure regimen where the time interval between the 0.1 Gy priming dose and the larger challenge dose was extended to 5 h (instead of 3 h in previous experiments), an interesting result was obtained. The no priming dose control for the

pre-conditioning (0.1Gy-5h-2Gy) was shown as “0Gy-5h-2Gy” and the no priming dose control for the post-conditioning (2Gy-5h-0.1Gy) was shown as “2Gy-5h-0Gy”. Surprisingly, the clonogenic survival of the no priming dose control for the pre-conditioning was significantly higher than that of the no priming dose control for the pre-conditioning (Figure 6). The pre-conditioning clonogenic survival was significantly lower than its no priming dose counterpart whereas the post-conditioning clonogenic survival was significantly higher than its no priming dose counterpart (Figure 6). Therefore, under these experimental conditions, pre-conditioning sensitized radiation responses whereas post-conditioning induced RAR in HCT116 p53<sup>+/+</sup> cells. When the TP53 gene coding p53 protein was knocked out in HCT116 p53<sup>+/+</sup> cells (as in the resulting HCT p53<sup>-/-</sup> subclone), the clonogenic survival was the same in pre- and post-conditioning as well as in their no priming dose control counterparts (Figure 7A); thus the observed radiosensitization/adaptive effect was abolished. This was also true when the challenge dose increased to 5 Gy (Figure 7B). This clearly shows that p53 regulated the mechanisms that led to the radiosensitization in pre-conditioning and RAR in post-conditioning in HCT116 p53<sup>+/+</sup> cells in response to high-dose radiation.

When the priming dose was lowered to 5 mGy and the challenge dose remained to be 2 Gy, the degree of radiosensitization by pre-conditioning was greatly reduced whereas the degree of RAR by post-conditioning was greatly enhanced in HCT116 p53<sup>+/+</sup> cells (Figure 8). Interestingly, when comparing “2Gy+5h+0.1Gy” (Figure 6) to “2Gy+5h+0.005Gy”



(Figure 8) in post-conditioning, the clonogenic survival was significantly higher ( $p < 0.05$ , student's t-test) when cells were primed with 5 mGy than with 0.1 Gy.

This shows that 5 mGy was a more effective priming dose than 0.1 Gy in inducing post-conditioning RAR in HCT116 p53<sup>+/+</sup> cells. Collectively, the data suggest that the magnitude of the priming dose was also important in dictating the cells' radiation response outcomes.

Correlation data between pre-/post-conditioning treatments on cell lines

For each experimental trial, cell survival from the pre-conditioning treatment was compared with the post-conditioning treatment (same priming and large challenge dose, just in reverse order) against the standard large-dose only control. The data were then plotted in Figure 9 as a difference in survival fraction between pre-/post-conditioning where the changes in survival fraction per experiment could be observed. A Pearson's Correlation Coefficient was calculated using the 2 arrays of difference in survival fraction from pre-conditioning and difference in survival fraction from post-conditioning per experimental trial, resulting in a parallel comparison between the strength of pre-conditioning and that of post-conditioning on the cells. A positive correlation of  $r = 0.86$  was found which suggests that as there is an increase in the effects from a pre-conditioning treatment, there is similarly an increase of similar magnitude in the effects

on survival fraction from post-conditioning treatment within the same trial. The data for the correlation holds the time prior to first radiation treatment constant at 6h to constrain parameters and keep experimental conditions consistent.

Overall, our results show that radiation conditioning responses are complex and depend on at least the following factors: the magnitude of priming/challenge dose, the time interval between priming and challenge dose, p53 status, cell seeding time prior to the first radiation treatment.

## DISCUSSION

The current study presents a unique parallel comparison between pre-conditioning and postconditioning in different human cell types in response to gamma radiation. As radiation preconditioning had already been well established to exert an adaptive response, a particular focus in this work was to determine the consequence of post-conditioning and compare to that of pre-conditioning. The priming (smaller) and challenge (larger) doses were the same in both conditioning methods; the only difference was the opposite delivery order of the doses to delineate pre- and post-conditioning principles.

In the glioblastoma T98G cells, the observed RAR in pre-conditioning in the current work agreed with what Ryan et al. reported in 2009 using Cobalt-60 as the gamma source. The current study showed, for the first time, that the RAR could develop in glioblastoma cells when the priming dose was introduced after a large challenge dose in post-conditioning. Similar levels of increase in clonogenic survival in pre- and post-conditioning in T98G suggests that a common cellular mechanism is very likely involved in inducing protective effects induced by both conditioning methods. In general, the protective effect a result of post-conditioning was consistent with the conclusions in mouse studies by Day et al. (2007) and Lemon et al. (2017a).

In the normal keratinocyte HaCaT cells, no RAR was observed in both pre- and post-conditioning. The inability of HaCaT cells to develop an RAR in pre-conditioning also agreed with Ryan et al. (2009). The concurrent lack of RAR in both pre- and post-conditioning, in contrast to T98G, also suggests that a common cellular mechanism driving RAR may be absent in HaCaT cells. The observed differential outcomes perhaps mirror some of the results by Liu and Wu (2015). In one instance, these authors found that post-conditioning had no effect in the hamster lung fibroblast V79S cell line but had a protective effect in the human intestinal carcinoma HT-29 cell line.

In the colorectal carcinoma HCT116 p53<sup>+/+</sup> cells, cellular responses after pre- and post-conditioning were complex. No RAR was observed in pre-conditioning at either the priming dose of 5 mGy or 0.1 Gy. This result was surprising because (1) cells displaying

the HRS/IRR trait could develop RAR (Ryan et al., 2009) and HCT116 p53<sup>+/+</sup> had HRS characteristics (Enns et al., 2004), and (2) 5 mGy had been shown to be effective in inducing pre-conditioning RAR in HCT116 p53<sup>+/+</sup> recently by Murley et al. (2017). As Murley et al. (2017) used a high dose rate while the lower dose rate was used in this study, dose rate may be a differentiating factor in eliciting the RAR induction. In the present study, a protective effect was observed in post-conditioning at both priming doses of 5 mGy or 0.1 Gy. In contrast to how T98G and HaCaT cells responded to radiation conditioning, HCT11 p53<sup>+/+</sup> did not develop RAR in preconditioning but did develop RAR in post-conditioning.

The noted difference between the “0Gy+5h+2Gy” and “2Gy+5h+0Gy” clonogenic survival was a surprising observation. The “0Gy+5h+2Gy” flasks were at 29 h post seeding prior to irradiation and the “2Gy+5h+0Gy” clonogenic flask were at 24 h post seeding prior to irradiation. It is possible that there were more cells that doubled at 29 h than those at 24 h. Therefore, we performed two additional experiments to see if this was a possible reason. In the first experiment, we seeded 1 million cells in T25 flasks and counted the total cell numbers in the flasks 24 or 29 h post seeding. We found that the cell numbers at 24 and 29 h were statistically indifferent from each other (Figure S1). As the cell status can be influenced under an extremely low-cell-density environment, in the second experiment we seeded cells at the clonogenic cell density in T25 flasks, stained the flasks with the fuchsin carbol dye 24 or 29 h post seeding, and microscopically scored the number of singlets (single cells) and doublets (cells that already doubled). We found

that the singlet percent was the same at 24 and 29 h and the doublet percent was also the same at 24 h and 29 h (Figure S2). Therefore, observed differences in the clonogenic survival cannot be explained by the unmatched percentages of cells that have or have not divided at 24 h and 29 h. It remains possible that the observed differences could be attributable to a cell synchronization effect. However, while the 2Gy dose could arrest cells, as long as the pre- or postconditioning flasks are assessed relative to the correct control (24 or 29 hrs), this should not be an issue. It could however provide an explanation for a post-conditioning protective effect if the cell synchronisation led to more cells being in a radioresistant cell cycle phase at the time the conditioning dose was applied. Since the conditioning dose is very small it is unlikely to cause the effect seen but the possibility is presented here for consideration. We consider it more likely that parallel processes are induced by small and large doses and that the precise order of administration of the high and low doses are less important than the absolute fact of two-dose administration. On the other hand, differences seen in cells seeded 6 h or 24 h before irradiation could be due to cell cycle arrest, synchronization or “lag” after trypsinization.

T98G and HaCaT have a mutant p53 whereas HCT116 p53<sup>+/+</sup> cells have a wild-type p53 and the different p53 status could influence the outcome of RAR. Indeed, Miller et al. (2016) and Marley et al. (2017; 2018) tested a collection of mammalian cell lines with different p53 status and found that wild-type p53 cells (including HCT116 p53<sup>+/+</sup>) developed RAR whereas mutant or null p53 cells developed a radiosensitive response

instead. In the current study, we also found that HCT116 p53<sup>+/+</sup> with a wild-type p53 developed RAR with the priming dose of 5 mGy as well as 0.1 Gy. We also found that when cells (HCT116 p53<sup>-/-</sup>) had no p53 expression, RAR disappeared but was not replaced with a radiosensitizing response as previously reported by Miller et al. (2016) and Marley et al. (2017; 2018). On the other hand, in contrast to those authors' work, T98G and HaCaT with a mutant p53 also did not develop radiosensitizing response. In T98G cells, p53 has a Met237 mutation (Van Meir et al., 1994) and has no functional activities (Schmidt et al., 2001). HaCaT has His179 and Arg282 mutations (Lehman et al., 1993) and has partial functions. Arg282 is one of the hotspot mutations and frequently mutated in many cancers (Kamaraj and Bogaerts, 2015). Arg282 mutation has been shown to acquire a gain of function (Zhang et al., 2016) and is attributable to an alternative radio-responsive apoptosis pathway in HaCaT cells (Henseleit et al., 1997). The likely contribution of different p53 mutations to the different responses of cells to low-dose biophoton radiation was recently linked by Le et al. (2017b). Our results suggest that there are other factors besides p53 that regulate RAR.

The mutual relationship between HRS/IRR and RAR phenomena has been previously implicated (Marples and Joiner 1995; Ryan et al., 2009). T98G and HCT116 p53<sup>+/+</sup> were HRS/IRR-positive (Short et al 1999; Enns et al., 2004) and developed RAR whereas HaCaT and HCT116 p53<sup>-/-</sup> were HRS/IRR-negative (Enns et al., 2004; Ryan et al., 2009) and did not develop RAR. Although common molecular players that participate in the orchestration of mechanisms that enable HRS/IRR and RAR are not known, our data in

this work further corroborated the previous notion that both phenomena may share some interconnected biochemical pathways activated by low-dose radiation.

The most surprising finding in the current study was with HCT116 p53<sup>+/+</sup>. Pre-conditioning had either no effect or radiosensitizing effect while post-conditioning could induce both radiosensitizing and radioresistant traits and the difference in outcomes was due to how the conditioning conditions were formulated. Our results have implications in clinical oncology where diagnostic imaging doses may present a potential challenge affecting the treatment outcome for cancers with HRS/IRR traits as well as in health physics concerning occupationally exposed nuclear workers or bystander residents living in radioactive-contaminated areas.

#### ACKNOWLEDGEMENTS

The authors acknowledge support from the Canada Research Chairs program, the Natural Sciences and Engineering Research Council (NSERC) Collaborative Research and Development program and NSERC Discovery Grants program, the National CFIDS (Chronic Fatigue and Immune Deficiency Syndrome) Foundation Inc, Bruce Power and the CANDU Owner's Group (COG). The authors kindly acknowledge Scott McMaster (McMaster University) for assistance with the use of the irradiation facility as well as dose uniformity

analysis. The authors also acknowledge Dr. Cristian Fernandez-Palomo for his cultivation of T98G and passing this line to us.

#### DECLARATION OF INTEREST

The authors declare no conflict of interest.



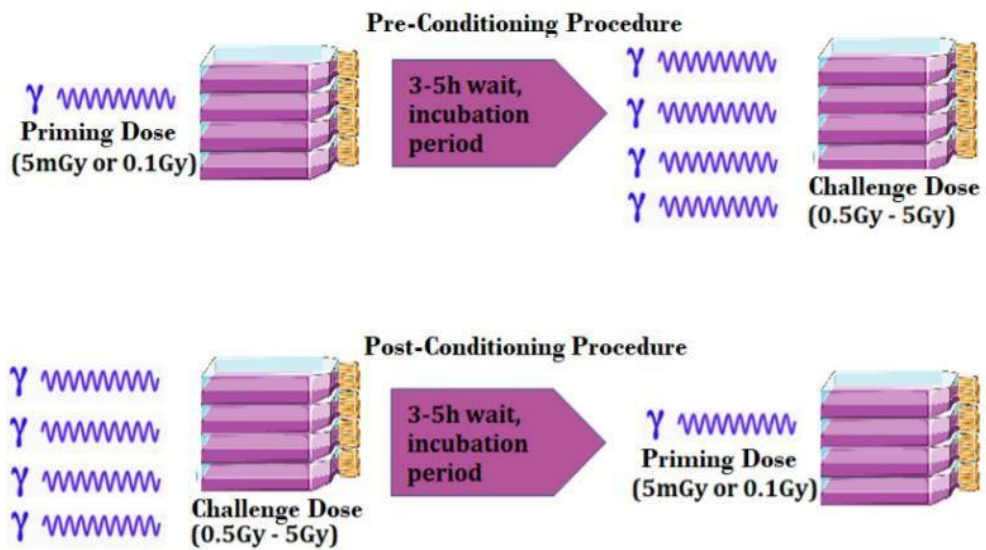


Figure 1: Scheme of the experiments. For both pre-conditioning and post-conditioning treatments, 20-60 cells/cm<sup>2</sup> were seeded in triplicate T25 clonogenic flasks. The priming doses were smaller doses and either 5mGy or 0.1 Gy. The challenge doses were larger doses and 0.5-5 Gy. In pre-conditioning, the priming dose preceded the challenge dose. In post-conditioning, the challenge dose preceded the priming dose.

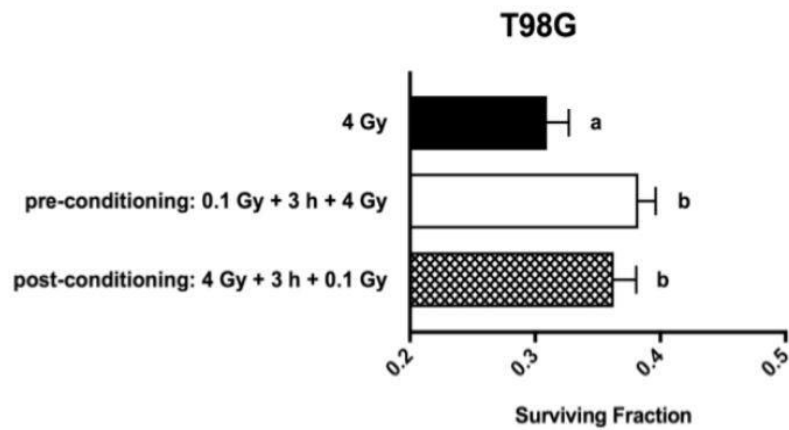


Figure 2. Effects of pre-conditioning and post-conditioning on the clonogenic survival of the human glioblastoma T98G cell line. Irradiation was performed 6 h after seeding cells at 40 cells/cm<sup>2</sup> in triplicate T25 flasks. The priming dose was 0.1 Gy and the challenge dose was 4 Gy. The time interval between the priming and challenge dose was 3 h. The data are shown as survival fraction  $\pm$  SEM (n=9) per treatment group. Based on the one-way ANOVA with Tukey's post-test, groups with different letters are statistically significant ( $p < 0.05$ ) and groups sharing the same letter are not.

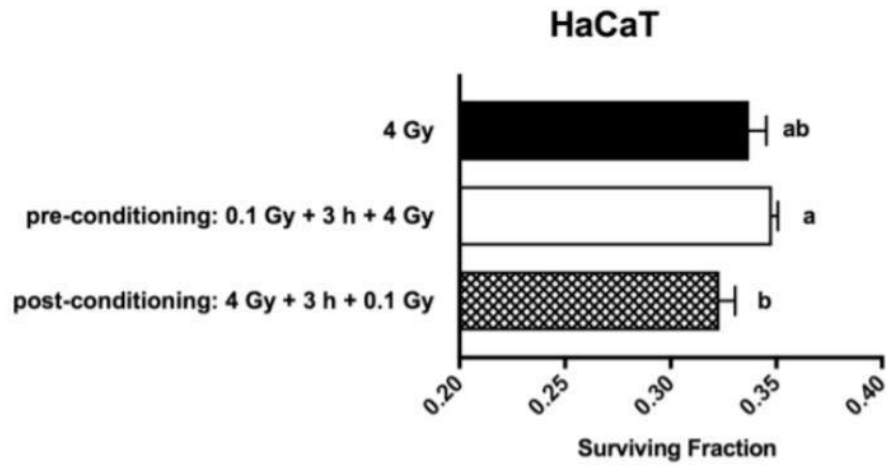


Figure 3. Effects of pre-conditioning and post-conditioning on the clonogenic survival of the normal human keratinocyte HaCaT cell line. Irradiation was performed 6 h after seeding 36 cells/cm<sup>2</sup> in triplicate T25 flasks. The priming dose was 0.1 Gy and the challenge dose was 4 Gy. The time interval between the priming and challenge dose was 3 h. The data are shown as survival fraction  $\pm$  SEM (n=9) per treatment group. Based on the one-way ANOVA with Tukey's post-test, groups with different letters are statistically significant ( $p < 0.05$ ) and groups sharing the same letter are not.

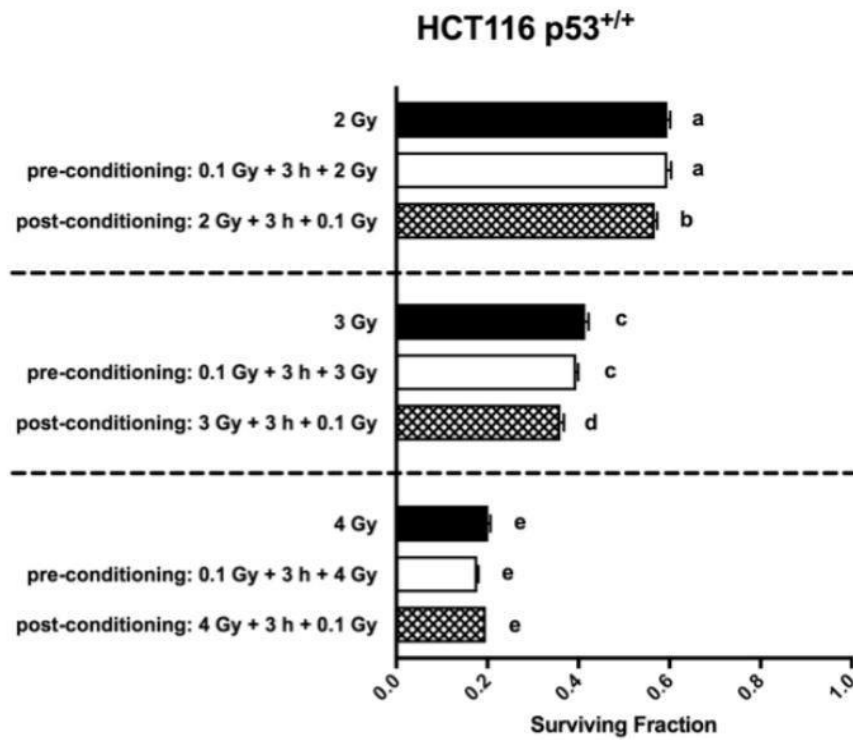


Figure 4. Effects of pre-conditioning and post-conditioning on the clonogenic survival of the human colorectal carcinoma HCT116 p53<sup>+/+</sup> cell line. Irradiation was performed 6 h after seeding 40 cells/cm<sup>2</sup> in triplicate T25 flasks. The priming dose was 0.1 Gy and the challenge dose was 2, 3 or 4 Gy. The time interval between the priming and challenge dose was 3 h. The data are shown as survival fraction  $\pm$  SEM (n=9) per treatment group. Based on the one-way ANOVA with Tukey's post-test, groups with different letters are statistically significant ( $p < 0.05$ ) and groups sharing the same letter are not.

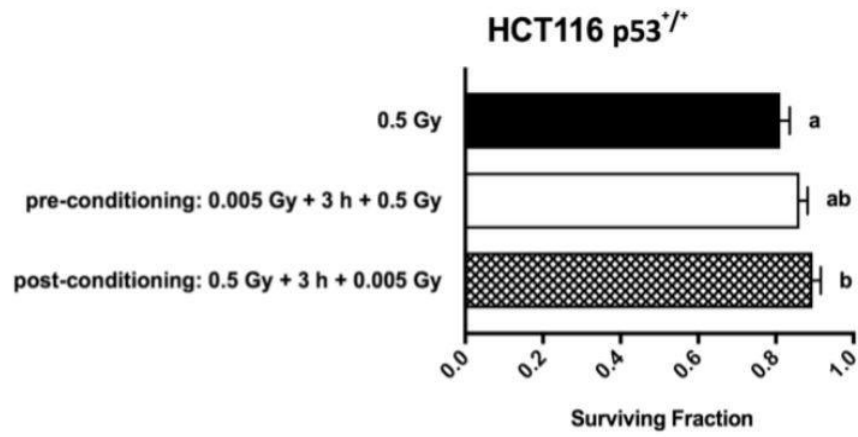


Figure 5. Effects of very low-dose radiation pre-conditioning and post-conditioning on the clonogenic survival of the human colorectal carcinoma HCT116 p53<sup>+/+</sup> cell line. Irradiation was performed 6 h after seeding 40 cells/cm<sup>2</sup> in triplicate T25 flasks. The priming dose was 5 mGy and the challenge dose was 0.5 Gy. The time interval between the priming and challenge dose was 3 h. The data are shown as survival fraction  $\pm$  SEM (n=9) per treatment group. Based on the one-way ANOVA with Tukey's post-test, groups with different letters are statistically significant ( $p < 0.05$ ) and groups sharing the same letter are not.

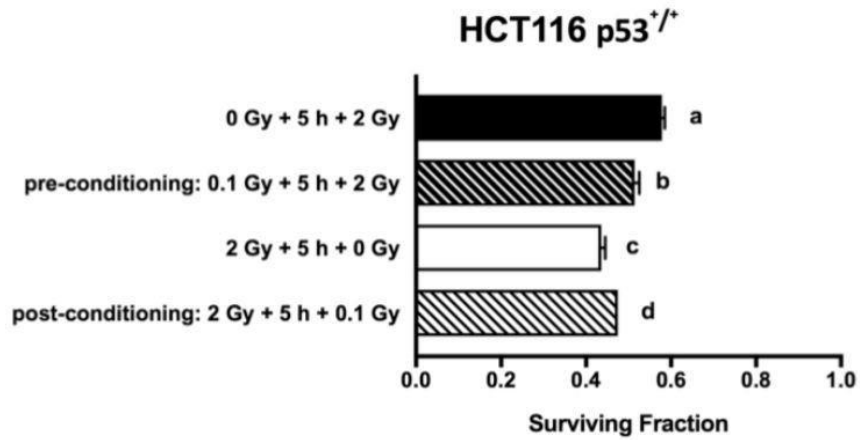


Figure 6. Effects of varied conditions of pre-conditioning and post-conditioning on the clonogenic survival of the human colorectal carcinoma HCT116 p53+/+ cell line. Irradiation was performed 24 h after seeding 20 cells/cm<sup>2</sup> in triplicate T25 flasks. The priming dose was 0.1 Gy and the challenge dose was 2 Gy. The time interval between the priming and challenge dose was 5 h. The data are shown as survival fraction  $\pm$  SEM (n=12) per treatment group. Based on the one-way ANOVA with Tukey's post-test, groups with different letters are statistically significant ( $p < 0.05$ ) and groups sharing the same letter are not.

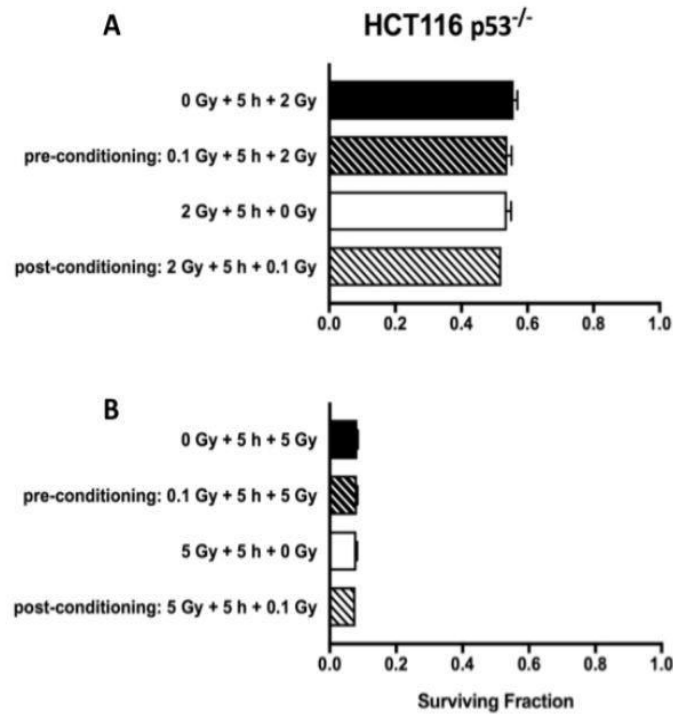


Figure 7. Effects of varied conditions of pre-conditioning and post-conditioning on the clonogenic survival of the human colorectal carcinoma HCT116 p53<sup>-/-</sup> cell line. Irradiation was performed 24 h after seeding 20 cells/cm<sup>2</sup> (for 2-Gy irradiation challenge) or 60 cells/cm<sup>2</sup> (for 4-Gy irradiation challenge) in triplicate T25 flasks. The priming dose was 0.1 Gy and the challenge dose was 2 or 5 Gy. The time interval between the priming and challenge dose was 5 h. The data are shown as survival fraction  $\pm$  SEM (n=9 or n=12) per treatment group. Based on the one-way ANOVA with Tukey's post-test, groups with different letters are statistically significant ( $p < 0.05$ ) and groups sharing the same letter are not.

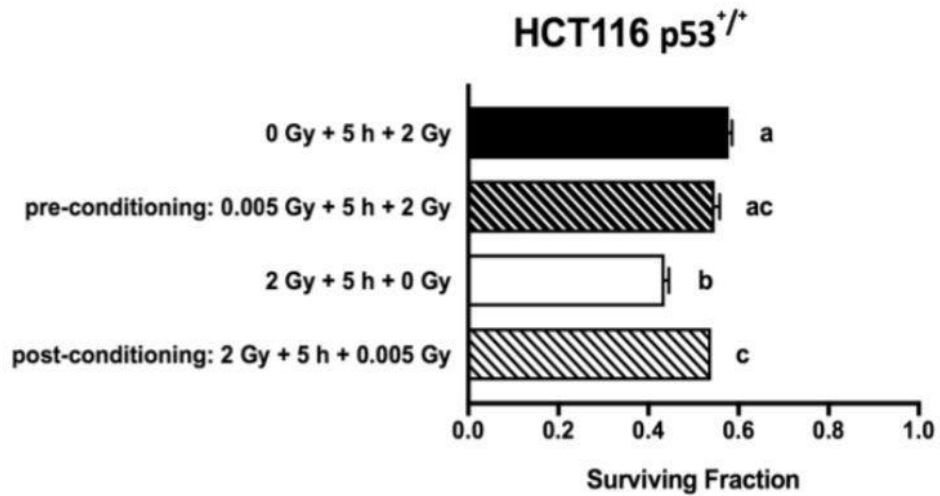


Figure 8. Influence of the 5 mGy priming dose on pre-conditioning and post-conditioning radiation outcomes in the human colorectal carcinoma HCT116 p53<sup>+/+</sup> cells irradiated with a challenge dose of 2 Gy 24 h after seeding 20 cells/cm<sup>2</sup> in triplicate T25 flasks. The time interval between the priming and challenge dose was 5 h. The data are shown as survival fraction  $\pm$  SEM (n=9) per treatment group. Based on the one-way ANOVA with Tukey's post-test, groups with different letters are statistically significant (p<0.05) and groups sharing the same letter are not.



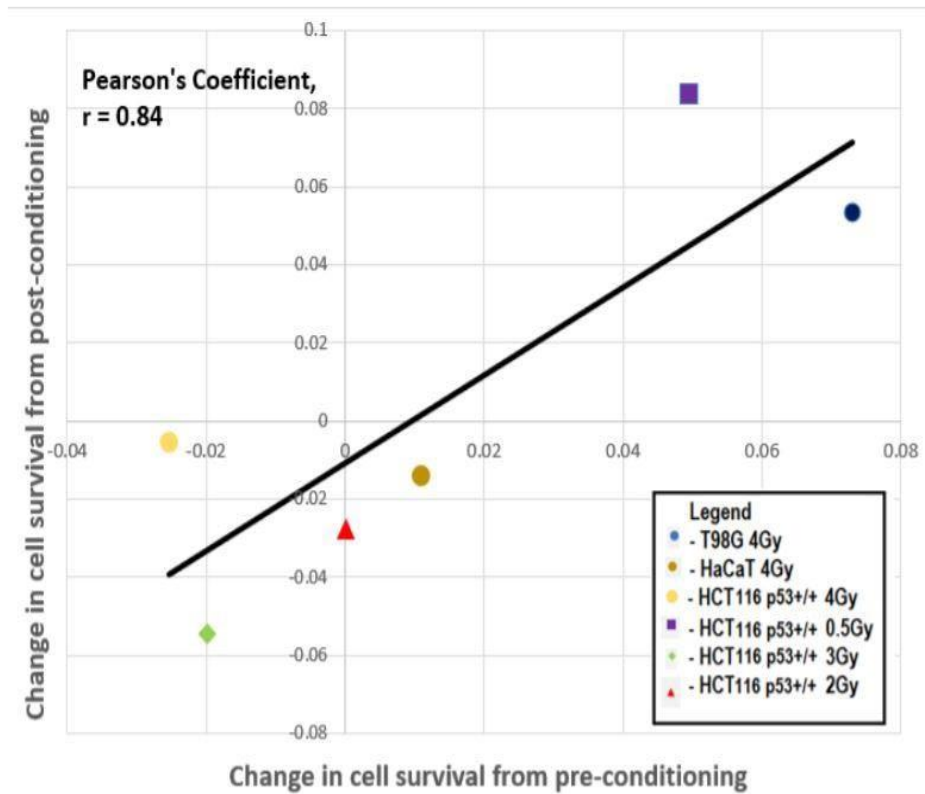


Figure 9. Correlation in change in cell survival after pre-conditioning and post-conditioning treatments for three cell lines (glioblastoma cells T98G, normal keratinocytes HaCaT, and colorectal carcinoma epithelial cells HCT116 p53+/+). The challenge dose was 0.5Gy, 2Gy, 3Gy, or 4Gy. Each data point represents a mean of three independent trials.

#### 4.1 Supplemental Material

In this section, it was tested whether the HCT116 p53 +/- cells doubled within the time span of the above experiments. Since several of the experiments radiation treatment was performed 24 hours after seeding, and then the 2<sup>nd</sup> dose of radiation five hours that (at the 29 hour mark), checking to see if cells were doubling during this time frame would help determine whether the pre-/post-conditioning treatments had an

additional variable that might have to be considered. It is useful to know whether or not the cells doubled especially during the 5 hour window as this might be another area to consider when determining the factors by which the pre-/post-conditioning treatments affected the clonogenic survival.

In **Figure 8 (or Figure S1)**, an experiment was performed using the BioRad Automated Cell Counter TC10. Briefly, 1 million cells were seeded into triplicate T25 Falcon flasks with 5mL of culture medium, and then trypsinized, a single cell suspension created at a time 24 hours and 29 hours later. From the single cell suspension, 10  $\mu$ L was taken and placed into the automated counter via a counting slide. The counter had determined the results of the cell concentration. It can be shown from the results that there is no apparent difference between the cell concentrations at 24 hours and 29 hours, for n=3 replicated flasks.

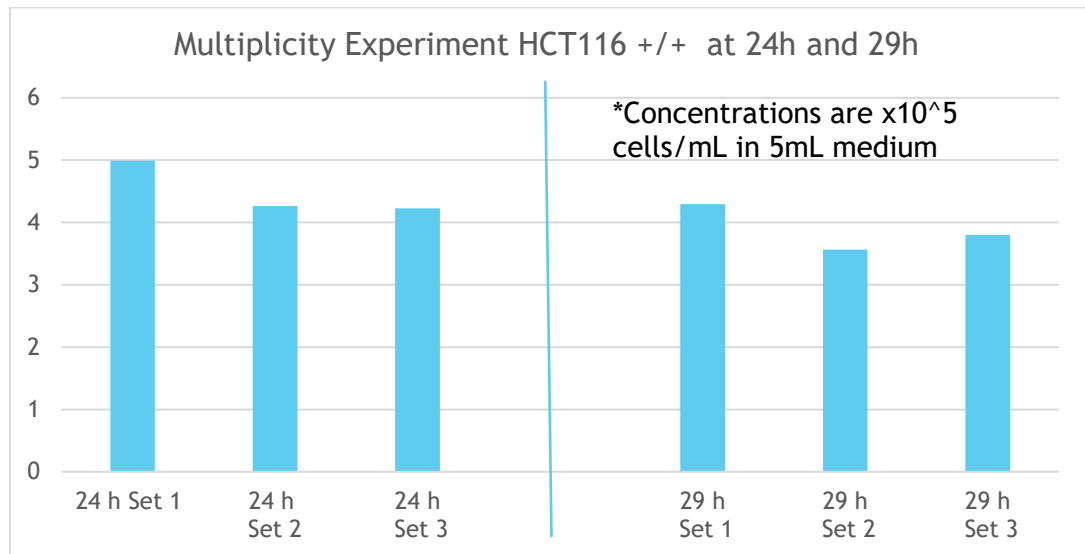


**Figure 8: Cell concentrations check at 24h and 29h after seeding using an Automated Cell Counter**

Afterwards, a follow up experiment was performed to test for cell doubling using a very small number of cells, within the typical clonogenic assay range. Briefly 500 cells were seeded in T25 Falcon Flasks containing 5mL cell culture medium, with  $n=3$  triplicates. After 24 hr and 29 hr the flasks were removed of medium and stained with Carbol Fuchsin (1:4 dilution to water). Cell singlets and doublets were manually counted under a microscope and scored manually as well, with the results shown in **Figure 9 (or Figure S2)**. The results show that in each case at 24h and 29h, there are slightly higher number of doublets than singlet cells. However, comparing 24h to 29h, the percentage doublet cells were no more at 29 hours than at 24 hours.

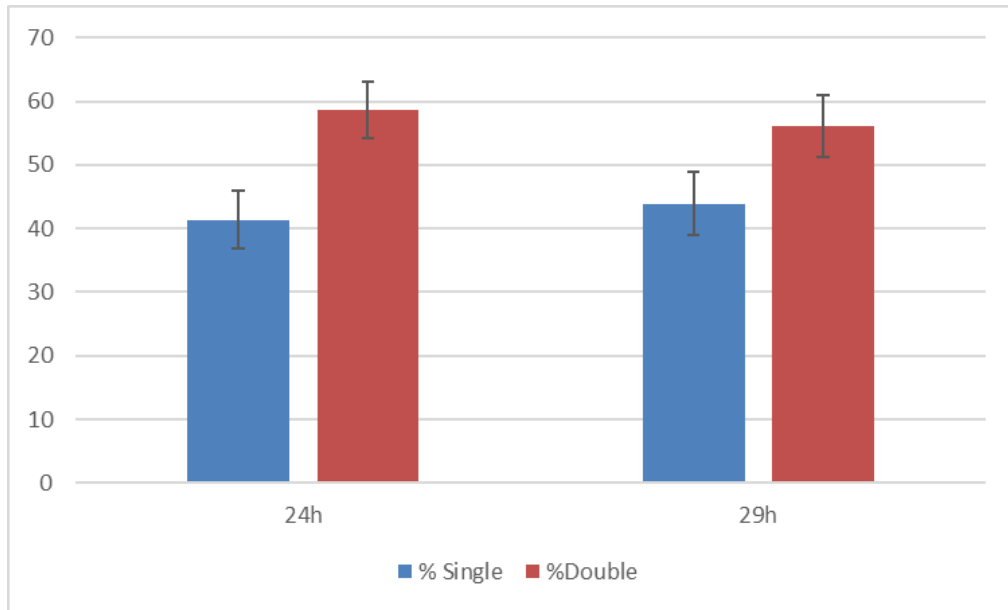


Figure 9: Cell singlet and doublet percentage at 24h and 29h for n=3 triplicates. The method was done using 500 cells seeded and stained at the times given, then manually counted under the microscope.

## 5 Protein Expression Resulting from Pre-/Post-Conditioning

### 5.1 Western Blotting Materials and Methods

The Western Blot technique was used to examine protein expression in their isolated forms after a given treatment. The Western Blot method used in this thesis had five main components: protein isolation, protein quantification via BCA assay, gel electrophoresis, transfer to blot membrane, and finally blocking along with primary and secondary antibody addition.

The HCT116 p53+/+ cell line was tested and a confluent T75 flask was trypsinized with 0.25% trypsin-0.48 mM EDTA in DPBS, neutralized with equal or greater volume of cell culture medium, and then centrifuged and resuspended in fresh cell culture medium. Cells were then counted using a BioRad TC20 Automated Cell Counter to get concentration/mL and then it was calculated which volume would be required to seed 1 million cells per T25 experimental flask. Cells were then seeded at densities of 40,000 cells/cm<sup>2</sup> in 25 cm<sup>2</sup> Falcon (Corning) flasks and then incubated for 24 h. Following incubation, the lids on the flasks were tightened and the cells were carried in a Styrofoam container across campus to the Cs137 TRS to

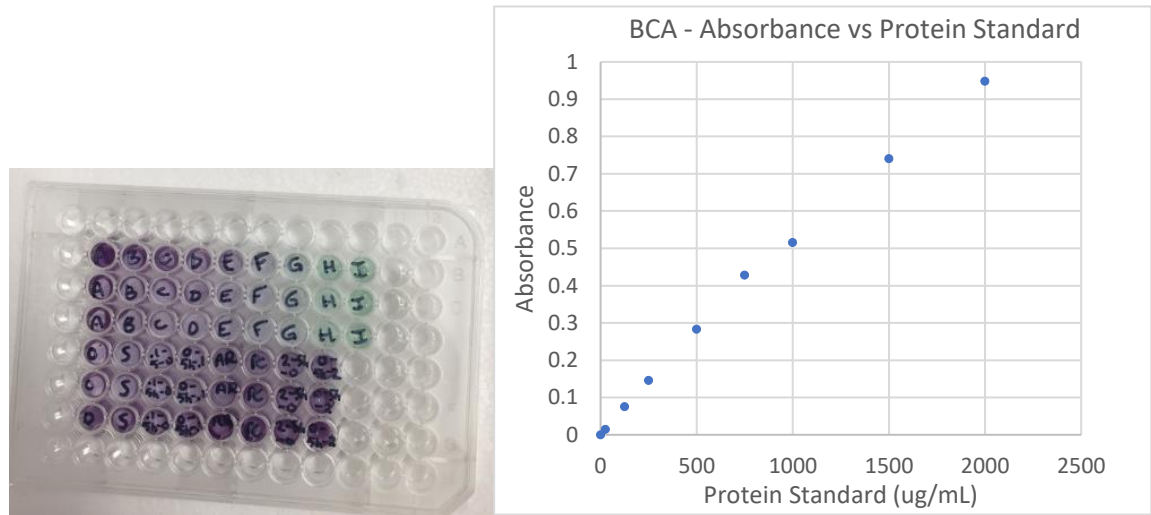
be irradiated. There were 8 flasks set up total: 0 Gy Control, 0 Gy Sham Control, 0Gy – 5h – 0.1Gy Control, 0.1Gy – 5h – 0Gy Control, 0Gy – 5h – 2Gy Control, 2Gy – 5h – 0Gy Control, 0.1Gy – 5h – 2Gy Treatment, and 2Gy – 5h – 0.1Gy Treatment. All flasks except the 0 Gy Control were carried to the radiation source room, with the 0 Gy Sham Control just being a carry control but also remaining unirradiated just as the 0Gy Control. The notation “x” Gy – 5h – “y” Gy means that the cells had received a dose of “x” Gy, then incubated for a time of 5 hours before receiving a 2<sup>nd</sup> irradiation of dose “y” Gy. All Cells brought to the radiation room were kept in a non-CO<sub>2</sub> incubator immediately beside the radiation room for the 5 hour period between the 1<sup>st</sup> and 2<sup>nd</sup> irradiation. After the 2<sup>nd</sup> irradiation, cells were returned to the main lab, caps were unscrewed until loosely fitted for air and CO<sub>2</sub> circulation, and then kept in a 95% air and 5% CO<sub>2</sub> incubator for another 12 hours.

The next morning (12h later), the cells were then subcultured in the same manner as they had been from the original T75 flask, then protein isolation began. Protein isolation started with collecting the cell pellets and washing the growth medium off with PBS a few times. The cells were then lysated in the protein lysis buffer using NP-40 buffer and protease inhibitor and kept on ice at all times. Centrifugation involved 14000g at 4C for 10 minutes. Afterwards, the supernatant was transferred to new tubes without disturbing the cell pellets. The supernatant was considered purified protein lysate.

Next the protein concentrations had to be measured for each of the 8 treatment groups mentioned above. This is to ensure equal loading for the gel electrophoresis stage. The Pierce™ BCA Protein Assay Kit from Thermo Fisher (CAT: 23227) was used. Diluted Albumin (BSA) Standards were prepared in 9 tubes to get a total of 9 final BSA concentrations ranging from 0 to 2000 ug/mL. Then the BCA working reagent (WR) was preparing using the following equation:

$$(\# \text{ standards} + \# \text{ unknowns}) \times (\# \text{ replicates}) \times (\text{volume of WR per sample}) \\ = \text{total volume WR required}$$

Since the experiment had 9 standards from above, and 8 unknown samples (treatment groups) as well as the decided 3 replicates and 0.2mL of WR per sample, a total of 10.4 mL of WR was made. The WR comprised of a 50:1 dilution of reagent A (containing sodium carbonate, sodium bicarbonate, bicinchoninic acid and sodium tartrate in 0.1M sodium hydroxide) to reagent B (containing 4% cupric sulfate). Finally, an 96-well microplate (BD Falcon) was set up by adding in first the 9 standards (control), and then adding 3 replicates of each treatment which contained 10 uL of sample with unknown protein concentration with 0.2 mL of WR per well, for a total of 51 wells (9 standards control and 8 treatment samples of unknown concentration each replicated 3 times). The plate was covered, incubated at 37°C for 30 min. and then taken to the BioInterfaces Institute at McMaster to measure the absorbance spectrum at 562 nm on a plate reader. The results were tallied and graphed below of **Figure 10 A B**:



A

B

Figure 10:

A: Microplate with working reagent and protein standards control (top three rows), and working reagent with unknown protein concentration samples. Note that the image was captured a couple of hours after creating the WR and protein samples, colors have faded in some areas.

B: Absorbance versus Protein Standard Curve based on control known protein standards, from which a best fit equation was acquired and used to interpolate absorbance data from unknown protein samples to solve for the corresponding protein concentration.

A best fit equation was generated from the data points of the standards and interpolated to get a protein concentration of each samples based on the absorbance values. Finally, the volume to be pipetted to achieve 40 ug of protein from each sample was added to 4x



loading dye, water, and 500 mM dithiothreitol, for a final volume of 25  $\mu$ L of each sample to be loaded in to the gel electrophoresis wells. All samples were boiled at 95°C for 5 minutes.

In the Gel Electrophoresis stage, NuPAGE MES SDS Running Buffer (20x) was diluted to achieve 1x SDS running buffer, which was used to fill the chambers of the tank. Novex Life Technologies precast gels were loaded with a volume of the protein mixed in the solution from the previous stage. Novex Sharp Pre-stained Protein Standard was also loaded into one of the wells to get a protein standard contrast to compare the protein migration to. The gel was run at 150 V for 1 hour at room temperature.

Next the mini-blot Module was used for Protein Electrotransfer (transfer gel to blot nitrocellulose membrane). Each gel, prepared in the previous stage described above, was placed as a sandwich in the following order from cathode surface: sponge, filter paper, nitrocellulose membrane, gel, filter paper, and sponge. 1x ice-cold transfer buffer was used to fill the module core and entire chambers. The transfer was run for 60 minutes at 10 V.

The final stage, after electrotransfer, involves blocking and antibody additions. Blots were blocked in 5% milk-TBST solution for 60 minutes at room temperature while on a rocker. Then rabbit polyclonal anti-p53 primary antibody (cat. no. 9282; Cell

Signaling Technology, Danvers, MA) added to a blot at a dilution of 1:1,000. On another blot, rabbit monoclonal anti-p21 primary antibody (cat. no. ab109520; Abcam, Cambridge, MA) at a 1:1,000 dilution was added and both blots were left overnight at 48C. The next morning, the primary antibody solution was discarded, the blots were washed with TBS-T for three times at 5 minute intervals, and the secondary anti-body of 1:5000 donkey anti-rabbit (peroxidase-linked) was added in a 5% blocking solution to each blot for 60 minutes at room temperature. The secondary anti-body was discarded from each blot and then each blot was rinsed thoroughly with TBS-T again. It should also be noted that in addition to the p53 and p21 proteins of interest, a loading control, actin (42 kDa), was used by blocking the a section of blot (that was cut, removed, and blocked in a separate container) and subsequently incubated with rabbit anti-actin primary antibody (cat. no. A5060; Sigma-Aldrich). Finally the blots were reading for imaging, using the ECL+ Detection (Thermo Scientific cat no: 32209). 0.5 mL of this enhanced chemiluminescent substrate was placed on the blots for 5 minutes and then the blots were imaged using a ChemiDoc MP (BioRad Laboratories Inc., Hercules, CA) under colormetric and chemiluminescent options. This was done to get overlaid images of the protein standard (ladder) and the protein bands of interest.

## 5.2 Results

The results show that the following systematic controls were in place starting with the actin protein at 42 kDa. The Actin protein acts as a placeholder to show that the Western Blotting technique has been performed to precision and addresses the locality of protein separation as per the designated scale on the edge of the blotting membrane.

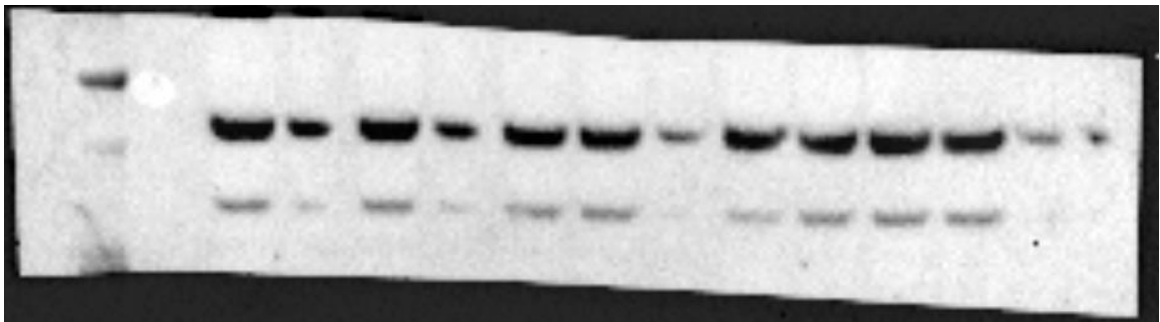


Figure 11: Actin control at 42 kDa in Wells 1, 3, 5, 6, 8-11 (from left-right).

After having the controls set up, the results of **Figures 12 and 13** show the Western Blotting results for the p53 status after the experiments were completed. The results are shown as a BioRad ChemiDoc Imaging file which has chemiluminescence and colorimetric overlay to show on the far edge a scale which confirms the molecular weight and thus the protein. The results show that based on the quantity of stain (thickness of the band) which is proportional to quantity of protein expression, there was the least

protein expression of p53 for the AR adaptive response treatment (pre-conditioning). Interestingly, the post-conditioning PC treatment had the highest p53 expression according to thickness of band division.

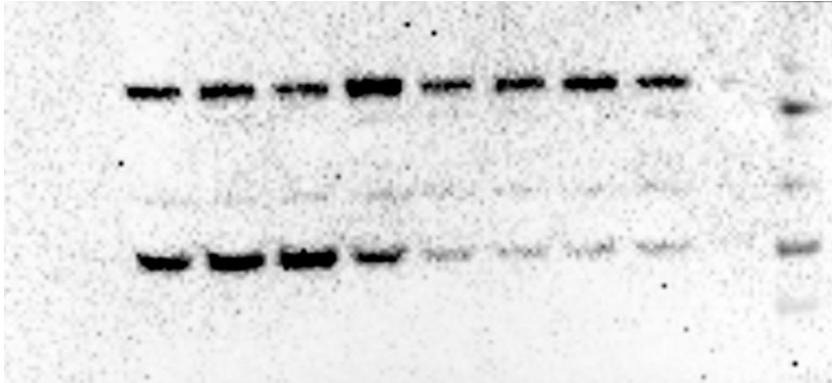


Figure 12: Original image of Western blot membrane investigating p53 status after pre-/post-conditioning treatments and controls, with visible protein standard ladder on the right side.

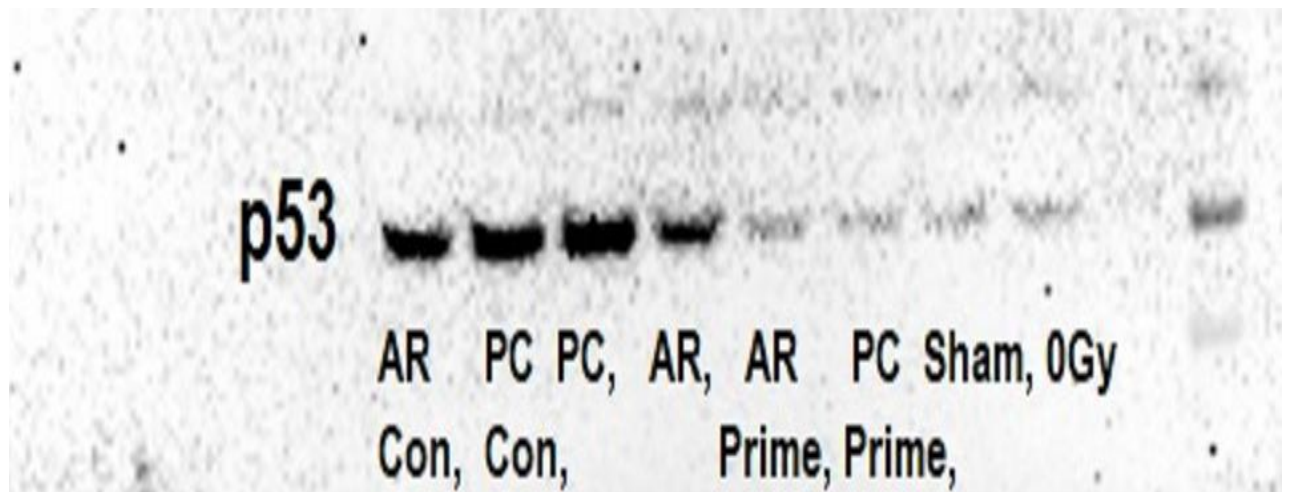
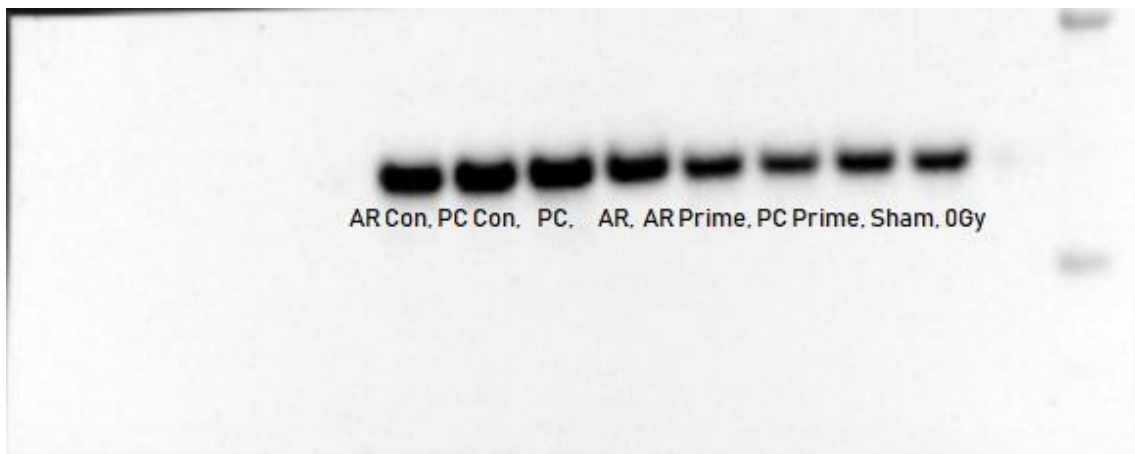


Figure 13: Close-up and labelled p53 protein expression from each of the 8 treatment groups used in this experiment with the HCT116 p53+/+ cell line.

**Figure 14** shows p21 expression as a result of various experimental treatments. According to the visual representation of protein expression from the blotting protocol, there were no remarkable differences in protein expression across all treatment groups. The higher dose treatments received more p21 expression than did the low priming or zero dose treatments.



**Figure 14:** p21 western blotting results. Image taken from BioRad ChemiDoc as an overlay of colorimetric and chemiluminescent image.

### 5.3 Discussion

It is shown from the Western Blotting techniques that the expressions for protein p53 have varying results from the pre/post-conditioning treatments compared to control large or small dose only.

The results for p53 status suggest that there is less p53 expression from the pre-conditioning treatment compared to post-conditioning treatments. The post-conditioning treatment (large dose followed by smaller dose after some time) clearly indicates the largest p53 protein expression. Visually the band is quantifiably almost twice in thickness for the post-conditioning treatment (PC) compared to the pre-conditioning treatment (AR). Interestingly, the post-conditioning control (2Gy – 5h – 0Gy) has thicker band formation, suggesting higher p53 presence, than the pre-conditioning control (0Gy – 5h – 2Gy). In the previous results of section 3 of this thesis, parallel comparison of pre-/post-conditioning using clonogenic cell survival endpoints, the clonogenic survival of these controls also differed. This may suggest that the timing windows play a role, whether the large dose is administered as 2Gy – 5h – 0Gy, as in the case for the post-conditioning control, or as 0Gy – 5h – 2Gy, as for the pre-conditioning control. For the p21 protein expression as a signal cascade, there were no notable differences in protein expression.

## 6 Quantifying Cell Luminescence in a Gamma Field via Photon Detection

### 6.1 Photon Detection Overview

The purpose of the following experiments was to show and quantify photon emissions, also referred to as cellular luminescence or BioPhotons, of biological material from gamma-radiation. The photon emission data upon irradiation of colorectal carcinoma cells (HCT116 p53<sup>+/+</sup>) was assessed following gamma ray exposure from the Cs-137 source previously described in the beginning of the thesis. A single-photon-counting system was used and shielded with lead to reduce counts from stray gammas reaching the detector. In the presence of gamma radiation, a higher photon emission was observed when cells were present and being irradiated compared to background without cells. In a gamma-field, photon emission quantity depended somewhat on the cell density. The results show that there is an increase in photons present upon cells being irradiated by gamma radiation. The amount of photons emitted in the presence of cellular material depend on, but are not limited to, cellular density and wavelength of release.

## 6.2 Materials and Methods

### Cell Cultures

The human colorectal cancer cell line HCT116 p53<sup>+/+</sup> was used to investigate the emission of biophotons from human cells upon direct gamma irradiation. The cell line was cultured in the Roswell Park Memorial Institute (RPMI)-1640 medium supplemented with 10 % fetal bovine serum (FBS), 2 mM L-glutamine, 25 mM HEPES, 100 U/ml penicillin, and 100 µg/ml streptomycin. All tissue culture reagents were obtained from Gibco/Life Technologies (Grand Island, NY), unless otherwise specified. The cell line was provided by Dr. Shane Harding (University Health Network and University of Toronto, Toronto, ON). The cell line was grown at 37°C in an atmospheric environment equilibrated at 5% CO<sub>2</sub> and 95% air. Subculturing was performed with trypsin/EDTA as previously described (Cohen et al., 2019; Vo et al., 2017).



### **Single Photon Counting**

The single photon detection unit consisted of a Hamamatsu R7400P photomultiplier tube (PMT) (Hamamatsu Photonics, Bridgewater, NJ, USA) configured with a specific interference-type band filter of choice. The detection unit had been previously used to quantify the UV biophoton emissions from cultured human cells irradiated with beta particles (Ahmad et al 2013; Le et al 2015; 2017). The PMT was set to a high voltage -800V. In some cases, for the gamma irradiation measurements -1000V was tested to see if there was any difference between the treatment groups as a result, and there were no observable differences between the groups from this.

### **$\gamma$ -Irradiation**

Densities of 250k, 500k, 750k, 1m and 4m cells were seeded into 75-cm<sup>2</sup> tissue culture flasks (BD Falcon) containing 15 mL of the growth medium. Control flasks had the same medium but without cells and served as a control for the experiment. After 24h incubation, all flasks were brought to the McMaster University's Taylor Radiobiology Suite that had Cs-137 as the gamma source.

The single photon counter was set up 75 cm directly below the circular opening of the Cs-137 source containment unit. In one instance, with 4m cells, the single photon counter was either set up as closely as possible to the radiation source (~22cm) or as far away as possible from the radiation source (~150cm) to briefly test whether large fluctuations in dose rate had an effect on cell luminescence. The detector lies within a chamber that is light tight, in order to prevent any outside light sources from affecting measurements. The detector is angled and facing downwards with the detector window directly parallel to the wall of the T75F that cells would anchor to. Directly above the detector was 2.2" of lead shielding held on top by a Styrofoam piece, and behind the detector were two – 1" blocks of lead shielding. Because the detector was several cm away from the flask, it was arranged so that the detector would be shielded and the flask would be as exposed as possible to the direct opening of the Cs-137 source. Measurements were run up to 20 times on five independent sessions and exposure times lasted 30s each run.

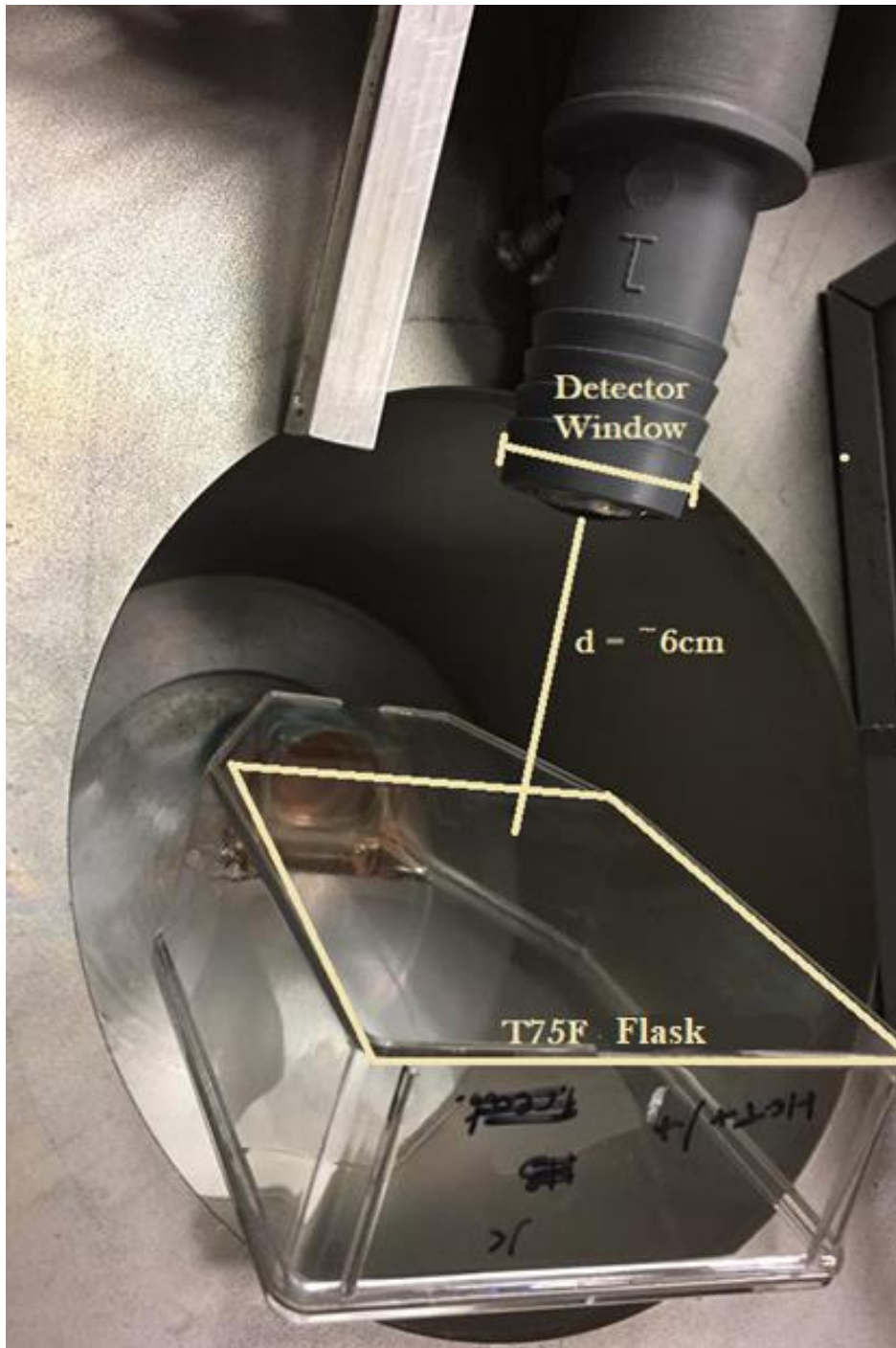


Figure 15: A top-down view of the exact setup in how measurements took place. The flask is angled so that the wall containing the cells (or lack thereof) is parallel to the detector

window, ~6 cm away. When the lid is on, this entire area is dark and free from stray light.

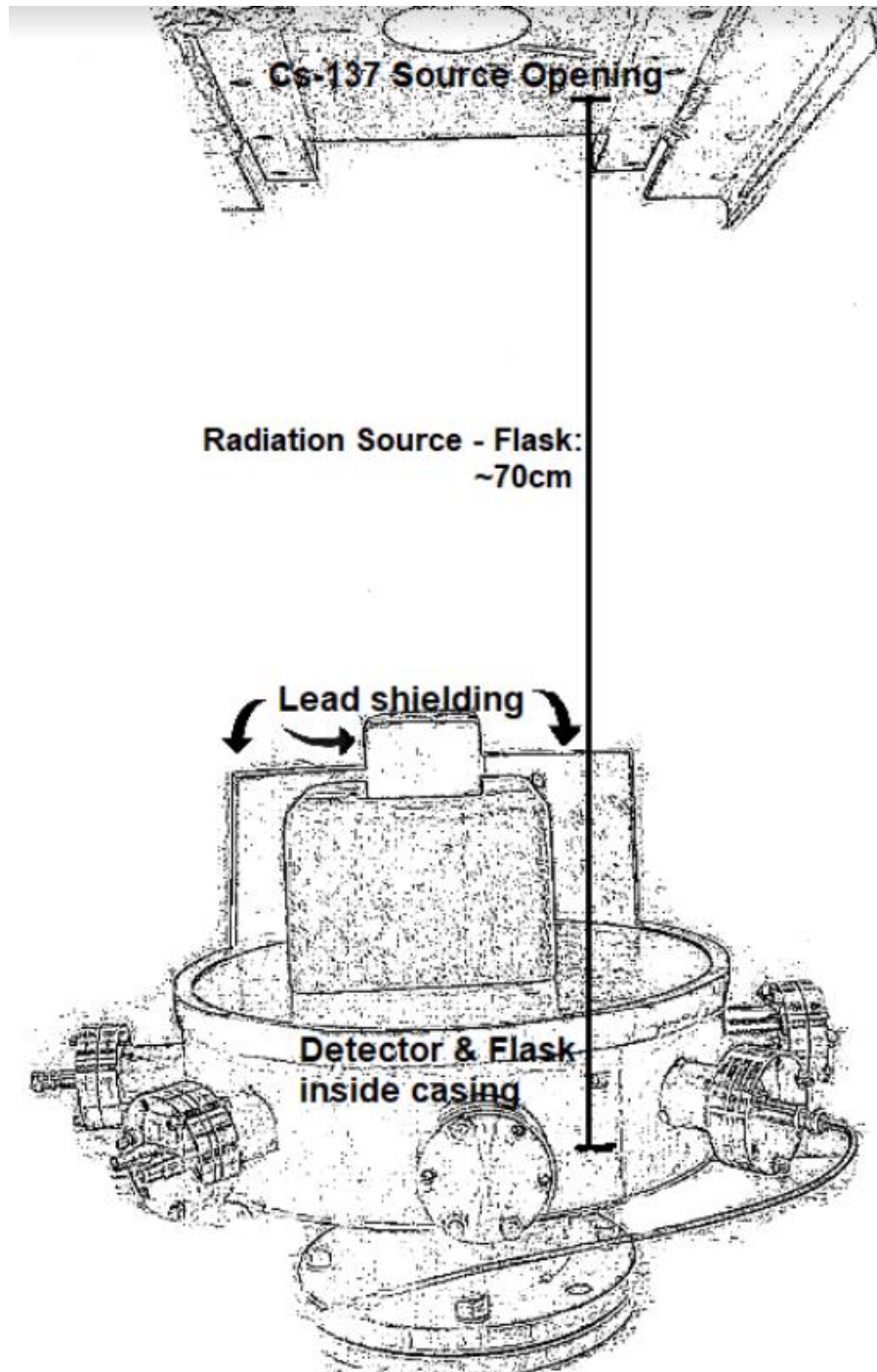


Figure 16: A schematic of the photon detector in the gamma-irradiator

### Shielding, detector factors and background considered

The background counts without any radiation or cells present was very low, approximately 1 count per 3 to 5 seconds. Next, it was checked whether tritium-water in the cells, which involved  $\beta$ - interactions, would elicit a BioPhoton response. This study was previously performed using the same detector with similar settings (Michelle Le, McNeill, Seymour, Rainbow, & Mothersill, 2015). This was done by setting up a 100mm x 15mm 56.5cm<sup>2</sup> petri dish (Falcon) containing ~200,000 cells which were originally seeded with 5mL fresh cell culture medium, and the medium was replaced with ~15mL of tritiated water (unknown activity). Tritium waste from previous experiments was reused by filtering with Acrodisc Syringe Filter with HT Tuffryn Membrane (Pall\* Life Sciences 0.2 um Pore Size) with a 30mL syringe tube. This was to remove any cellular debris and sterilize the tritium solution so that only diluted tritium would be used. However, because the tritium was diluted in multiple experiments prior to this study, the activity of tritium per unit volume of solution was unknown. The original activity of tritium was 1 mCi per 1 mL of pure H<sub>2</sub>O. Consulting to previous tritium users (experimenters) allowed to find a better estimate of approximate tritium activity from the waste container. It was found that a minimum of ~25 mCi (25mL) of tritium was used and the waste container that contained the tritium was ~1500mL. Regardless of this second hand knowledge and

primary observations, the tritium concentration could not be quantified with certainty at the time of the experiments. After the 15mL of tritium solution was placed in the petri dish containing 200,000 cells, the dish was placed directly below the detector at ~3cm from the cells to the detector window. Counts were measured for 300 seconds, and the total count output was  $292 \pm 17$  Counts, or 1 cps. Then 15mL of tritium solution was placed in another petri dish without cells, and for another 300 seconds the measurement took place. The total count output without cells was measured at  $346 \pm 19$  Counts, or 1.2 cps. Therefore from this observation there was little to no measurable difference with cells present. However, it appears that compared to background counts without any tritium dishes present, which was measured at approximately 1 count ever 3-5 seconds, that there is a very small amount of interaction of the tritium with the materials in the dish itself.

After control measurements were taken, the experiment was set up to allow for gamma-ray interactions to be observed. HCT116 p53+/+ cells were seeded at a densities between 250,000 cells, 500,000 cells, 750,000 cells, 1 million cells, and 4 millions cells.

Attenuation from the shielding would still result in background coming from photons that pass through the lead (Pb), including what is called a build-up factor. The

Build-up factor is the ratio of photons at a point to those that make it to the point without being scattered. When the gamma radiation reaches the Pb material, it will interact with Pb and some of the radiation will scatter or produce secondary radiation. This secondary source of radiation can make it through the shielding material, along with the less than 0.5% that did not at all get blocked by the shielding material. The build-up factor depends on photon energy, shielding material and thickness of shielding material, and the build-up factors are found in tables from Nuclear Data. For 660 keV gamma-ray photons passing through 5.5cm of the Pb shielding material:

Without considering the build-up factor, approximately 5.5 cm of lead shielding will block >2 TVLs or about 99.5% of the initial gamma radiation. However, the buildup radiation will result in the following equation:

$$I = I_0 * b * e^{-\mu x}$$

Where I is the gamma radiation from the source that reaches the detector,  $I_0$  is the gamma radiation that is initially present before reaching the Pb shielding, b is the build-up factor for Cs-137 radiation upon Pb material, and the  $e^{-\mu x}$  is the attenuating factor by which the shielding reduces the incident gamma radiation to the detector.

To calculate the build-up factor first the number of mean free paths (mpf) is required,

which is based on the mass attenuation coefficient and the density of Pb:

$$\# \text{ mfp} = \frac{\mu}{\rho} \rho = (0.1102 \text{ cm}^2 \text{ g}^{-1})(11.35 \text{ cm}^3 \text{ g}) = 1.25 \text{ cm}^{-1}$$

$$\mu \cdot x = (1.25 \text{ cm}^{-1})(5.5 \text{ cm}) = 6.875$$

The information to find the mass attenuation coefficient for 662 keV gamma-rays is found here in another table (United States National Institute of Standard and Technology, NIST Physical Measurement Laboratory). Next, the buildup factor can be easily found in the table (Nucleonica European Atomic Energy Community, Dosimetry & Shielding) based on the # mfp and the energy. Therefore, the build-up factor for this scenario is 2.31.

Using the tables provided, for a point source in Pb, and interpolating for 0.661 MeV, and then interpolating for mfp = 1.25, yields B = ~2.31. The Cs-137 radiation source was approximately 500 Ci at the time of measurements, and the detector 70 cm away from the source, resulting in the branching ratio for the 0.661 MeV gamma rays to be 0.85. The unshielded fluence rate at the time of measurements is given as:

$$(500 \cdot 3.7 \times 10^{10} \cdot 0.85)/(4 \pi \cdot 70^2) = 255.4 \cdot 10^6 \gamma \cdot \text{cm}^{-2} \cdot \text{s}^{-1}$$



Therefore shielded (full energy) fluence rate would be  $266.8 \times 10^3 \gamma \cdot \text{cm}^{-2} \cdot \text{s}^{-1}$ .

Scattered gamma rays can be roughly approximated to be half the energy of full energy gamma rays. The fluence rate, in terms of photon number, after the 5.5 cm Pb shield would be about be  $120 \times 10^4 \text{ photons} \cdot \text{cm}^{-2} \cdot \text{s}^{-1}$ .

It must be stressed that the actual number of biophotons emitted is actually a lot greater than what was being detected. This is in part due to attenuation from the photons passed through the cellular material, followed by the flask, and then through the space between the emission source and the detector window. Additionally, only due to the solid angle of the detector to the plane of cells, the limited geometry of a small windowed detector which is not all-encompassing across the cellular emissions results in most of the biophotons being undetected. The following equations represent that loss of detection due to i) Solid angle and ii) Attenuation through various media:

i) Solid Angle of detector to plane of cells

$\Omega = \iint_S \sin \theta \, d\theta d\varphi$ . The solid angle, defined as the surface area of a sphere that is enveloped by the projection onto the sphere, or  $\Omega$ , is found by integrating over the surface S across its polar ( $\theta$ ) and azimuthal ( $\varphi$ ) angles. Ideally if the entire range of photons were picked up by the detector across all cells on the plane, the solid angle  $\Omega = 4\pi$ . However, because there is a plane (or slab) of cells which are emitting photons across

all directions in a spherical geometry around them, and a detector of a small circular window that is approximately situated in the middle of the slab and 6 cm away (Figure 2), the approximate solid angle would be  $\sim 0.0079$ , which is  $\sim 0.8\%$  of the entire solid angle. This means that only less than 1% of the cell luminescence observed above background is being detected by the detector. Therefore, if a detector setup existed that was able to receive 100% of the biophoton signal coming from the cells, then it would theoretically have a 100-times increase in the number of photons detected from cellular emissions (Zaluzec, N.J XEDS Tools Solid Angle Calculator TelePresence Microscopy Collaboratory; Zaluzec N.J 2014)..

ii) Attenuation of biophotons due to i) cellular material ii) flask material iii) air/space between emission source and detector window

$$\text{Incident photons} = \text{Initial photons} \times e^{-(\mu_{cell} \cdot x_1 + \mu_{flask} \cdot x_2 + \mu_{air} \cdot x_3)}$$

Where:

$$\mu_{cell} = \sim 0.2 \text{ cm}^{-1} \text{ for } 0.05 \text{ mm of tissue}$$

$$\mu_{flask} = 0.178663 \text{ cm}^{-1} \text{ for paraffin wax of close structure to the flask}$$

$$\mu_{air} = 0.0001039 \text{ cm}^{-1}$$

(Chen et al. 2015; Mousa A, Kusminarto K, Suparta G B 2017; The Risk Assessment Information System, University of Tennessee 2018)

$x_1$  = distance for biophotons to pass through the cell, or cell diameter = 0.00174cm

(Tahara et al., 2014)

$x_2$ = distance for biophotons to pass through thickness of flask wall = ~2mm

$x_3$ = distance from flask wall to detector window = ~6cm

Taking the above factors into consideration, indicating that the biophotons detected (currently seen as a significant increase above background) is still much less than the actual biophoton emission after the solid angle and attenuations limitations are realized. The following equation approximates the true number of biophotons that were theoretically present at the time of measurements:

$$I_{observed} = I_{true} \times e^{-(\mu_{cell} \cdot x_1 + \mu_{flask} \cdot x_2 + \mu_{air} \cdot x_3)} \times \Omega$$

$$I_{true} = \frac{I_{observed}}{e^{-(\mu_{cell} \cdot x_1 + \mu_{flask} \cdot x_2 + \mu_{air} \cdot x_3)} \times \Omega}$$

If we take the case of 340 nm measurements, which observed a detected Biophoton count rate (above background levels) as 19974 cps, then the actual number of

Biophotons emitted at the time of detection was:

$$I_{true} = \frac{19.974 \times 10^3 \text{ cps}}{e^{-(\mu_{cell} \cdot x_1 + \mu_{flask} \cdot x_2 + \mu_{air} \cdot x_3)} \times 0.0079}$$

$$I_{true} = 2.623 \times 10^6 \text{ cps}$$

Therefore the true biophoton rate of emission at the time of measurement was theoretically  $2.623 \times 10^6$  cps.

## 6.3 Results

### **$\gamma$ -Irradiation**

The results from gamma-irradiation show an observed difference in photon emission when cellular material is present. In **Figure 17** it is shown that a polystyrene flask irradiated for 30s, at ~70 cm from the presence of a 50 Ci Cs-137 gamma-source resulted in an average non-significant increased emission of 26,000 Counts. Compared to a polystyrene flask alone, a flask containing 500,000 cells reached 79,000 Counts above background, which is approximately 53,000 Counts above the flask alone, and higher than both of the calculated individual errors.

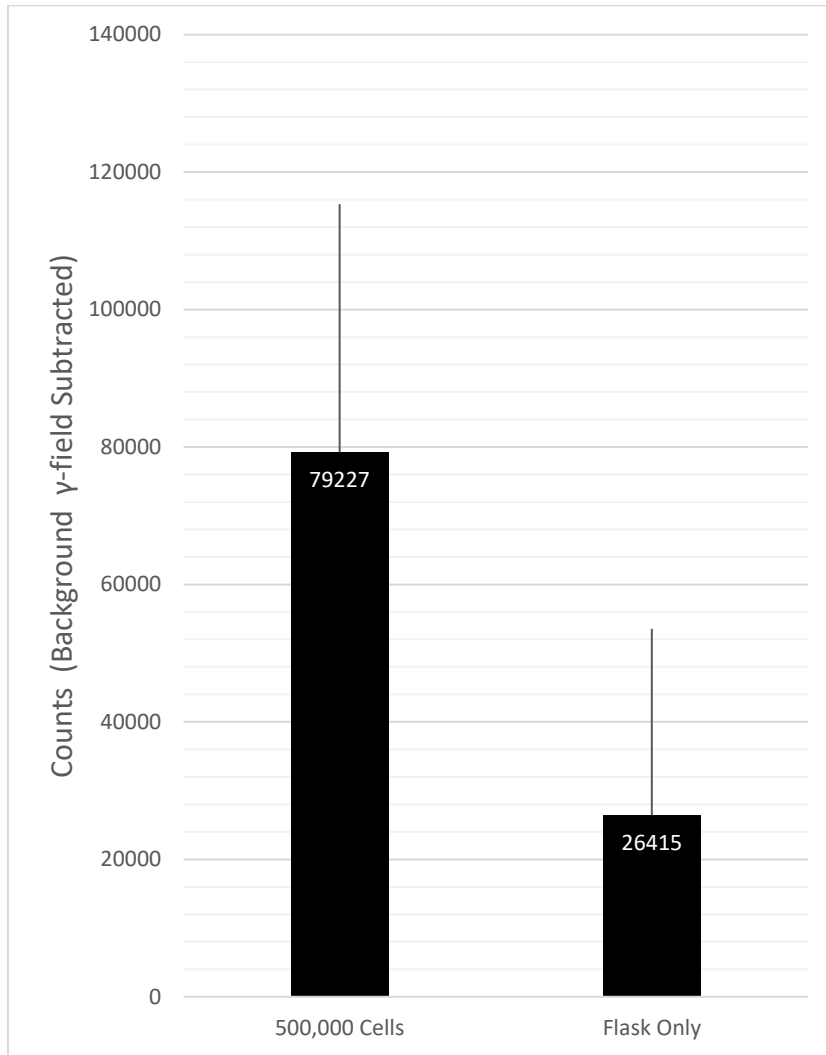


Figure 17: Average Counts from 30s exposure to  $\gamma$ -Irradiation with a 610nm filter. The counts were subtracted from background (detection of stray gammas only) for each independent trial.

Additionally, it is shown in **Figure 18** that changes in cell density may result in changes in cell-luminescence output (shown as count rate in counts per second). The experiments were performed such that each flask was placed in front of the detector, the measurement took place for 30s while the Cesium 137 gamma-source was exposed, and then afterwards the flask was replaced with a flask of different cell density, going from Flask Only (no cells), to 250,000 cells, 500,000 cells, 750,000 cells, and 1 million cells. The filter that was on the detector during all measurements was that for 610 nm.

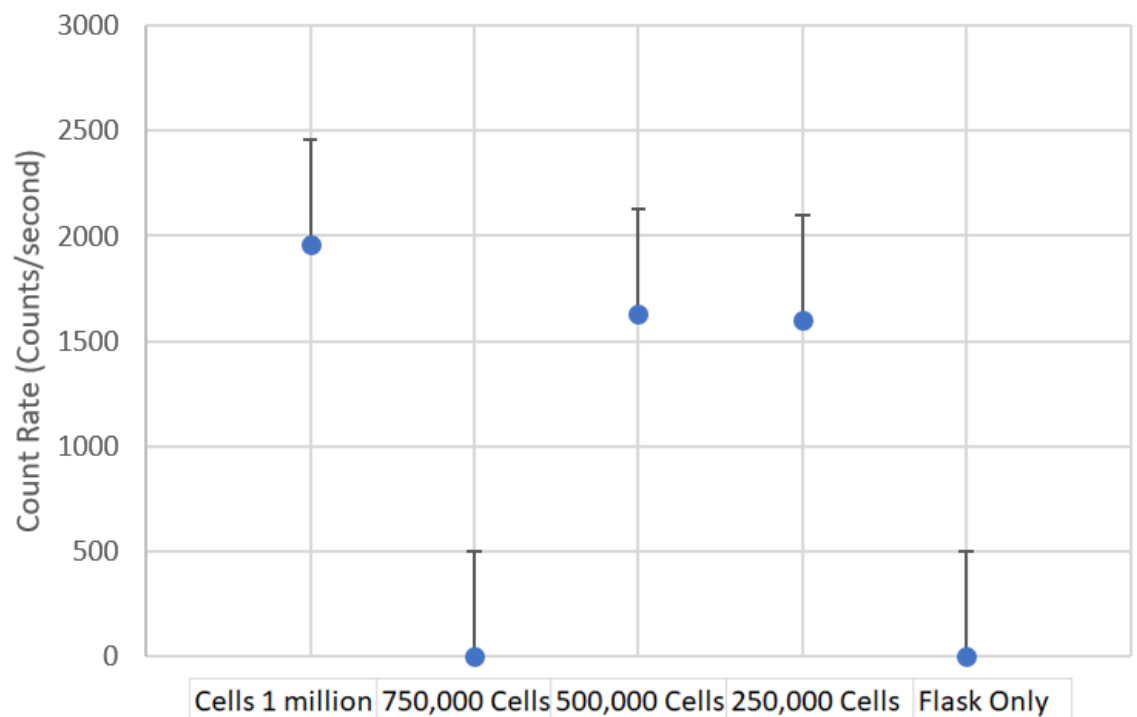
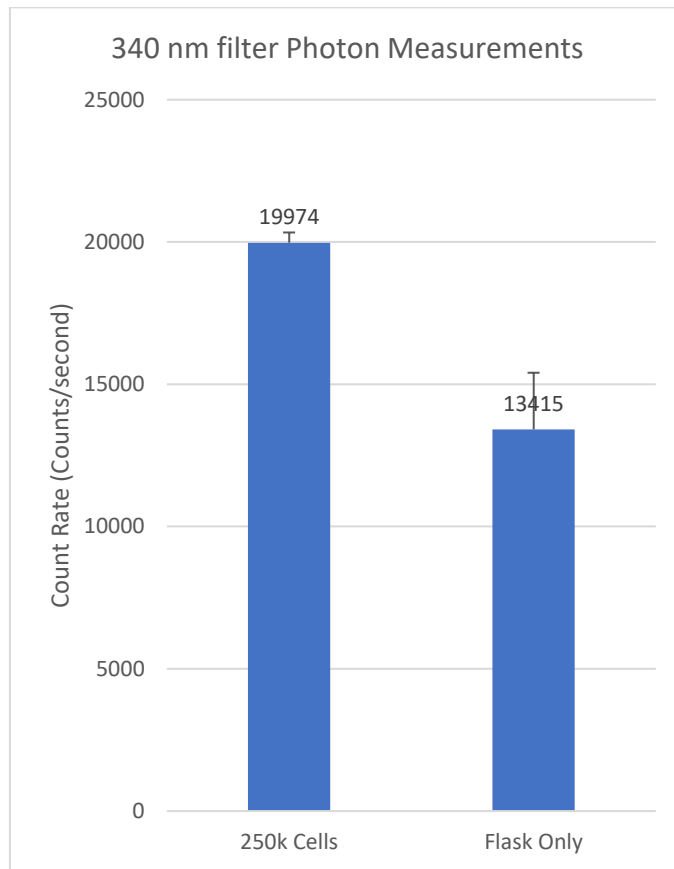


Figure 18: Average Count rate from 30s exposure to  $\gamma$ -Irradiation with a 610nm filter.

The count rates above were background corrected (subtracted from the detection of

stray gammas only, with no flasks present) for each independent trial, n=9. Different cell densities were used with Flask Only indicating no cells present during the measurements.

Afterwards, the filter was changed to encompass the 340 nm Ultraviolet A (UV-A) wavelength. It is shown in **Figure 19** the count rate from 250,000 cells under detection in a gamma field for 30s compared to a detector facing only a flask (no cells). The results are tabulated as a count rate (counts per second) after being converted to count rate from dividing the total counts recorded in the 30 s run by the 30 s time.



**Figure 19: Average Count rate from 30s exposure to  $\gamma$ -Irradiation with a 340nm filter. The count rates above were background corrected (subtracted from the detection of stray gammas only, with no flasks present) for each independent trial.**

For the case of 340nm, which was of particular interest, further measurements were set up to track any effects of distance from radiation source (dose rate) versus count rate from the cell luminescence of 4 million cells. Compared to no cells (Flask Only), there was no difference in count rate either at 23cm (highest possible Dose Rate of 0.35Gy/min), nor the lowest dose rate at roughly 150cm from the Cs137 radiation source



(Dose Rate of roughly 0.012Gy/min), as depicted in **Figures 20 and 21**. Note that the actual dose rate following a  $\frac{1}{r^2}$  inverse-square law would result in  $\sim 0.008$ Gy/min, however the dose rate estimates at a distance of around 150cm were based on a conservative model, adding some height for the flask being inside the detector, and the casing being several centimetres above ground.

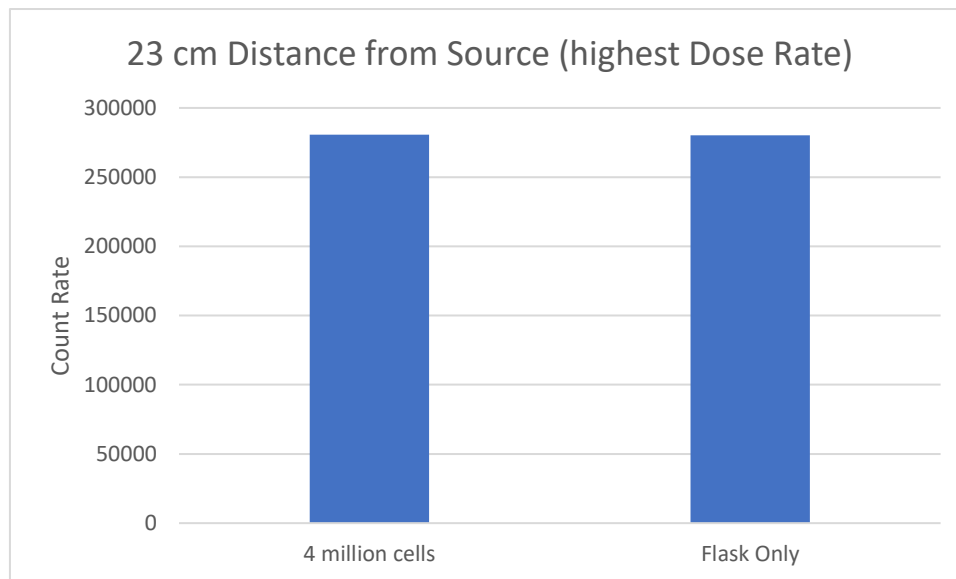
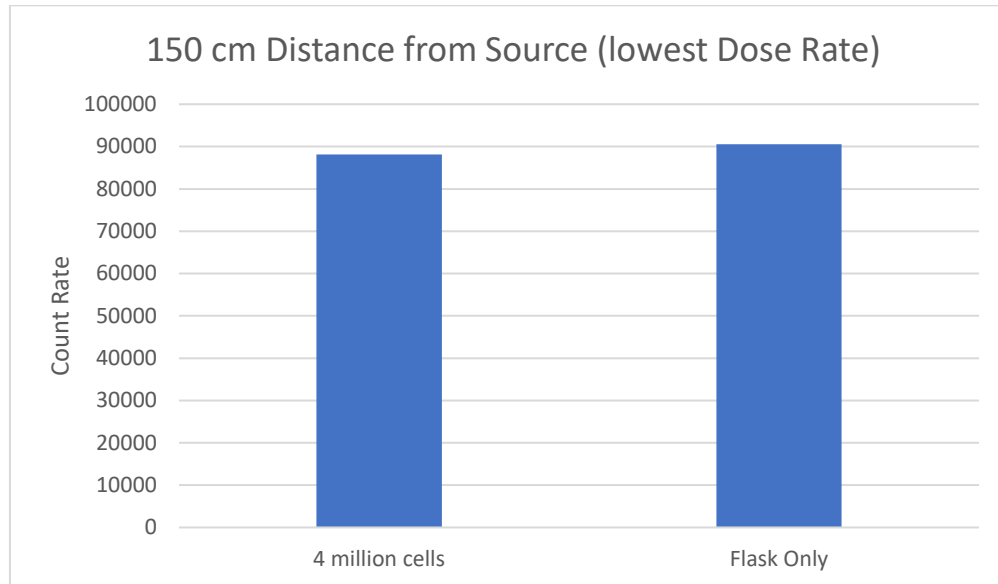


Figure 20: 4 million cells seeded, and no differences in observed count rate from changes in dose rate at highest dose rate 0.35Gy/min.



**Figure 21: 4 million cells seeded, and no differences in observed count rate from changes in dose rate at lowest possible dose rate for the Cs137 source 0.012Gy/min.**

Finally, it was tested as to whether the cell luminescence was dependent upon a continuously damaging source, or if cell luminescence would remain still after the damage source had effectively been removed. **Figure 22** shows the count rate of 4 million cells that were exposed to a high dose rate, acute dose of 4Gy over an 8 minute period. Immediately after irradiation, the cells were taken to the radiation detector which was placed outside of the gamma-irradiation room for these experiments. The count rate was compared to that of background and that of just a flask only (no cells). Both the flask only and the 4 million cells did not reach count rates higher than background. It should be noted that although background appears quite high, the background count was run last after the detector had been

exposed to a fair amount of bright light due to opening and closing the lid of the unit several times, and the light in the room the detection system was in at the time was much brighter than the irradiation room.

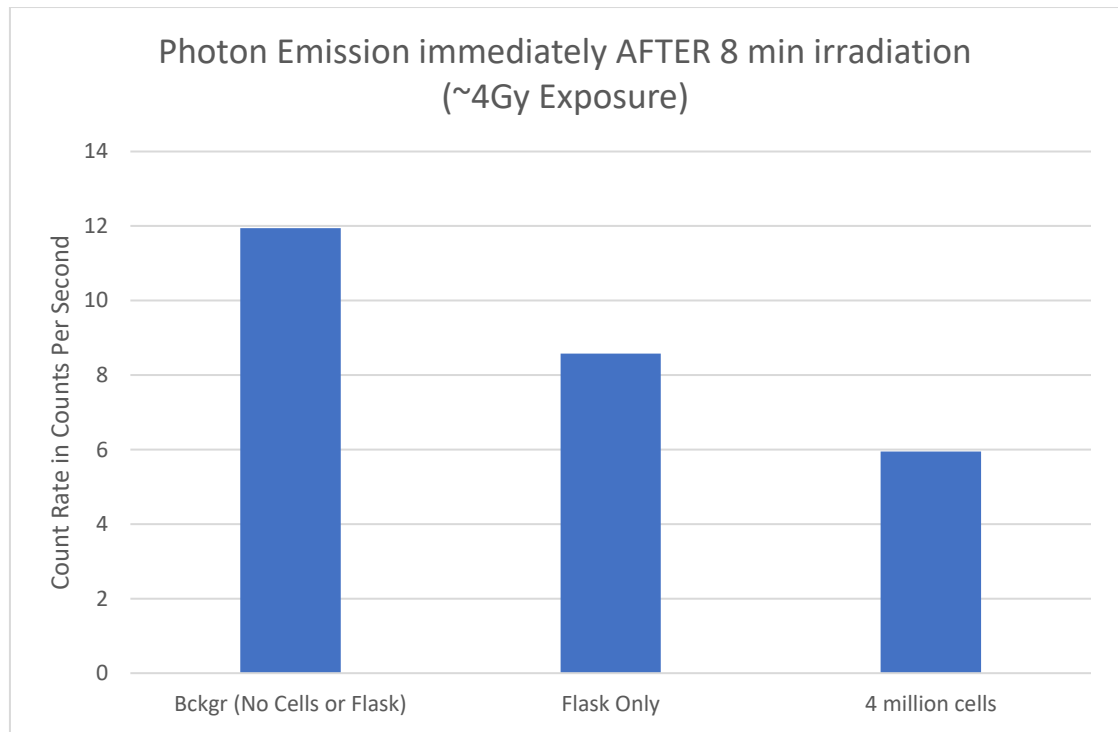


**Figure 22: Photon emission detected immediately AFTER irradiation for 4 million cells, and compared to natural background or flask only.**

#### 6.4 Discussion

Though this is the first reported work on BioPhotons and Cell Luminescence attempted using gamma-radiation as the radiation damaging source, it is important to note that the work was extended from the recent advances made using beta- radiation

sources (Ahmad B S 2012; Le M 2018). The work that was done in this thesis using gamma-radiation can be compared to the previous two beta sources in Table below:

Source & Activity (or Dose Rate):	Cells-Detector Distance:	Background Counts per Second ( <u>absence of cellular material</u> ):	Fluorescent Counts per Second ( <u>with cells</u> ):
Yttrium-90, 703 $\mu\text{Ci}$  (Max $E(\beta) = 2.28$ MeV; Avg $E(\beta) = 0.933$ MeV)	2cm	2767 counts/s	45,000 counts/s (with 10,000 cells/5mL)
Tritium-Water ( $\text{H}_3$ ), 857.5 $\mu\text{Ci}$	4cm	(?)	1200 counts/s (with 2000 cells/cm <sup>2</sup> , 200,000 cells total)

<p>(0.347 mGy/min,  <b>total dose = 0.5Gy</b>)</p> <p>(Max <math>E(\beta)</math> = 18.6  keV;  Avg <math>E(\beta)</math> = 5.7 keV)</p>			
<p><b>Cs-137,</b>  ~7500 Ci</p> <p>(Dose rate at 60cm =  0.052 Gy/min.)</p>	<p>6cm</p>	<p>140,000  counts/s</p>	<p>2000-20,000 counts/s (with varying cell densities  and filters)</p>

It can be shown that the gamma-source used in these experiments is very high in the dose rate used to irradiate the cells compared to the previous research on the tritium irradiated HaCaT cells (Michelle Le et al., 2015). It should be noted that the background counts are quite high due to reasons mentioned in the explained

section of the methods under background. However, even still, for when a 610 nm filter is used, the count rate from a flask containing cells jumps to up to 2000 counts/second higher than background. Since radioactive decay is modelled by the Poisson distribution, if the mean background is 140,000 counts/second then counting statistics error can take the square root of the mean background counts and then divide by the run time of the measurements which gives approximately

$$\frac{4,200,000 \pm \sqrt{4,200,000}}{30} = \frac{4,200,000 \pm 2049}{30} = 140,000 \pm 68 \text{ cps as the background.}$$

Measurements taken with values higher than the background and above the error can be comparatively, namely irradiated cell concentrations of 250,000 cells, 500,000 cells and 1 million cells per 75 cm<sup>2</sup> flask at 610 nm wavelength filtering.

Additionally, at the 340 nm wavelength filter which was of interest due to the UVA characteristic emissions, count rates reached as high as 20,000 counts/s above background levels for cellular concentrations of 250,000 cells/75cm<sup>2</sup> flask. This characteristic 340 nm is also noted to result in highest count rates in previous biophoton work performed (Ahmad et al., 2013; Michelle Le et al., 2015).

In the cases where 4 million cells were used with a 340nm filter, interesting results were shown in **Figures 20, 21, and 22** around varying the dose rate or intensity of damage to the count rate of cell luminescence as well as testing

cell luminescence immediately following radiation damage. However, there were no notable changes across these experiments and results could be followed up with using different cell densities to confirm these findings or to see any patterns thereof.

## **7 Radiation Induced Bystander Effects and BioPhoton Cell-Cell Signalling**

### **7.1 Radiation Induced Bystander Effects and BioPhoton Emission**

#### **Quantification Materials and Methods**

In order to observe any effects of cell communication from BioPhotons after incident gamma irradiation, primary considerations must first be made to develop an experimental apparatus to host the cells. First, a light tight box containing black paper inside was used as a holder for all cells, direct irradiated and reporters. There was a lid on top of the box that could be easily opened and closed moderately tightly in order to place and retrieve cells. The reporter cells were to made taped with a very thin, clear piece of tape to the inside top center of the box, which will sit directly below the source opening with heavy lead shielding (which will be discussed further below) place in between the radiation source and those cells.

Next, 4 larger T75 flasks containing 300,000 cells would be placed at  $\sim 45^\circ$  angles at the sides of the box, without shielding at the top. Geometry was an important

consideration to minimize  $\frac{1}{r^2}$  photon density distribution and maximize fluence.

The trade-off was that the cells had to be placed far enough to be exposed by full intensity gamma radiation while being close enough to the shielded reporter flasks to minimize the inverse square dependence of distance for UV photon dose. A distance of ~4-10cm was achieved (4cm being the closest and 11cm being at the bottom ends of the flasks). After taking into account the type of box used, the shielding, and geometry, the next consideration was dose of gamma radiation to be delivered to the directly irradiated flasks. In previous work (Michelle Le et al., 2015) it was observed that as the radiation dose increased, the BioPhoton emission will also increase. However, this dose delivered is another trade-off with the fifth consideration, temperature, because the cells are being irradiated in a room with ambient temperature ~22°-26°, which is much colder than the standard incubation temperature of 37.5° Celsius. Therefore the cells should be irradiated with exposure times less than around 25-35 minutes, as above this time the cells will reach a low enough temperature where cell function can be compromised. Finally, the sixth consideration was the number of cells to seed in the directly irradiated flasks. Previous research has shown that seeding numbers above 2000 cells/cm<sup>2</sup> would reduce the UV photon damage received by the reporter flasks (Michelle Le et al., 2015). To maximize the photon output while keeping a consistent cell density within this boundary, large T75 flasks (Falcon) were used with surface area ~75cm<sup>2</sup> which is almost an additional 20 cm<sup>2</sup> cell growth area, or 25% larger, cell growth



area than the petri dishes used in the previous research. Additionally, in contrast to the previous research done, there were 4 of the 75cm<sup>2</sup> Flasks used as directly irradiated flasks in these experiments compared to 1 petri dish at 56.5cm<sup>2</sup> (Falcon).

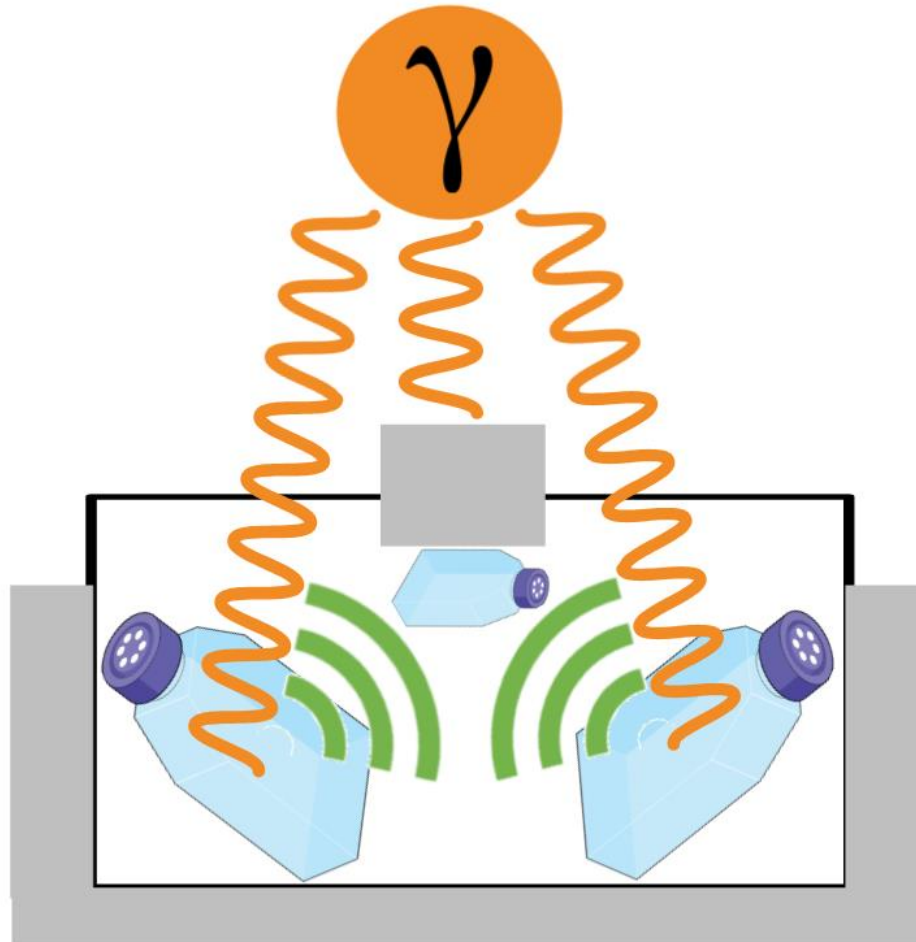


Figure 23: Schematic of flask arrangement to perform crude testing of cell-cell signalling through UV BioPhotons. Grey color here represents shielding, whereas black represents the enclosed case that was kept dark during measurements. The orange color represents gamma irradiation and the green represents potential BioPhoton signals.



Figure 24: A layout of the flasks before the top cover was placed directly over the rest of the enclosure.

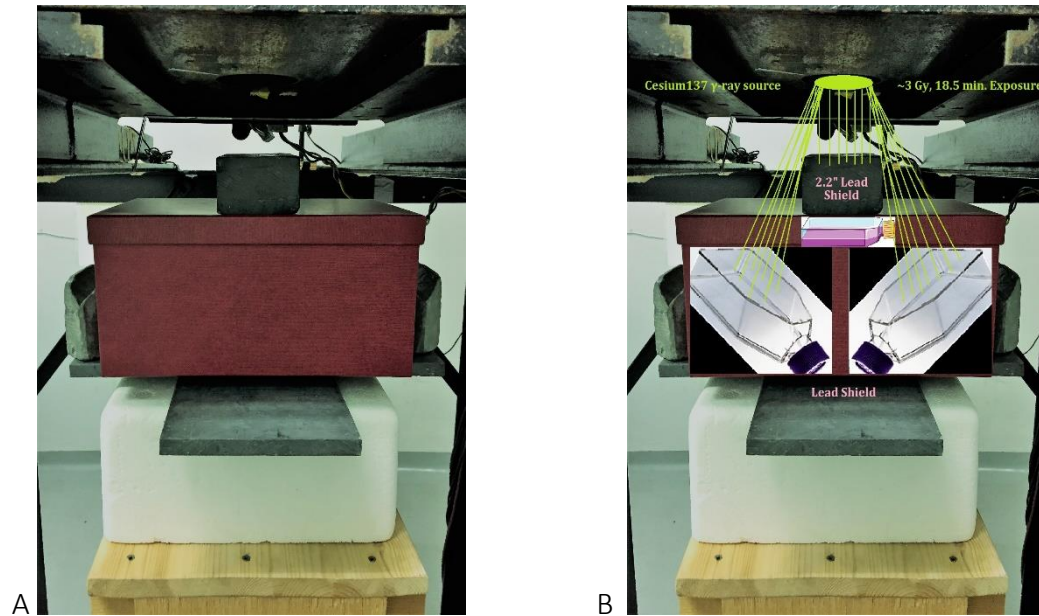


Figure 25: A shows the direct setup of the experiment just before irradiation, including the shielding placement. B shows a rough schematic using stock images of how the flasks were placed relative to the Cesium 137 radiation source opening.

The distance from the flasks to the radiation source was chosen to be 30cm, with a dose rate of  $\sim 0.211$  Gy/min. Appropriate shielding was estimated using lead blocks surrounding the flask enclosure. To define shielding, the Tenth Value Layer (TVL) was looked at which is defined as the thickness needed to reduce radiation intensity to 1/10 of the original value. The equation given:

$$TVL = \frac{2.3}{\mu} = \frac{2.3}{(\mu/\rho)\rho}$$

(U.S NRC Regulatory Documents – Basic Health Physics – 32 Shielding Radiation;

Research University of Cincinnati – Isotopes: Cs137)

Represents the TVL for any source where  $\mu/\rho$  is the mass attenuation coefficient ( $\text{cm}^2/\text{g}$ ) and  $\rho$  is the density of the shielding material. For Cs-137 shielded by lead (Pb), the thickness required for 1 TVL is approximately 0.9". In all experiments it was decided that 2.2" of lead (or 2.44 TVL) will be used to shield directly above (and directly below the Cs137 radiation source opening) of the "unirradiated reporter flasks". The sides will be partially shielded with ~2" of lead, and the bottom will be shielded with 1"-2" of lead (2" directly below the reporter flasks).

For a Cs-137 1 kCi  $\gamma$ -Source at ~27.1 cm away there is a general uniform photon distribution within marginal error of 3% (estimations for error based on error from 20.3 cm distance). The build-up factors for  $\gamma$ -energies over 500 keV were calculated using Taylor's form:

$$B(x) = A(E, Z) \cdot e^{-a_1(E, Z)x} + (1 - A(E, Z)) \cdot e^{-a_2(E, Z)x}$$

(McMaster University Radiation Sciences Graduate Program – Medical Physics 775 Byun S H, 2016)

For an assumed point isotropic source, the equation used for finding the reduced dose based on a given thickness of lead shielding is:

$$\dot{D}' = \dot{D} \cdot B \cdot e^{-\mu R} ; \quad \text{Where } \dot{D} = \frac{\Gamma \cdot A}{d^2}$$

This equation shows that the dose rate (in Gy) after shielding is equal to the original dose rate (without shielding) multiplied with the build-up factor, and an exponential attenuation containing the linear attenuation coefficient for shielding material ( $\mu$ , in  $\text{cm}^{-1}$ ) and the thickness of the shield ( $R$ ). The original dose rate is a product of Activity of the source and specific gamma constant ( $\Gamma = 0.33$  for  $\text{Cs137}$ ) divided by the square of the distance from the source. Both the build up factor  $B$  and linear attenuation coefficient  $\mu$  are found in respective tables based on lead (Pb) shielding.

From the calculations above it was found that based off of 2.4 TVLs (or 2.2" of Pb shielding) would result in 6142 mR/h exposure =  $1.706 \times 10^{-5}$  Gy/s. This would result in  $\sim 10$  mGy dose to cells in  $\sim 10$  minutes exposure.

Another consideration was that in a gamma field contained within a closed room as this setup, there will be stray gamma rays from backscatter against the walls or other surfaces. The gamma rays after scatter are dependent on the scattering angle,  $\theta$ .

Most of the gammas hitting any wall will require at least  $120^\circ$  scattering angle in order to reach the unirradiated reporter flasks in the areas where shielding is not

present, reducing the gamma energy to 250 keV or less, roughly 1/3 of its original energy (Nuclear Physics Compton Scattering Calculators, 2019).

## 7.2 Results

The results in **Figure 26** and **Figure 27** represent the outcome from the biophoton experiments. A positive control was attempted in order to try to confirm that the HCT p53 +/+ and p53 -/- cells were functioning in a manner relative to what was generally seen in this lab before. The positive controls are represented in each **Figure 26 and 27** by CCCM and ICCM which mean Irradiated Cell Control Conditioned Medium and Irradiated Cell Conditioned Medium. This would mean that the CCCM was the clonogenic survival control for the bystander effect, having received medium transfer from cells that were not irradiated and remained healthy, and ICCM is the clonogenic survival of the cells that had received medium bathing previously irradiated cells (receiving ~2Gy at a time of 1 hour prior to medium transfer). The results for HCT p53+/+ for this positive control show an approximately 13% decrease in survival from the bystander effect compared to the control. The results for the HCT p53-/- show no difference in survival between the CCCM and ICCM. These two results are relatively consistent with previous findings

For the BioPhoton Cell-Cell Communication of HCT p53+/+, it is shown that compared to the control of flasks only (no cells) on the signalling end, the clonogenic survival of cells that were “signalled” by flasks of 200,000 cells receiving ~3Gy of direct gamma irradiation were higher by 6%. In contrast, for the HCT p53-/-, there was no difference between the control flask only signals versus the flasks with cells signalling to the shielded reporter cells.

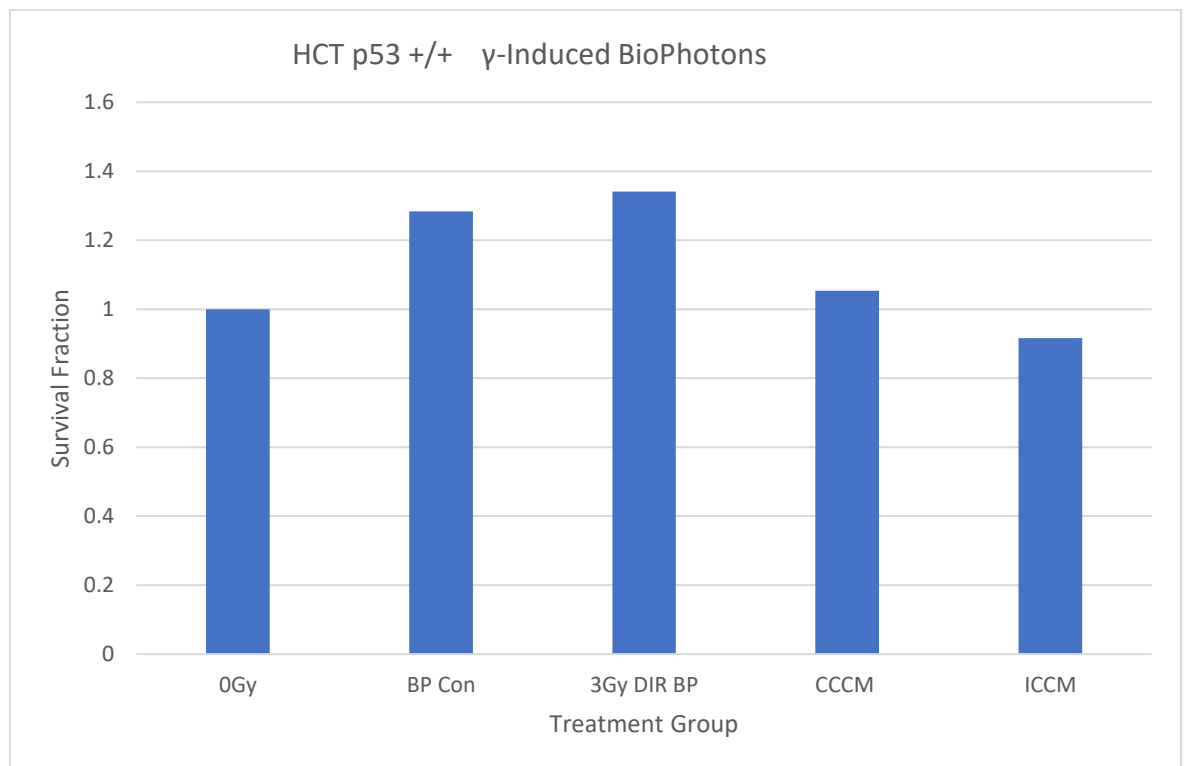


Figure 26: HCT116 p53+/+ summary of experimental results, n=9, 3 independent trials. 0Gy control is completely unirradiated, control plating efficiency, BP Con is the BioPhoton control of flasks only signalling to 500 shielded reporter cells, 3Gy DIR BP

is flasks containing 200,00 cells receiving ~3Gy Direct irradiation to signal towards 500 shielded reporter cells, and CCCM and ICCM are the bystander medium transfer positive controls. The graph is representing the survival fraction on according to various treatments.

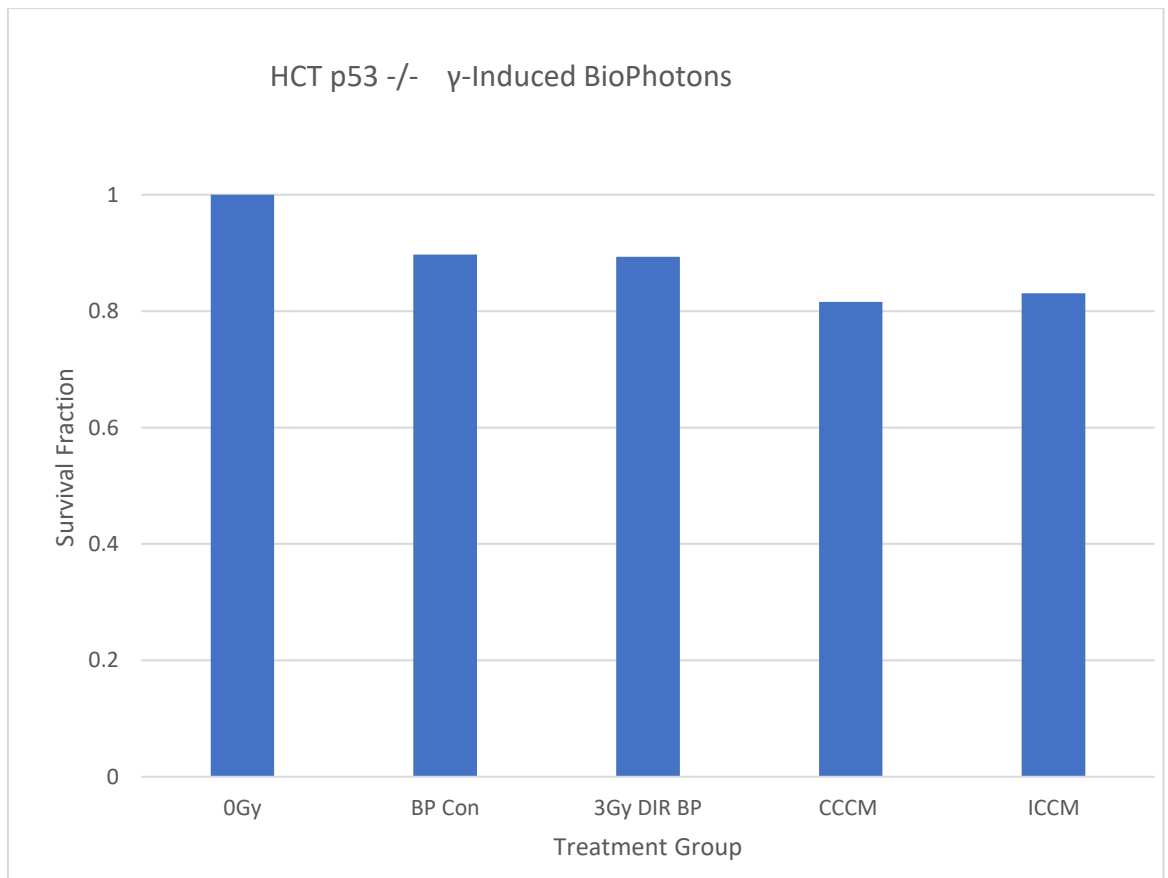


Figure 27: HCT116 p53-/- summary of experimental results, n=9, 3 independent trials. 0Gy control is completely unirradiated, control plating efficiency, BP Con is the



BioPhoton control of flasks only signalling to 500 shielded reporter cells, 3Gy DIR BP is flasks containing 200,00 cells receiving ~3Gy Direct irradiation to signal towards 500 shielded reporter cells, and CCCM and ICCM are the bystander medium transfer positive controls. The graph is representing the survival fraction on according to various treatments.

### 7.3 Discussion

HCT116 p53+/+ cells, which have been previously shown to have a strong bystander response through both cellular medium via medium transfer techniques as well as BioPhoton signalling through chronic exposure to Triated  $\beta^-$  irradiation, were explored in this study to test whether acute gamma irradiation can induce a significant enough UV emission to cause a change in cell survival in unirradiated reporters (M. Le, Mothersill, Seymour, Rainbow, & McNeill, 2017). As explained above, positive controls were set up as it has been previously shown that this cell line with a p53 wild-type presence has significant changes in cell survival from bystander medium transfer experiments. There was a difference in cell survival between the CCCM, or control conditioned cell medium (medium transfer to reporter flasks where there was no irradiation involve to the donor flasks), and the

ICCM, or irradiated cell conditioned medium, where 200,000 donor cells were irradiated with 1.5Gy and then the medium was transferred to the reporter cells one hour later. This difference is shown in the **Figure 26** and was ~10%.

For the testing of whether irradiated cells would be able to communicate damage from radiation through UV photons, which would in turn damage unirradiated reporter cells enough to be an observed effect in the clonogenic survival of HCT116 p53+/, it can be seen there was a 6% non-significant increase in cell survival between the BP Con, which is the control representing reporter flasks exposed to irradiated Falcon flasks without any cells present to be directly irradiated, and the 3Gy DIR BP, which is the set of the reporter flasks which have been exposed to cells directly irradiated with an acute dose of ~3Gy in 18min. Additionally, the HCT116 p53-/- had shown no difference in clonogenic survival of the reporter cells signalled by the 200,000cells irradiated by 3Gy (3Gy DIR BP), compared to the control which were exposed to only empty flasks without cells present.

## 8 Future Directions

In the pre-/post-conditioning work, there are many endpoints and even more modifications to the experiments to gather more information and insights in the mechanisms and patterns. For one, flow cytometry could be used to investigate cell cycle stage relationship to pre-/post-conditioning. Another important factor aside from cell cycle, is investigating cell density and how cell density may affect the relative response mechanisms and signalling of cells. Furthermore, and also alluded to in the publication shown in this thesis, investigating type of radiation and/or dose-rate on pre-/post-conditioning would show insight and possibly result in the normalization of the adaptive response across different radiation research modalities.

Following up on the Western Blotting on protein expression, creating a western blot procedure at the time 5 hours after the priming dose of radiation (for pre-conditioning this is when the adaptive effects are likely to kick-in) and/or right after the priming dose for post-conditioning, may show more and provide enhanced results, as opposed to the work in the current thesis which had utilized the blotting procedure at a quite a bit later than that.

For the experiments of using a photon counter to detect cell-luminescence as a

result of direct irradiation, there are many parameters that can be changed and considered. Of such parameters, considering the utilization of more shielding and the placement of shielding around the detector, while ensuring the cells are still receiving the right dose of radiation, will be paramount in reducing background counts. Additionally, using more filters and cell densities may help to map out further patterns in cell luminescence and to relate to and confirm previous findings.

The experiments of the BioPhoton cell-cell signalling were only one arrangement of a large potential of arrangements of the system. Creating a new apparatus or geometry to irradiate cells while keeping them as close as possible to the unirradiated reporter cells would result in a better possibility of seeing effects, as the  $\frac{1}{r^2}$  photon density distribution decreases. The use of reflective mirrors could be a useful application in order to create more concentrated BioPhoton signals to reach either reporter cells or a photon detector. The purpose of the mirror would be to project BioPhotons that are emitted in all directions from an irradiated flask, and then direct the BioPhotons to the target (reporter cells or detector) which were not on an original path towards that target. The most important consideration when using a mirror is its reflectance. Normally mirrors sold for everyday purposes have a glass surface, or substrate, with a sheet of aluminum underneath, which could result in much of the UV photons being absorbed and not effectively transmitted. Lab purpose mirrors such as first surface mirrors which have a high reflectance coating on the first surface and therefore incoming photons do not need

to pass through another material first before being reflected or enhanced metal coating, can be quite useful in these applications (Edmund Optics Resources - Metallic Mirror Coatings, 2019). Additionally, dielectric mirrors, or enhanced metal coatings, can also enhance the reflectance (Edmund Optics Resources - Metallic Mirror Coatings, 2019). The chart below shows below that DUV Aluminum would be ideal for increased reflectance from 120-400nm wavelength range.

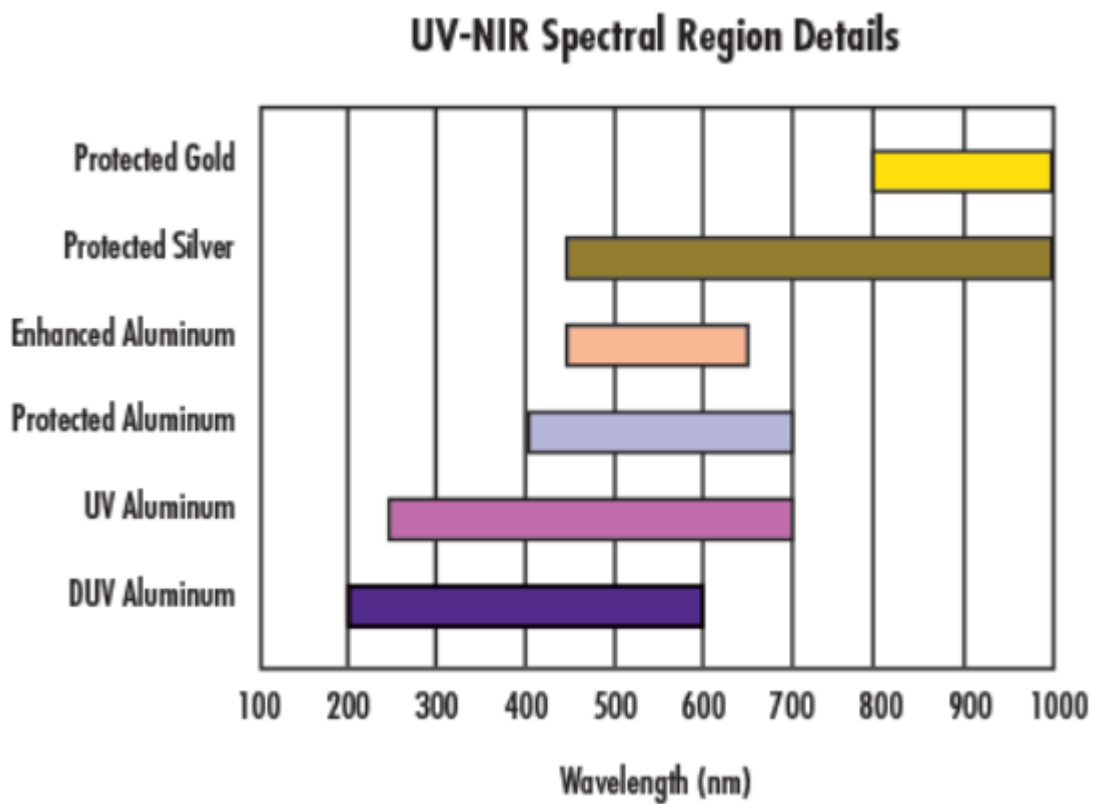


Figure 28: UV-NIR Spectrum and the most suitable reflecting materials as provided by the Edmund Optics Company

Additionally, exposing the cells for a longer, chronic period of time to radiation while keeping them in appropriate temperature conditions would be optimal, especially to follow off of previous BioPhoton experiments where the tritium irradiated cells were chronically irradiated and signalling to the reporter cells while in the incubator for 24 hour periods.

## 9 References

Ahmad, S.B. "SIGNIFICANCE OF ION INDUCED LUMINESCENCE FOR RADIATION INDUCED BYSTANDER EFFECTS" PhD Thesis Dissertation, McMaster University, 2012.  
<https://macsphere.mcmaster.ca/bitstream/11375/14804/1/fulltext.pdf>

Ahmad, S. B., McNeill, F. E., Byun, S. H., Prestwich, W. V., Mothersill, C., Seymour, C., Fernandez, C. (2013). Ultra-violet light emission from hpv-g cells irradiated with low let radiation from 90Y; consequences for radiation induced bystander effects. *Dose-Response*, 11(4), 498–516. <https://doi.org/10.2203/dose-response.12-048.ahmad>

Aimo A, Borrelli C, Giannoni A, Pastormerlo LE, Barison A, Mirizzi G, Emdin M, Passino C (2015). Cardioprotection by remote ischemic conditioning: Mechanisms and clinical evidences. *World J Cardiol* 7(10):621-632.

Audette-Stuart M, Yankovich T (2011). Bystander effects in bullfrog tadpoles. *Radioprotection* 46:S497– S502.

Azzam EI, Raaphorst GP, Mitchel RE (1994). Radiation-induced adaptive response for protection against micronucleus formation and neoplastic transformation in C3H 10T1/2 mouse embryo cells. *Radiat Res* 138(1 Suppl):S28–31.

Boreham, D. Adaptive Response: Modulation of Response by Low Dose Diagnostic Radiation, Exercise, and Diet. *Dose Response Conference* 2015.

Boukamp P, Petrussevska R, Breitkreut D, Hornung J, Markham A, Fusenig N (1988). Normal keratinization in a spontaneously immortalized aneuploid human keratinocyte cell line. *The journal of cell biology*, 106(3):761-771.

Brattain MG, Fine WD, Khaled FM, Thompson J, Brattain DE (1981). Heterogeneity of malignant cells from a human colonic carcinoma. *Cancer Res* 41(5):1751-1756.

Bunz F, Dutriaux A, Lengauer C, Waldman T, Zhou S, Brown JP, Sedivy JM, Kinzler KW, Vogelstein B (1998). Requirement for p53 and p21 to sustain G2 arrest after DNA damage. *Science* 282:1497-1501.

Cai L, Yang G, Yu D, Li W, Zhao Y, Wen X, Liang X, Zhang X, Zhou L, Hu J, Niu C, Tian H, Han F, Chen X, Dong L, Cui J. Distinct Biological Effects of Low-dose Radiation on Normal and Cancerous Human Lung Cells Are Mediated by ATM Signaling. *Oncotarget* 2016; 7(44): 71856-71872.

Calabrese EJ, Bachmann KA, Bailer AJ, Bolger PM, Borak J, Cai L, Cedergreen N, Cherian MG, Chiueh CC, Clarkson TW, Cook RR, Diamond DM, Doolittle DJ, Dorato

MA, Duke SO, Feinendegen L, Gardner DE, Hart RW, Hastings KL, Hayes AW, Hoffmann GR, Ives JA, Jaworowski Z, Johnson TE, Jonas WB, Kaminski NE, Keller JG, Klaunig JE, Knudsen TB, Kozumbo WJ, Lettieri T, Liu SZ, Maiseu A, Maynard KI, Masoro EJ, McClellan RO, Mehendale HM, Mothersill C, Newlin DB, Nigg HN, Oehme FW, Phalen RF, Philbert MA, Rattan SI, Riviere JE, Rodricks J, Sapolsky RM, Scott BR, Seymour C, Sinclair DA, Smith-Sonneborn J, Snow ET, Spear L, Stevenson DE, Thomas Y, Tubiana M, Williams GM, Mattson MP (2007). Biological stress response terminology: Integrating the concepts of adaptive response and preconditioning stress within a hormetic dose-response framework. *Toxicol Appl Pharmacol* 222(1):122-128.

Calabrese EJ, Mattson MP (2017). How does hormesis impact biology, toxicology, and medicine? *Aging and Mechanisms of Disease*, 3:13

Conceptual Physics, Decay Level Scheme of Cesium-137. 2014.

<http://www.conceptualphysicstoday.com/2014/04/decay-level-scheme-of-cs-137.html>. Retrieved on September 2018.

Day TK, Zeng G, Hooker AM, Bhat M, Scott BR, Turner DR, Sykes PJ (2006). Extremely Low Priming Doses of X Radiation Induce an Adaptive Response for Chromosomal Inversions in pKZ1 Mouse Prostate. *Radiat Res* 166:757–766.



Day TK, Zeng G, Hooker AM, Bhat M, Scott BR, Turner DR, Sykes PJ (2007). Adaptive response for chromosomal inversions in pKZ1 mouse prostate induced by low doses of X radiation delivered after a high dose. *Radiat Res* 167:682–692.

de Toledo SM, Asaad N, Venkatachalam P, Li L, Howell RW, Spitz DR, Azzam EI (2006). Adaptive responses to low-dose/ low-dose-rate gamma rays in normal human fibroblasts: The role of growth architecture and oxidative metabolism. *Radiat Res* 166:849–857.

Enns L, Bogen KT, Wizniak J, Murtha AD, Weinfeld M (2004). Low-Dose Radiation Hypersensitivity Is Associated With p53-Dependent Apoptosis. *Mol Cancer Res* 2(10):557-566.

Fernandez-Palomo C, Seymour C, Mothersill C (2016). Inter-relationship between low-dose hyperradiosensitivity and radiation-induced bystander effects in the human T98G glioma and the epithelial HaCaT cell line. *Radiat Res* 185(2):124-133.

Guéguen, Y., Bontemps, A., & Ebrahimian, T. G. (2019). Adaptive responses to low doses of radiation or chemicals: their cellular and molecular mechanisms. *Cellular and Molecular Life Sciences*, 76(7), 1255–1273. <https://doi.org/10.1007/s00018-018-2987-5>

Hamada, N., Matsumoto, H., Hara, T., & Kobayashi, Y. (2007). Intercellular and intracellular signaling pathways mediating ionizing radiation-induced bystander

effects. *Journal of Radiation Research*, 48(2), 87–95.

<https://doi.org/10.1269/jrr.06084>

Henseleit U, Zhang J, Wanner R, Haase I, Kolde G, Rosenbach T (1997). Role of p53 in UVB-induced apoptosis in human HaCaT keratinocytes. *J Invest Dermatol* 109:722–727.

Ikushima, T. (1987). Chromosomal responses to ionizing radiation reminiscent of and adaptive response in cultured Chinese hamster cells. *Mutation Research - Fundamental and Molecular Mechanisms of Mutagenesis*, 180(2), 215–221.

[https://doi.org/10.1016/0027-5107\(87\)90217-X](https://doi.org/10.1016/0027-5107(87)90217-X)

Joiner, A. M. C., & Johns, H. (2019). Renal Damage in the Mouse : The Response to Very Small Doses per Fraction Published by : Radiation Research Society Stable URL : <https://www.jstor.org/stable/3577233> REFERENCES Linked references are available on JSTOR for this article : You may need to lo. 114(2), 385–398.

Joiner, M. C., Denekamp, J., & Maughan, R. L. (1985). The use of “top-up” experiments to investigate the effect of very small doses per fraction in mouse skin. *International Journal of Radiation Biology*, 49(4), 565–580.

<https://doi.org/10.1080/09553008514552811>

Kamaraj B, Bogaerts A (2015). Structure and Function of p53-DNA Complexes with Inactivation and Rescue Mutations: A Molecular Dynamics Simulation Study. *PLoS One* 10(8):e0134638.

Le M, Fernandez-Palomo C, McNeill FE, Seymour CB, Rainbow AJ, Mothersill CE (2017a). Exosomes are released by bystander cells exposed to radiation-induced biophoton signals: Reconciling the mechanisms mediating the bystander effect. *PLoS One* 12(3):e0173685.

Le, M., Mothersill, C. E., Seymour, C. B., Rainbow, A. J., & McNeill, F. E. (2017). An Observed Effect of p53 Status on the Bystander Response to Radiation-Induced Cellular Photon Emission. *Radiation Research*, 187(2), 169–185.  
<https://doi.org/10.1667/rr14342.1>

Le, Michelle, McNeill, F. E., Seymour, C., Rainbow, A. J., & Mothersill, C. E. (2015). An Observed Effect of Ultraviolet Radiation Emitted from Beta-Irradiated HaCaT Cells upon Non-Beta-Irradiated Bystander Cells. *Radiation Research*, 183(3), 279–290.  
<https://doi.org/10.1667/rr13827.1>

Lehman TA, Modali R, Boukamp P, Stanek J, Bennett WP, Welsh JA, Metcalf RA, Stampfer MR, Fusenig N, Rogan EM, Hurries CC (1993). p53 mutations in human immortalized epithelial cell lines. *Carcinogenesis* 14:833–839.

Lemon JA, Phan N, Boreham DR (2017a). Multiple CT scans extend lifespan by delaying cancer progression in cancer-prone mice. *Radiat Res* 188(4.2):492-504.

Lemon JA, Phan N, Boreham DR (2017b). Single CT Scan Prolongs Survival by Extending Cancer Latency in Trp53 Heterozygous Mice. *Radiat Res* 188(4.2):505-511.

Lin PS, Wu A (2005). Not all 2 Gray radiation prescriptions are equivalent: Cytotoxic effect depends on delivery sequences of partial fractionated doses. *Int J Radiat Oncol Biol Phys* 63(2):536-544.

Liu, Z., Mothersill, C. E., McNeill, F. E., Lyng, F. M., Byun, S. H., Seymour, C. B., & Prestwich, W. V. (2006). A Dose Threshold for a Medium Transfer Bystander Effect for a Human Skin Cell Line. *Radiation Research*, 166(1), 19–23.  
<https://doi.org/10.1667/rr3580.1>

Maguire P, Mothersill C, McClean B, Seymour C, Lyng FM (2007). Modulation of radiation responses by pre-exposure to irradiated cell conditioned medium. *Radiat Res* 167(4):485-492.

Maguire, P., Mothersill, C., Seymour, C., & Lyng, F. M. (2006). Medium from Irradiated Cells Induces Dose-Dependent Mitochondrial Changes and BCL2 Responses in Unirradiated Human Keratinocytes. *Radiation Research*, 163(4), 384–390.  
<https://doi.org/10.1667/rr3325>

Marples B, Joiner MC (1995). The elimination of low-dose hypersensitivity in Chinese hamster V79-379A cells by pretreatment with X rays or hydrogen peroxide. *Radiat Res* 141(2):160-169.

Marples, B., & Joiner, M. C. (1993). The response of Chinese hamster V79 cells to low radiation doses: evidence of enhanced sensitivity of the whole cell population.

Radiation Research, 133(1), 41–51. Retrieved from

<http://www.ncbi.nlm.nih.gov/pubmed/8434112>

Marples, B., Wouters, B. G., & Joiner, M. C. (2006). An Association between the Radiation-Induced Arrest of G<sub>2</sub>-Phase Cells and Low-Dose Hyper-Radiosensitivity: A Plausible Underlying Mechanism? *Radiation Research*, 160(1), 38–45.

<https://doi.org/10.1667/rr3013>

Marples, B., Wouters, B. G., Collis, S. J., Chalmers, A. J., & Joiner, M. C. (2006). Low-Dose Hyper-radiosensitivity: A Consequence of Ineffective Cell Cycle Arrest of Radiation-Damaged G<sub>2</sub>-Phase Cells. *Radiation Research*, 161(3), 247–255.

<https://doi.org/10.1667/rr3130>

Matsumoto H, Hayashi S, Hatashita M, et al (2001). Induction of radioresistance to accelerated carbon-ion beams in recipient cells by nitric oxide excreted from irradiated donor cells of human glioblastoma. *Int J Radiat Biol*, 76:1649–57.

Matsumoto H, Hayashi S, Hatashita M, Ohnishi K, Shioura H, Ohtsubo T, Kitai R, Ohnishi T, Kano E (2001). Induction of radioresistance by a nitric oxide-mediated bystander effect. *Radiat Res* 155:387–396.

Matsumoto H, Hayashi S, Hatashita M, Shioura H, Ohtsubo T, Kitai R, Ohnishi T, Yukawa O, Furusawa Y, Kano E (2000). Induction of radioresistance to accelerated carbon-ion beams in recipient cells by nitric oxide excreted from irradiated donor cells of human glioblastoma. *Int J Radiat Biol* 76:1649–1657.

Matsumoto H, Takahashi A, Ohnishi T (2007). Nitric oxide radicals choreograph a radioadaptive response. *Cancer Res* 67:8574–8579.

Matsumoto, H., Hayashi, S., Hatashita, M., Ohnishi, K., Shioura, H., Ohtsubo, T., ... Kano, E. (2006). Induction of Radioresistance by a Nitric Oxide-Mediated Bystander Effect. *Radiation Research*, 155(3), 387–396.

Matsumoto, H., Takahashi, A., & Ohnishi, T. (2005). Radiation-Induced Adaptive Responses and Bystander Effects. *Biological Sciences in Space*, 18(4), 247–254.  
<https://doi.org/10.2187/bss.18.247>

Matsumoto, H., Takahashi, A., & Ohnishi, T. (2007). Nitric oxide radicals choreograph a radioadaptive response. *Cancer Research*, 67(18), 8574–8579.  
<https://doi.org/10.1158/0008-5472.CAN-07-1913>

McMaster, Scott. Manager, McMaster Accelerator Laboratory. McMaster University Taylor Radiobiology Source Cs-137 Source Check Documents.

Michelle Le, “INVESTIGATING THE GENERATION OF BIOPHOTONS INDUCED BY LOW-DOSE BETA-IRRADIATION AND THEIR ROLE IN THE RADIATION-INDUCED BYSTANDER EFFECT” PhD Thesis Dissertation, McMaster University, 2017.  
[https://macsphere.mcmaster.ca/bitstream/11375/22773/4/Le\\_Michelle\\_2017December\\_PhDRadiationBiology.pdf](https://macsphere.mcmaster.ca/bitstream/11375/22773/4/Le_Michelle_2017December_PhDRadiationBiology.pdf).

Miller RC, Murley JS, Rademaker AW, Woloschak GE, Li JJ, Weichselbaum RR, Grdina DJ (2016). Very low doses of ionizing radiation and redox associated modifiers affect survivin-associated changes in radiation sensitivity. *Free Radic Biol Med* 99:110-119.

Mitchel RE, Jackson JS, McCann RA, Boreham DR (1999). The adaptive response modifies latency for radiation-induced myeloid leukemia in CBA/H mice. *Radiat Res* 152:273–279.

MIURA, Y. (2004). Oxidative Stress, Radiation-Adaptive Responses, and Aging. *Journal of Radiation Research*, 45(3), 357–372. <https://doi.org/10.1269/jrr.45.357>

Mothersill C, Seymour C. Radiation-induced bystander effects and adaptive responses – the Yin and Yang of low dose radiobiology? *Mutation Research/Fundamental and Molecular Mechanisms of Mutagenesis* 2004; 568(1): 121-128.

Mothersill C, Bristow RG, Harding SM, Smith RW, Mersov A, Seymour CB (2011). A role for p53 in the response of bystander cells to receipt of medium borne signals from irradiated cells. *Int J Radiat Biol* 87(11):1120-1125.

Mothersill C, Seymour C, Fernandez-Palomo C. Inter-Relationship between Low-Dose Hyper-Radiosensitivity and Radiation Induced Bystander Effects in the Human T98G Glioma and the Epithelial HaCaT Cell Line. *Radiation Research* 2016; 185(2):124-133.

Mothersill C, Seymour C (2004). Radiation-induced bystander effects—implications for cancer. *Nat Rev Cancer.*, 4(2): 158-164.

Mothersill C, Seymour CB (1993). Recovery of the radiation survival curve shoulder in CHO-K1, XRS-5 and revertant XRS-5 populations. *Mutat Res* 285(2):259-266.

Mothersill C, Seymour, C, Joiner, M. Relationship between Radiation-Induced Low-Dose Hypersensitivity and the Bystander Effect. *Radiation Research* 2002; 157(5):526-532.

Mothersill C, Smith R, Wang J, Rusin A, Fernandez-Palomo C, Fazzari J, Seymour C (2018). Biological Entanglement-Like Effect After Communication of Fish Prior to X-Ray Exposure. *Dose Response*, 16(1): 1-17

Mothersill, C. (1997). Medium from irradiated human epithelial cells but not human fibroblasts reduces the clonogenic survival of unirradiated cells. *International Journal of Radiation Biology*, 71(4), 421–427. Retrieved from <http://informahealthcare.com/doi/abs/10.1080/095530097144030>

Mothersill, Carmel, & Seymour, C. B. (2006a). Bystander and Delayed Effects after Fractionated Radiation Exposure. *Radiation Research*, 158(5), 626–633. [https://doi.org/10.1667/0033-7587\(2002\)158\[0626:badeaf\]2.0.co;2](https://doi.org/10.1667/0033-7587(2002)158[0626:badeaf]2.0.co;2)

Mothersill, Carmel, & Seymour, C. B. (2006b). Cell-Cell Contact during Gamma Irradiation Is Not Required to Induce a Bystander Effect in Normal Human Keratinocytes: Evidence for Release during Irradiation of a Signal Controlling Survival into the Medium. *Radiation Research*, 149(3), 256. <https://doi.org/10.2307/3579958>



Mothersill, Carmel, Seymour, C. B., & Joiner, M. C. (2002). Relationship between radiation-induced low-dose hypersensitivity and the bystander effect. *Radiation Research*, 157(5), 526–532. Retrieved from <http://www.ncbi.nlm.nih.gov/pubmed/11966318>

Mousa, A., Kusminarto, K., & Suparta, G. B. (2017). A new simple method to measure the X-ray linear attenuation coefficients of materials using micro-digital radiography machine. *International Journal of Applied Engineering Research*, 12(21), 10589–10594.

Murley J, Miller R, Weichselbaum R, Grdina D (2017). TP53 Mutational Status and ROS Effect the Expression of the Survivin-Associated Radio-Adaptive Response. *Radiat Res* 188(5):579-590.

Murley J, Miller R, Weichselbaum R, Grdina D. TP53 control of the survivin-mediated radio-adaptive response in human tumors. *Cancer Res* 2017; 77(13).

Murley JS, Arbiser JL, Weichselbaum RR, Grdina DJ (2018). ROS modifiers and NOX4 affect the expression of the survivin-associated radio-adaptive response. *Free Radic Biol Med* 123:39-52.

Murley, J. S., Miller, R. C., Weichselbaum, R. R., & Grdina, D. J. (2017). TP53 Mutational Status and ROS Effect the Expression of the Survivin-Associated Radio-Adaptive Response. *Radiation Research*, 188(5), 659–670. <https://doi.org/10.1667/rr14831.1>

Ojima, M., Eto, H., Ban, N., & Kai, M. (2011). Radiation-induced bystander effects induce radioadaptive response by low-dose radiation. *Radiation Protection Dosimetry*, 146(1–3), 276–279. <https://doi.org/10.1093/rpd/ncr169>

Olivier, Gregorio, Bodycote, Judy, Wolff, Sheldon (1984). Adaptive Response of Human Lymphocytes to Low Concentrations of Radioactive Thymidine. *Science*, 223(4636), 594–597.

Paglia, Pasquale, & Penna, Claudia (2011). Cardiac Postconditioning. *Antioxidants & Redox Signaling*. 14(5).

Paraswania N, Thohb M, Bhilwadeb H, Ghosha A. Early antioxidant responses via the concerted activation of NF- $\kappa$ B and Nrf2 characterize the gamma-radiation-induced adaptive response in quiescent human peripheral blood mononuclear cells. *Mutation Research/Genetic Toxicology and Environmental Mutagenesis* 2018; 831:50-61.

Parkins, C. S., & Fowler, J. F. (1986). The linear quadratic fit for lung function after irradiation with X-rays at smaller doses per fraction than 2 Gy. *The British Journal of Cancer. Supplement*, 7, 320–323.

Popanda O, Zheng C, Magdeburg JR, Buttner J, Flohr T, Hagemüller E, Thielmann HW (2000). Mutation analysis of replicative genes encoding the large subunits of DNA polymerase alpha and replication factors A and C in human sporadic colorectal cancers. *Int J Cancer* 86:318–324.

Puck T, Marcus P (1956). Action of X-rays on mammalian cells. *J Exp Med* 103:653-666.

Ryan L, Joiner M, Seymour C, Mothersill C (2009). Radiation-induced adaptive response is not seen in cell lines showing a bystander effect but is seen in lines showing HRS/IRR response. *Int J Radiat Biol* 85(1):87-95.

Ryan LA, Seymour CB, O'Neill-Mehlenbacher A, Mothersill CE (2008). Radiation-induced adaptive response in fish cell lines. *J Environ Radioact* 99(4):739-747.

Ryan, L. A., Seymour, C. B., Joiner, M. C., & Mothersill, C. E. (2009). Radiation-induced adaptive response is not seen in cell lines showing a bystander effect but is seen in lines showing HRS/IRR response. *International Journal of Radiation Biology*, 85(1), 87–95. <https://doi.org/10.1080/09553000802635062>

Sanderson, B.J, Morley, A.A. (1986). Exposure of human lymphocytes to ionizing radiation reduces mutagenesis by subsequent ionizing radiation. *Mutat Res.* 164(6), 347–351.

Schmidt F, Rieger J, Wischhusen J, Naumann U, Weller M (2001). Glioma cell sensitivity to topotecan: the role of p53 and topotecan-induced DNA damage. *Eur J Pharmacol* 2001 412(1):21-25.

Short S, Mayes C, Woodcock M, Johns H, Joiner MC (1999). Low dose hypersensitivity in the T98G human glioblastoma cell line. *Int J Radiat Biol*, 75:847–55

Short, S. C., Bourne, S., Martindale, C., Woodcock, M., & Jackson, S. P. (2006). DNA Damage Responses at Low Radiation Doses. *Radiation Research*, 164(3), 292–302. <https://doi.org/10.1667/rr3421.1>

Smith D, Raaphorst G (2003). Adaptive responses in human glioma cells assessed by clonogenic survival and DNA strand break analysis. *International Journal of Radiation Biology*, 79:333-339.

Smith RW, Mothersill C, Hinton T, Seymour CB (2011). Exposure to low level chronic radiation leads to adaptation to a subsequent acute X-ray dose and communication of modified acute X-ray induced bystander signals in medaka (Japanese rice fish, *Oryzias latipes*). *Int J Radiat Biol* 87(10):1011-1022.

Snyder, A. R. (2004). Review of radiation-induced by bystander effects. *Human and Experimental Toxicology*, 23(2), 87–89. <https://doi.org/10.1191/0960327104ht423oa>

Stecca, C., & Gerber, G. B. (2002). Adaptive Response to DNA-Damaging Agents. *Biochemical Pharmacology*, 55(7), 941–951. [https://doi.org/10.1016/s0006-2952\(97\)00448-6](https://doi.org/10.1016/s0006-2952(97)00448-6)

Szumiel, I. (2005). Adaptive response: Stimulated DNA repair or decreased damage fixation? *International Journal of Radiation Biology*, 81(3), 233–241. <https://doi.org/10.1080/09553000500077047>

Tahara, M., Inoue, T., Sato, F., Miyakura, Y., Horie, H., Yasuda, Y., Sugano, K. (2014). The Use of Olaparib (AZD2281) Potentiates SN-38 Cytotoxicity in Colon Cancer Cells by Indirect Inhibition of Rad51-Mediated Repair of DNA Double-Strand Breaks. *Molecular Cancer Therapeutics*, 13(5), 1170–1180. <https://doi.org/10.1158/1535-7163.mct-13-0683>

Takahashi A (2001). Different inducibility of radiation- or heat-induced p53-dependent apoptosis after acute or chronic irradiation in human cultured squamous cell carcinoma cells. *Int J Radiat Biol* 277:215– 224.

Tang H, Chen L, Liu J, Shi J, Li Q, Wang T, Wu L, Zhan F, Bian P (2016). Radioadaptive Response for Reproductive Cell Death Demonstrated in In Vivo Tissue Model of *Caenorhabditis elegans*. *Radiat Res* 185(4):402-410.

Tanya D, Guoxin Z, Atony H, Madhava B, Bobby S, David T, Pamela S. Adaptive Response for Chromosomal Inversions in pKZ1 Mouse Prostate Induced by Low Doses of X Radiation Delivered after a High Dose. *Radiation Research* 2007: 167(6):682-692.

Tapio, S., & Jacob, V. (2007). Radioadaptive response revisited. *Radiation and Environmental Biophysics*, 46(1), 1–12. <https://doi.org/10.1007/s00411-006-0078-8>

Van Meir EG, Kikuchi T, Tada M, Li H, Diserens AC, Wojcik BE, Huang HJ, Friedmann T, de Tribolet N, Cavenee WK (1994). Analysis of the p53 gene and its expression in human glioblastoma cells. *Cancer Res* 54(3):649-652.

Vo NTK, Sokeechand BSH, Seymour CB & Mothersill CE (2017a). Characterizing responses to gamma radiation by a highly clonogenic fish brain endothelial cell line. *Environ Res* 156:297–305.

Vo NTK, Sokeechand BSH, Seymour CB, Mothersill CE (2017b). Influence of chronic low-dose/dose-rate high-LET irradiation from Radium-226 in a human colorectal carcinoma cell line. *Environ Res* 156:697-704.

Wodarz, D., Sorace, R., & Komarova, N. L. (2014). Dynamics of Cellular Responses to Radiation. *PLoS Computational Biology*, 10(4).

<https://doi.org/10.1371/journal.pcbi.1003513>

Wolff S (1998). The adaptive response in radiobiology: evolving insights and implications. *Environ Health Perspectives* 106(1):277-283.

Zhang Y, Coillie SV, Fang JY, Xu J (2016). Gain of function of mutant p53: R282W on the peak? *Oncogenesis* 5:e196.

## 10 Appendix A: Raw Data

### Pre-/Post-Conditioning Experiments:

#### 1. 5Gy HT29

	0Gy	5Gy	AR5	PC5
Trial 1	0.37	0.328	0.376	0.321
	0.394	0.296	0.321	0.332
	0.406	0.336	0.327	0.313
Trial 2	0.418	0.269	0.403	0.364
	0.404	0.381	0.333	0.324
	0.436	0.232	0.359	0.370
Trial 3	0.296	0.388	0.343	0.392
	0.256	0.329	0.427	0.308
	0.326	0.290	0.469	0.308
AVG	1.00	0.32	0.37	0.34
SEM	0.020	0.017	0.017	0.010
	0Gy	5Gy Control	Adaptive R	Post-Conditioning
AVG	100.0	31.7	37.3	33.7
SEM	2.0	1.7	1.7	1.0

#### 2.

<u>2Gy HCT+/-</u>	Plating Controls		Pre-Conditioning Group			Post-Conditioning Group			NOTES	NOTES
	0Gy	Sham	2Gy Only Control AR	5mGy-5h-2Gy	0.1Gy-5h-2Gy	2Gy Only Control PC	2Gy-5h-5mGy	2Gy-5h-0.1Gy	NOTES	NOTES
<b>TRIAL 1</b> Raw Counts	203	351	244	No data	215	195	No data	189		
	203	358	221	No data	210	149	No data	200		
	206	345	243	No data	214	163	No data	150		
Averaged Survival Fraction Trial 1		0.70	0.48	-	0.43	0.34	-	0.37		
<b>TRIAL 2</b> Raw Counts	170	180	80	58	53	50	73	70		
	174	170	84	57	50	58	74	72		
	190	196	80	86	72	46	66	70		
Averaged Survival Fraction Trial 2			0.56	0.46	0.40	0.35	0.49	0.49	< Trial 2 Survival Fraction was calculated using Trial 3 Sham PE	
<b>TRIAL 3</b> Raw Counts	169	138	79	67	80	64	78	78		
	180	146	86	70	112	80	79	80		
	164	150	101	83	76	85	72	74		
Averaged Survival Fraction Trial 3		0.29	0.61	0.51	0.62	0.53	0.53	0.53		
<b>TRIAL 4</b> Raw Counts	174	187	127	135	100	112	110	82		
	204	190	107	127	108	71	131	108		
	186	191	140	119	135	113	100	100		
Averaged Survival Fraction Trial 4		0.38	0.66	0.67	0.60	0.52	0.60	0.51		

**3.**

***T98G Data (collected in 2015)***

					Pre-Conditioning	Post-Conditioning	NOTES	NOTES	NOTES
		0Gy	Sham	4Gy Only Control	0.1Gy-3h-4Gy	4Gy-3h-0.1Gy	NOTES	NOTES	NOTES
<b>Trial 1</b>	Raw Counts			45	45	56			
				26	58	43			
				39	46	50			
	Averaged Survival Fraction Trial 1			0.29	0.40	0.40	← Trial 1 Survival Fraction was calculated using Trial 8 Sham PE		
<b>Trial 2</b>	Raw Counts	153	160	101	127	120			
		146	159	111	115	115			
		148	163	105	116	116			
	Averaged Survival Fraction Trial 2	0.30		0.35	0.40	0.39			
<b>Trial 3</b>	Raw Counts	70	60	43	22	67	Red highlight = excluded from analysis		
		61	69	42	30	56	Red highlight = excluded from analysis		
		80	62	57	20	56	Red highlight = excluded from analysis		
<b>Trial 4</b>	Raw Counts			71	22	63	Red highlight = excluded from analysis		
				73	14	41	Red highlight = excluded from analysis		
				75	24	58	Red highlight = excluded from analysis		
				59		69	Red highlight = excluded from analysis		
				68		68	Red highlight = excluded from analysis		
<b>Trial 5</b>	Raw Counts			83		59	Red highlight = excluded from analysis		
				58		60	Red highlight = excluded from analysis		
				76		53	Red highlight = excluded from analysis		



***T98G Data (collected in 2015)***

				Pre-Conditioning	Post-Conditioning	NOTES	NOTES	NOTES	
				0.1Gy-3h-4Gy	4Gy-3h-0.1Gy	NOTES	NOTES	NOTES	
	0Gy	Sham	4Gy Only Control						
<b>Trial 6</b>	Raw Counts			89	24	103	Red highlight = excluded from analysis		
				91	26	106	Red highlight = excluded from analysis		
				94	39	95	Red highlight = excluded from analysis		
				108		89	Red highlight = excluded from analysis		
				84		83	Red highlight = excluded from analysis		
				86		100	Red highlight = excluded from analysis		
<b>Trial 7</b>	Raw Counts			64	76	70			
				66	90	73			
				68	81	68			
	Averaged Survival Fraction Trial 7			0	0.35	0.30	< Trial 7 Survival Fraction was calculated using Trial 3 0Gy PE		
<b>Trial 8</b>	Raw Counts	42	37	23	33	32	Red highlight = excluded from analysis		
		36	39	33	27	21	Red highlight = excluded from analysis		
		42	37	32	38	22	Red highlight = excluded from analysis		

\*Trials that were excluded due to low plating efficiency or experimental errors (ie. wrong irradiation times)

**4.**

<b><i>0.5Gy HCT+/-</i></b>				Pre-Conditioning	Post-Conditioning	NOTES	NOTES	NOTES	
				5mGy-3h-0.5Gy	0.5Gy-3h-5mGy	NOTES	NOTES	NOTES	
	0Gy	Sham	0.5Gy Only Control						
<b>TRIAL 1</b>	Raw Counts	90	68	166	224	168	Red highlight = excluded from analysis		
		107	50	161	177	199	Red highlight = excluded from analysis		
		78	56	205	184	304	Red highlight = excluded from analysis		
	Averaged Survival Fraction Trial 1								
<b>TRIAL 2</b>	Raw Counts	140	174	247	237	267			
		139	146	256	278	260			
		168	143	292	276	293			
	Averaged Survival Fraction Trial 2	0.31	0.86	0.85	0.89		< Trial 2 Survival Fraction normalized to Sham		
<b>TRIAL 3</b>	Raw Counts	141	150	265	256	246			
		165	187	254	268	287			
		158	172	208	269	276			
	Averaged Survival Fraction Tri	0.31	0.78	0.85	0.87		< Trial 3 Survival Fraction normalized to 0Gy		
<b>TRIAL 4</b>	Raw Counts	136	159	219	257	230			
		140	164	203	220	232			
		116	135	199	208	265			
	Averaged Survival Fraction Tri	0.26	0.79	0.87	0.93		< Trial 4 Survival Fraction normalized to 0Gy		

\*Trial 1 excluded due to poor plating efficiency for Sham and 0 Gy controls

**5.**

<b>HaCaT Line</b>					
Received the Data from 2015,					
	0Gy	Sham	4Gy	AR	PC
Trial 1	26,28,30/300	82,80,82/300	83,91,87/900	69,61,62/900	81,84,87/900
Trial 2	41,46,36/300	77,70,63/300	54,51,55/900	45,45,49/900	59,55,60/900
Trial 3	Data acquired and included in 3 Trials average below				
Results 3 Experimental Trials, N=9formulated					
	0Gy	Sham	4Gy	AR	PC
Mean plating efficiency	0.342	0.318	0.337	0.348	0.323
Standard error of mean	4.85	4	7.44	2.44	6.74

**6.**

**HCT+/- 2,3,4Gy w. 0.1Gy Primer, 6h incubation before irradiation**

0	S	2Gy	AR2	PC2	3Gy	AR3	PC3	4Gy	AR4	PC4
Trial 1										
0.30	0.31							0.20	0.15	0.18
Trial 2										
0.34	0.34							0.18	0.12	0.17
Trial 3										
0.26	0.31							0.23	0.26	0.24
Trial 4										
0.33	0.31	0.69	0.69	0.70	0.52	0.49	0.48			
Trial 5										
0.35	0.41	0.72	0.67	0.68	0.53	0.51	0.44			
Trial 6										
0.31	0.29	0.37	0.43	0.39	0.20	0.19	0.16			

## 7.

### ***HCT-/- 2Gy and 5Gy***

		0Gy	S	ARCon 2	AR2	PCCon 2	PC2	ARCon 5	AR5	PCCon 5	PC5
<b>TRIAL 1</b>	Raw Counts		238	180	177	171	155	59	129	69	67
			296	169	185	177	163	76	60	80	86
			288	153	154	179	177	107	60	100	72
	Averaged Survival Fraction Trial 1		0.55	0.49	0.51	0.54	0.52	0.09	0.07	0.09	0.08
<b>TRIAL 2</b>	Raw Counts	189	No Data	No Data	No Data	No Data	No Data	62	26	44	60
		178	No Data	No Data	No Data	No Data	No Data	30	26	31	21
		183	No Data	No Data	No Data	No Data	No Data	33	36	19	21
	Averaged Survival Fraction Trial 2	0.367						0.082	0.071	0.060	0.060
<b>TRIAL 3</b>	Raw Counts		145	67	67	61	65	31	40	43	42
			152	70	61	53	70	34	30	37	42
			142	72	58	57	45	43	54	56	28
	Averaged Survival Fraction Trial 3		0.293	0.476	0.424	0.390	0.410	0.082	0.094	0.103	0.085
<b>TRIAL 4</b>	Raw Counts		154	85	66	67	65	34	43	24	34
			150	70	84	77	69	23	29	23	28
			159	86	68	75	79	34	25	21	29
	Averaged Survival Fraction Trial 4		0.309	0.521	0.471	0.473	0.460	0.066	0.070	0.049	0.066

### **BioPhoton Experiments using single photon counting detector (data is in photon counts after 30s runs):**

#### **1. 610nm Wavelength Filter, ~70cm distance from Cs137 Gamma-radiation source, 30s runs:**

		Cells 1 million	750,000 Cells	500,000 Cells	250,000 Cells	Flask Only	Bckgr (No Cells or Flask)
<b>Experiment 1</b>	Trial 1	873211	805367	837521	905418	801519	831638
	Trial 2	879237	852491	828990	892860	812849	824649
	Trial 3	878538	797669	829081	889735	799818	828280
<b>Experiment 2</b>	Trial 1	887520	756407	795449	802703	732335	759715
	Trial 2	889438	747003	804901	783355	728480	752770
	Trial 3	871779	726257	784367	793550	726824	747308
<b>Experiment 3</b>	Trial 1	275161	271767	387760	269459	244261	302262
	Trial 2	265916	247440	349235	359015	321090	276368
	Trial 3	248916	274400	363731	275529	230800	294124

**2.** 250,000 cells seeded, 340nm Wavelength Filter, ~70cm distance from Cs137 Gamma-radiation source,  
30s runs

	Cells	Flask	Background
<b>Trial 1</b>	793574	533860	183196
<b>Trial 2</b>	790027	580442	189626
<b>Trial 3</b>	773329	652338	186447